ABSTRACT

PEARCE, BRADY LAWRENCE. Solution Based Functionalization of Nanostructured Oxides with Organic Molecules. (Under the direction of Dr. Albena Ivanisevic).

The surface modification of wide bandgap semiconductors with organic molecules provides novel functionalities to the composite material. These functionalities can include tuning of the optical properties, providing solution stability of the inorganic material, as well as many others. The use of an *in-situ* functionalization method for surface attachment of phosphonic group containing molecules to the surface of gallium nitride (GaN) has shown promise. This technique is particularly advantageous due to the etching and functionalization steps occurring at the same time, in the same beaker, as well as not being reliant on organic solvents or high temperatures. In this functionalization process, surface hydroxide groups are preferentially grown on the surface of GaN, which serve as attachment sites for phosphonic groups on organic moieties. Molecules with these hydroxyl groups available natively on their surface, such as AlOOH and GaOOH, provide a unique advantage. The requirement for an etching step is removed, and the functionalization process could be performed in a simple one-step modification. The work in this dissertation seeks to address the possibility of using these materials as the inorganic component in organic/inorganic composite material in devices. Of particular importance in solar cell and bioelectronic devices is the ability to withstand varying pH environments, and to avoid the leaching of toxic ionic species. Lysine has shown to reduce the leaching of ionic species, when particles of inorganic molecules are cross-linking agents for the amino acid. In this work, the aqueous stability of both AlOOH and GaOOH in a lysine environment will be explored. The optical and size characteristics observed in nanostructured forms of the mixed composition $Al_xGa_{1-x}OOH$ material system is of interest, due optical tunability providing a distinct advantage in optoelectronic devices

containing these organic/inorganic hybrids. Immobilizing phosphonic group containing organic dyes on the surface of GaN, GaOOH, AlOOH and mixed compositions of AlGaOOH using surface bonding sites, and possible covalent attachments mechanisms, seeks to provide an improvement in the long term stability of the inorganic/organic interface for devices. Future work in this area will test device efficiency using these hybrids, explore additional mixed oxyhydroxide composition systems and continue the advancement of the understanding of the important role of phosphonic groups in organic/inorganic devices. The nature of chemical and surface species in these materials will be characterized with Fourier Transformed-Infrared Spectroscopy (FT-IR) and X-Ray Photoelectric Spectroscopy (XPS). The optical properties of the materials were tested with photoluminescence (PL) spectroscopy, and the stability was examined with fluorescence spectroscopy. The crystallographic nature of the nanostructured inorganic materials before and after functionalization was determined with X-Ray Diffraction (XRD). Images of the nanostructures were obtained with mainly Scanning Electron Microscopy (SEM) as well as Transmission Electron Microscopy (TEM). The work in this dissertation seeks to address the improvement of the development of nanostructured inorganic/organic hybrid materials, the investigation of novel composites for these applications and the improvement of the long term stability in aqueous medium as well as of the organic/inorganic interface itself.

Solution Based Functionalization of Nanostructured Oxides with Organic Molecules

by
Brady Lawrence Pearce

A dissertation submitted to the Graduate Faculty of
North Carolina State University
in partial fulfillment of the
requirements for the degree of
Doctor of Philosophy

Materials Science and Engineering

Raleigh, North Carolina

2016

APPROVED BY:

_____	_____
Dr. Albena Ivanisevic Committee Chair	Dr. Michael Dickey
_____	_____
Dr. Joseph Tracy	Dr. Claude Reynolds Jr

BIOGRAPHY

Brady Pearce was born in Waukesha, Wisconsin and moved to the Raleigh, North Carolina area when he was 8 years old. He did his undergraduate at Appalachian State University as a double major in physics and chemistry. Brady also received a master's degree from Appalachian State in engineering physics. He worked with Albena Ivanisevic on surface functionalization of synthesized nanostructured oxyhydroxide materials at North Carolina State University after being accepted in the PhD progam for Materials Science and Engineering in 2014.

TABLE OF CONTENTS

LIST OF TABLES

LIST OF FIGURES

1. Introduction

1.1 Background

The main topic of this thesis involves a discussion of the viability of nanostructured gallium and aluminum oxyhydroxide materials, functionalized with organic molecules, as organic/inorganic interfaces for solar cell and biological applications. The use of dyes as the organic molecule in these interfaces presents one particular example, for use as dye-sensitized solar cells (DSSCs). Dyes with functional groups containing phosphonic sites provide the advantage of binding with the oxide layer native on GaOOH and present through controlled etching on GaN. Previous work has demonstrated the viability of using phosphonic group containing organics for the functionalization of GaN.[1] This covalent bond presents the unique advantage of prolonged device stability in environmental and biological conditions, such as those solar cells and biosensors are subject to.

The semiconductor molecules of interest in this work are gallium nitride (GaN), gallium oxyhydroxide (GaOOH) and aluminum oxyhydroxide (AlOOH). These inorganic materials are proposed for interfacing with various organic molecules for novel hybrid inorganic/organic composites. The organic molecules of specific interests are L-lysine and phosphonic group containing porphyrin dyes. Recent research has indicated that by etching and effectively growing a hydroxide layer on GaN, a means of covalent surface attachment for phosphonic, carboxylic group and thiol containing organic molecules is produced.[2] This attachment mechanism is identical to that of GaOOH, in that the surface layer on GaN that is used is present throughout the entire molecule. The native presence of this oxide layer on

GaOOH, as well as the native layer on AlOOH, presents a unique advantage of these materials for modification with functional organics.

1.2 Gallium Nitride, Gallium Oxyhydroxide and Aluminum Oxyhydroxide

Gallium nitride belongs to the class of materials known as III-nitrides, containing Ga as the III-group element. The crystal structures that GaN predominately exists in are wurtzite and zinc blende. [3] It is a direct, intrinsic semiconductor with a wide band gap of 3.4 eV.[4] As a direct bandgap containing semiconductor, it is suitable as a material for optoelectronic applications. The incorporation of functional groups to the surface of GaN has been used for a multitude of applications including thin films deposited on nanowires by atomic layer deposition,[5] field-effect transistors with recognition peptides attached to the surface,[6] thiol groups,[7] attachment of olefins,[8] alkyl groups,[9] incorporation of alkylphosphonic acids[10] and 1-alkenes[11] in an effort to add various functionality to the inorganic semiconductor surfaces.

The wide bandgap semiconductor, GaOOH, with a bandgap of 4.75 eV, provides a useful inorganic scaffold for the attachment of organic dyes for use as DSSCs and biosensing applications. The crystallinity of GaOOH has been shown to be that of an orthorhombic crystal system.[12] In recent work, GaOOH has been used as a precursor molecule for conversion to gallium oxide (Ga_2O_3)[13] as well as GaN.[14] With a direct bandgap, GaOOH is also suitable for optoelectronic devices. The Al analogue to this, AlOOH, also contains a direct bandgap which is known to be 4.51 eV.[15] The optical properties of AlN and GaN provide the unique capability of using ternary, mixed compounds to tune the specific wavelength of emission for LEDs and other optoelectronic devices. In general, III-nitride

materials have been identified as some of the most important compounds for driving the future of optoelectronic devices.[16]

It is of interest to investigate composite oxyhydroxide materials containing both Ga and Al. The aluminum oxide layer has shown to be an effective and highly stable material for interfacing with organics, such as poly-L-lysine.[17] Vogelson et. al. demonstrated the use of a simple reflux reaction to synthesize hybrids of AlOOH and lysine. This technique is environmentally friendly due to it relying on only DI water as a solvent. The temperatures used are lower than typical functionalization reactions, as well. By replacing the AlOOH nanoparticles with GaOOH nanostructured materials, it is believed that a composite with Ga can be synthesized.

1.3 In-situ Functionalization of Gallium Nitride Using the Surface Oxide Layer

Wide bandgap semiconductors are effective materials for functionalization with organic molecules for a number of reasons. The material properties of the inorganic semiconductor form the basis for optical and electrical characteristics of the functional device as well as determine the coherency of the interface between the two molecules. In the case of GaN and GaOOH, the effectiveness and stability of the interface is reliant on the oxide layer present on the surface of the two molecules. Hydroxide groups present on the surface have proven effective moieties for the attachment of phosphonic groups and covalent modification of the surface with an organic molecule.[18]

In-situ functionalization of GaN has been shown to be possible using simple, beaker based wet chemistry. This functionalization process has been performed with some success in the past with topographical, surface chemical, optical and electronic properties

characterized to determine differences before and after the modification. Changes in the optical properties due to the functionalization have been explored in detail due to the materials importance in light emitting diodes (LEDs).[19]

The mechanism of the *in-situ* surface attachment of organic moieties to GaN consists of a few steps for coverage to occur. It is noted that this approach is less time consuming and more environmentally friendly than previous reported methods of functionalization of semiconductors with organic molecules. There are four steps in this process including cleaning, etching and binding of the functional molecule and capping of the surface. During the cleaning process, any environmentally formed, uncontrolled oxide and carbon layer is removed from the surface to ensure a useful oxide layer can be formed for surface attachment. In the etching portion, oxides are formed and dissolved on the surface of the GaN sample and a controlled attachment layer is formed on the surface. In the *in-situ* functionalization of GaN, this etching step is done in conjunction with the binding step where the functional groups used for attachment interact and bind with the controlled oxide layer or, in some cases, the metal itself. Capping is done to ensure that no undesired molecules bind with the surface after the functionalization and any unreacted materials are washed and filtered away.

This methodology is particularly beneficial due to its environmentally friendly nature. Hydrochloric acid, used during the cleaning step, is the most abrasive and unsafe chemical used during the process. The etching process is done with the relatively safe phosphoric acid and simple DI water as solvents.

1.4 Applications of Organic/Inorganic Composites

One of the specific applications of interest for these novel, nanostructured organic/inorganic interfaces is that of DSSCs. Since these devices advent in 1991, in the work done by Grätzel and O'Regan[20], extensive research has been done to improve the efficiency and stability of them. For DSSCs, the focus of most recent research efforts is on the materials TiO_2[21] and ZnO.[22] Research into alternative materials has garnered recent attention due to TiO_2 having relatively low electron mobility.[23] Conversion efficiencies of the alternative ZnO have been cited as being low with the reasoning behind this being the dye interaction with the semiconductor at the surface.[24] Group III-nitride semiconductors, particularly in nanostructured form, have been identified as extremely important for devices which rely on optoelectronic phenomenon.[16] As indicated earlier, the oxide layer present on GaN provides the ability to bond phosphonic containing groups to the surface, thus increasing efficiency by increasing long term device stability.[2]

The search for efficient, renewable energy sources has driven the rise in research into increasing the efficiency and decreasing the cost and environmental effects of manufacturing solar cells. Advantages of DSSCs are numerous and include the low cost of fabrication[25] as well as the nature of the cell being environmentally friendly.[26] These types of cells are considered the third generation of solar cells and are diverse in chemical and structural makeup.[27] The principle behind their operation, however, remains the same and is reliant upon an organic dye molecule that can inject electrons from its highest occupied molecular orbital (HOMO) to the conduction band of a wide bandgap semiconductor that is in close

proximity of the dye. An electrolyte solution is used to regenerate electrons in the system by reducing them to the lowest occupied molecular orbital (LUMO) of the dye molecule. It is the incoming radiation that promotes these electrons from the LUMO to the HOMO where the dye-semiconductor transfer will occur again. The electrodes of DSSC are typically made of a transparent conducting oxide (TCO).

The typical method of attachment of dye molecule to semiconductor is by physisorption on the surface by various techniques. This has proven to be a useful technique; however issues of long term stability remain problematic. Recent work has been done to replace the solvent used in the electrolyte solution to address this.[28] We seek to add to this by using our unique interface which contains surface bonding and is believed to be capable of long term device stability in environmental conditions.

A second consideration for device implementation is the electronic and optical properties of direct wide bandgap semiconductors providing a method of incorporating an optically active organic molecule to tune these properties for sensing and energy harvesting. The band alignment that occurs between organic dye molecules and GaN and GaOOH is advantageous when compared to that of TiO_2. The band alignment of these wide band gap semiconductors provides evidence of these Ga containing semiconductors viability as suitable replacements for DSSCs.

Beyond solar cells, these organic/inorganic hybrid materials have been identified as especially useful for biosensors and other biological applications. The use of gallium containing materials for biological applications is viable due to its reported biocompatibility.[29] Using the amino acid lysine provides unique functionality for biological

applications of these composites. It has shown to improve cell adhesion[30] and biocompatibility[31] of various functional materials.

The aqueous stability of materials used in biological applications is important for toxicity considerations. Pourbaix diagrams of Al and Ga oxide materials demonstrate the importance of stabilizing these materials in aqueous environments. Both elements are passivated in small pH windows and in environments with varying pH, leaching of both is likely to occur. This is indicative of improving the stability of oxides of these materials by functionalization with a molecule such as lysine.

1.5 Advantages of Nanostructured Materials

A distinct advantage of the use of nanostructured materials for organic functionalization is the increased surface area and, therefore increased attachment sites for modification.[21] Specifically for photovoltaic applications, there is an increase in research for the use of GaN nanostructured materials. Various nanostructures of GaN have been investigated including nanobelts, nanowires and others. A microwave hydrothermal process has been used to synthesize nanorods of GaOOH.[31] Nanostructured AlOOH has been synthesized using a variety of methods, including the hydrothermal synthesis of γ-AlOOH nanotubes and nanorods.[32]

1.6 Examples of Synthesis Techniques for Nanostructured Materials

1.6.1 Solution Based Techniques

The literature describing various solution based techniques of forming nanostructured materials is extensive. Examples of solution based methods include microemulsion, hydrothermal, sol-gel and ultrasonic synthesis of materials.[33] Recent work has established

microwave hydrothermal synthesis which will be the focus of the next section. Hydrothermal synthesis techniques for metal oxide materials have recently been reviewed.[34] Typically, these reactions use metal nitrate salts as precursors. A hydrolysis reaction follows which forms a metal hydroxide. Dehydration of this hydroxide forms a precipitate which is that of a metal oxide. This is described below in Equation 1 and 2, adapted from Hayashi et. al.[34]

$$M(NO_3)_x + xH_2O \rightarrow M(OH)_x + xHNO_3 \quad (1)$$

$$M(OH)_x \rightarrow MO_{x/2} + x/2\ H_2O \quad (2)$$

Microemulsion techniques rely on three different components within one stable, single phase solution. A surfactant is used that is miscible in the solution along with two other components which are not. The stabilizer or emulsifier is a molecule with a polar head group and nonpolar tail. The emulsifier aligns itself with the nonpolar tail facing towards the surfactant and the polar head group facing towards what is typically an aqueous solution containing precursor materials. The emulsifier surrounds the reaction solution and dictates the size and shapes of crystallized product.

Sol-gel techniques rely on the polymerization of inorganic materials. The precursor materials in these reactions form gels through a hydrolysis reaction. The size of the particles is affected by rates of the hydrolysis reaction as well any condensation reactions that occur.[33] The removal of solvent from the gel is done using high temperature calcination. Other factors that affect the size of these particles are the composition and pH of the solution and the temperature of the reaction.[33]

The synthesis of nanomaterials using sonochemical methods uses ultrasounic radiation to promote chemical reactions. An advantage of this method is that it can be done

with no added pressure or temperature to the reaction. The high energy sound waves cause acoustic cavitation to occur which forms bubbles in the solution which continue to grow until they collapse.[33] These bubbles are thought to produce extremely high temperatures during the process of their collapse which are then rapidly cooled back to the ambient solution temperature.

1.6.2 Microwave Hydrothermal Synthesis

In traditional hydrothermal synthesis techniques, the solution is sealed and placed into an autoclave. The reaction temperature is set and it is left for periods of around 24 hours, typically. Recent work has shown that by replacing the autoclave with a microwave, these reactions can be done in less than an hour.[31] This can be done with no surfactant in an environmentally friendly way, with just DI water as a solvent.

The key advantage of microwave synthesis is the drastically reduced time restraints on the reaction process. Along with this, the process requires less energy than typical synthetic techniques which allows it to be considered a green chemistry technique.[35] Another advantage is that the microwave heating is capable of restricting the side reactions that take place during the synthesis.[36]

Radiation that resides in the frequency range between 0.3 and 300 GHz is considered microwave radiation. The two processes involved in microwave heating are dipolar polarization and ionic conduction. The microwave radiation aligns either the dipoles or ions with the oscillating electric field and their attempt to realign within the field causes heating effects.[36] The ionic conduction mechanism is a stronger heating mechanism than that of dipolar polarization. An ionic liquid is capable of reaching high temperatures in extremely

short periods of time, an advantage of microwave heating that cannot be reproduced by any other method. The various mechanisms behind the microwave's ability to drastically reduce reaction time are still under investigation with various theories explaining this phenomenon.

1.7 Advantages of Oxide Materials for Functionalization

The majority of previous research in solution based *in-situ* functionalization has focused on using GaN as the inorganic moiety of the hybrid material. The surface oxide layer that forms during the etching process has been hypothesized to be GaOOH or various other hydroxyl groups due to the high solubility of Ga_2O_3 in acidic conditions. It is beneficial, therefore, to investigate the solution based functionalization of GaOOH (as well as AlOOH) due to the inherent presence of this oxide layer with no etchant required. These materials could be functionalized with soluble phosphonic group containing molecules by simple prolonged contact in solution. This would eliminate any need for harmful etchants or cleaning agents and require simply DI water as a solvent. This process represents a highly scalable and environmentally friendly technique for forming organic/inorganic hybrids with long term interface stability.

The advantages and synthetic techniques of nanostructured forms of these oxide materials have already been discussed. The solution microwave techniques are, in particular, attractive due to their short time requirements and environmentally friendly nature. The solvent used in the microwave hydrothermal synthesis of GaOOH is simply DI water.[37] This technique has not been reported for the synthesis of AlOOH or composites of Al and Ga. This provides a unique additional time saving property of this synthetic technique. A water soluble organic molecule containing phosphonic linkage groups can be added with the

microwave precursors and the resulting product will be the desired inorganic/organic composite material.

1.8 Characterization Methodologies and Properties of Organic/Inorganic Interfaces

Various techniques exist which have proven effective at investigating the properties of organic/inorganic hybrid materials. Surface sensitive techniques for determining the chemical properties of the interfaces provide important information. This can be done using X-ray photoelectron spectroscopy (XPS) and Fourier transformed-infrared spectroscopy (FT-IR). The effects of functionalization on the crystalline nature of the inorganic materials are of particular interest for the synthesized nanostructures. X-ray Diffraction (XRD) measurements provide this information. The optical properties of the material are the main focus of their viability in optoelectronic devices. The emission wavelength under high energy photon excitation is of particular interest and can be measured using photoluminescence spectroscopy (PL). The stability of the organic material's attachment to the inorganic material can be assessed with experiments involving the use of fluorescence spectroscopy. High resolution atomic leaching and ratios can be obtained using inductively coupled plasma-mass spectrometry (ICP-MS). The morphological features of these nanostructured samples can be explored using scanning electron microscopy (SEM).

1.8.1 X-Ray Photoelectron Spectroscopy

XPS is a surface sensitive technique which provides valuable information about the surface chemistry of materials. It relies on the photoelectron effect which occurs when a high energy photon excites electrons within a material. Electrons within the material can be removed with a photon energy that is greater than the work function of the sample. The

removed electron will have a kinetic energy which is equal to the energy of the incoming photon minus the binding energy of the electron within the material.[38] This energy is measured and provides information about the atom and orbital shell attributed to the ejected electron. Observed energy shifts in these measured electrons are attributed to binding with various other atomic species.

Two x-ray sources are typically used in XPS instrumentation which includes Al Kα and Mg Kα. The energy of x-rays generated from these sources is 1486.7 and 1253.6 eV, respectively. Survey scans sweep through a large range of binding energies. These scans can be used for qualitatively understanding the atomic species present on the surface as well as quantitatively measuring the ratio of these species in the sample. Charging effects from insulating samples (such as GaN and the oxide materials of interest) cause the measured binding energies to shift from their real values. Due to this, a calibration standard has been established using the advantageous carbon peak in the carbon 1s regional scan to 284.8 eV.[39]

In order to provide higher resolution information for use in determining the nature of bond species to the atoms seen in the survey scan, regional scans are used. The range of these scans is much lower than the survey scan and they focus specifically on one orbital shell of an atom. A particularly useful high resolution region for the materials discussed in this chapter is the N 1s region. Organic materials containing N species can easily be identified in the N 1s region due to the high binding energy of N bound to organic species. Amide bonds can be found near 399.8 eV[40] and peaks around 399 and 402 eV for pyrolle N in porphyrin molecules.[41]

1.8.2 X-Ray Diffraction

Crystallographic information is of importance for these composites in order to observe the effects, if any, of the presence and attachment of the organic molecule to the crystalline nature of the nanostructured inorganic semiconductors. XRD is a widely used technique for addressing the crystalline nature of samples. In this work, Bragg-Brentano geometry will be the focus of discussion, since the materials are powders and nanostructured samples and not thin films. In this geometry, the angle of diffraction of the x-ray after interacting with the crystal structure of the material provides information about the orientation and planar spacing of the sample. In addition, the size of crystallites within the material can be determined using the Scherrer equation. The broadening of the spectral lines in the XRD can be used to calculate the size of crystallites.

1.8.3 Optical Properties and Photoluminescence Spectroscopy

A main focus of this chapter is the ability to use the inorganic/organic hybrids discussed in this work as optoelectronic and biosensing platforms for improving stability and, possibly, efficiency of devices. Of particular interest for these devices is the band matching between the semiconductor and optically active organic molecule. The interaction between the HOMO level of the organic material and the conduction band of the semiconductor provides the basis for electron transfer between the two molecules in devices such as DSSCs. One method of exploring the direct band gap of a semiconductor is by measuring the emission wavelength seen in a PL spectrum.

The mechanism of PL involves the creation of an exciton (electron-hole pair) by absorption of a high intensity photon source, such as a laser. If the energy of the incoming

photon is higher than the band gap of the semiconductor, the material will absorb it and release the energy in a number of different ways. Nonradiative recombination of the excitons releases phonons which is essentially the release of heat through lattice vibrations. In the case of radiative recombination, photons are release from the material and can be measured using a photodetector.

The maximum energy of the photons released from the material are from an exciton pair recombining across the full bandgap of the material. These are referred to as band edge recombinations and are seen at the lowest wavelength in PL spectra. For materials which are made with less regard to defect density as pristine wafers, the PL spectrum is broad and spans a wide range of wavelengths. The second, broad peak seen in these spectra is attributed to exciton recombination within defects levels which lie within the band gap themselves. Therefore, the photons emitted from these recombination processes have lower energy levels than the band edge and are seen at higher wavelengths.

An important consideration of PL measurements is size effects of nanoscale semiconducting materials. The dominant effect of size characteristics on the band gap of the materials is determined by the size ratio to the Bohr radius of the material as well as the general shape the materials conform to.

1.8.4 Stability and Fluorescence Spectroscopy

A key advantage of these novel composite materials is the mechanism of attachment between the organic and inorganic molecule providing the possibility of long term stability of the interface and, therefore the device. A key concern for these composites is the stability of the interface in aqueous media. Fluorescence spectroscopy provides a method of determining

the presence of soluble organic dye leached off of the semiconductor into solution. This can be accomplished by leaving the composite sedimented in solution for a long period of time. After filtering this solution to ensure none of the sediment remains, fluorescence spectroscopy can be done to determine if any soluble dye has leached off of the semiconductor and into solution.

1.8.5 Scanning Electron Microscopy

Imaging of materials with nanoscale features is possible with electron microscopy techniques. Homogeneity of nanostructured materials and other morphological information can be gained using SEM. In SEM, a source of electrons is excited and accelerated though a number of lenses before coming in contact with the sample. Electron interactions with the samples cause two types of electrons to be emitted, high energy backscattered electrons and secondary electrons. The backscattered electrons (BSE) have energies which are equal to that of the incoming electron beam. Secondary electrons (SE) are low energy electrons which are produced from inelastic collisions of the electron beam with other electrons within the sample itself. Both of these electron types are ejected from the sample and can be collected by a detector. The electron beam is rastered across the surface of the sample and an image can be produced using either the BSE or SE. For improved z-contrast, BSE images are used and for morphological and for depth of field information SE images are used.

1.9 Summary and Overview

The beneficial attributes of the inorganic wide bandgap semiconductors GaN, GaOOH and AlOOH have been reviewed. It is of interest to investigate the usefulness of these materials for inorganic/organic hybrid composites for use as optoelectronic platforms in

various devices. Tunability of the optical properties is thought to be possible by varying the Al and Ga composition. This is especially attractive for band matching with organic molecules which are optically active. In addition, the improvement of aqueous stability of these materials is of interest for the reduction of metal leaching for biological applications. The work in this thesis seeks to address these unmet areas of need for researching more effective and stable composites and their functionalization in interfaces useful for device applications.

Initially, an *in-situ* functionalization technique, with the ability to both etch and modulate the surface in the same step and beaker, will be performed on nanostructured GaN powder using a porphyrin dye. This will be followed by the investigation of the attachment of this dye molecule to the surface of a solution synthesized, nanostructured material GaOOH. This semiconductor contains the hydroxyl attachment site on it natively, which removes the need to etch before introducing the soluble dye. The incorporation of Al precursors in the microwave synthesis procedure will then be explored, to determine its effectiveness in providing optical tunability. The mixed Al-Ga oxyhydroxide system will also be functionalized with the porphyrin dye molecule, and the effects of the dye on the composite's optical properties will be explored. The effects of the incorporation of AlOOH and GaOOH with lysine on the aqueous stability of the semiconductors will be explored.

2. *In-situ* Functionalization of Gallium Nitride Powder with a Porphyrin Dye

Brady L. Pearce,[1] Stewart J. Wilkins,[1] Matthew S. Rahn,[2] Albena Ivanisevic[1*]

[1]Department of Materials Science and Engineering, North Carolina State University, Raleigh, North Carolina, 27695, USA

[2]Department of Materials Science and Engineering, Pennsylvania State University, State College, Pennsylvania, 16801, USA

2.1 Abstract

This work focused on the modification of milled GaN powder. Successful attachment of a porphyrin derivative to a GaN powder was performed via *in-situ* functionalization in the presence of phosphoric acid. The GaN powder was imaged using scanning electron microscopy and was found to be heterogeneous in nature, adopting no consistent geometry in the aggregates. The aqueous stability of the porphyrin used was observed in deionized water and a solution of phosphoric acid using ultra-violet-visible spectroscopy. Surface chemistry was characterized with x-ray photoelectron spectroscopy and infrared spectroscopy, which identified evidence of successful functionalization through the presence of characteristic peaks. The interface stability of the covalent bond between GaN and porphyrin was evaluated using fluorescence spectroscopy and demonstrated no leaching of dye in water solutions for 20 days.

2.2 Introduction

Research efforts into solution based surface functionalization of inorganic materials have sought to expand the knowledge base of the effects surface bound molecules have on their properties. Of these semiconducting materials, gallium nitride (GaN), a III-V material

with a band gap of 3.4 eV, is of significant interest.[4] The surface modification of GaN has been used to develop field effect transistors with a myriad of surface treatments such as recognition peptides[42], attached thiols[7], alkyl groups[9], DNA binders such as olefins[8], 1-alkenes[11], atomic layer deposition (ALD) thin films[5] and alkylphosphonic acids[10] for unique properties. The chemisorption of multiple molecules (haloanilines,[43] aniline,[44] pyrroline,[45] water,[46] and fluorine[47]) on GaN surfaces has traditionally been studied within controlled environments. Of the properties altered with surface chemistry, the modulation of optical properties of GaN is well documented[48] and remains a continuing endeavor. The rise in applications of functionalized gallium nitride is attributed to their documented chemical inertness[49] and biocompatibility through aqueous stability[50] when compared to other III-V semiconductors. Recent work has shown that wet etching gallium nitride with phosphoric acid in the presence of adsorbates alters the surface morphology as well as the surface chemical composition.[51] This combined process opens up the ability to change the semiconductor surface, which introduces opportunities for the development of functional interfaces as well as biosensing applications.

The attachment of dye molecules to semiconductor interfaces is beneficial for applications such as dye-sensitized solar cells (DSSC) and optical sensors.[52] In DSSCs, the dye is crucial as it allows a wider bandwidth of light to be absorbed. Previous research has documented evidence that porphyrin sensitizers provide high photon-to-electron conversion efficiency.[53] The most studied semiconductor in DSSCs so far is TiO_2. Due to TiO_2 having a low electron mobility (less than 1 $cm^2/V\ s$)[23], there is a focused effort into identifying alternative wide band gap materials. One alternative to TiO_2 that has been investigated is

ZnO;[24] however, the instability of the surface interaction between the dye and semiconductor is cited for the recorded low conversion efficiency. Recent use of GaN for DSSC applications has shown promise compared to transition metal oxides.[54] Incorporating GaN in DSSCs provides a semiconductor with higher electron mobility than traditional TiO_2. Additionally, the high chemical stability of GaN under different environmental conditions and various solvents is beneficial for future solar cell devices.[55]

In this study we report the surface modification of milled GaN powder with a porphyrin dye. The reported characterization focuses on the chemical stability of the bound dye to the GaN and nature of the dye bonding. The use of milled powder was originally employed due to its ease and cost when compared to traditional methods such as chemical vapor deposition (CVD).[56] Improvements in the milling process have allowed for the possibility of high quality crystal growth.[57] The high surface area of the powder GaN is beneficial for applications such as solar cells where one tries to maximize light conversion. In addition to the large surface area, the ability to convert the powder into a paste and deposit it onto large planar surfaces provides simplified processing beneficial for DSSCs fabrication. By altering the surface morphology with the aforementioned etching technique, the chemical stability of the porphyrin salt in the presence of phosphoric acid as well as in an aqueous environment was tested. The GaN powder was imaged with Scanning Electron Microscopy (SEM) to probe the size and homogeneity of the powder. Fourier Transformed-Infrared spectroscopy (FT-IR) was utilized to observe the incorporation of the organic dye on the GaN surface. Quantitative X-Ray Photoelectron Spectroscopy (XPS) determined elemental composition, binding shifts and the presence of surface species after porphyrin dye

attachment. The stability of the attachment of the dye to GaN is important to assess since it is directly related to device efficiency.[49] Fluorescence spectroscopy tracked the presence and possible leaching of dye from the powder after immersion in aqueous solutions for up to 20 days.

2.3 Materials and Methods

2.3.1 Powder Functionalization

The gallium nitride powder was obtained from Sigma-Aldrich (99.99 % trace metals basis) without pre-treatment. The powder was washed three times with acetone (Fisher Scientific) and three times with methanol (Sigma Aldrich). The samples were then rinsed with hydrochloric acid (Sigma Aldrich, 35-38 vole %) three times followed by three washes with deionized (DI) water (18.2 MΩ*cm).

A 7.125 μM solution of meso-tetra(4-phosphonomethylphenyl) porphine tetrasodium salt (TTP-PO_3) (Frontier Scientific) with DI water was prepared. This solution was added in a 1:1 (v:v) ratio to phosphoric acid (Fisher Scientific, 95%). The resulting solution was added to the washed and treated GaN powder and heated for a period of 120 minutes at 40°C. The powder was stirred throughout the duration of the treatment. A separate batch of powder was washed and stirred in phosphoric acid etchant only for the same time and under the same conditions. After 120 minutes, the GaN powder was washed with DI water three times and left overnight in a desiccator to dry.

2.3.2 Characterization

An Agilent Technologies Cary Series Ultraviolet-Visible Spectrophotometer (UV-Vis) was used to collect absorbance data. The 7.125 μM solution of TTP-PO_3 as well as a

solution of 50 vol.% 7.125 μM TTP-PO_3 and 50 vol.% phosphoric acid were tested. All spectra were collected in quartz cuvettes.

Pre-treatment GaN powder was imaged with a JEOL 6010 LE SEM with an accelerating voltage of 20kV. The working distance for the image was 10 mm with a spot size of 50. A magnification of 3,000x was used to take the micrograph. The IR data was gathered with a Bruker 1 95 9670 ALPHA Fourier-Transform-Infrared Spectrometer (FT-IR) equipped with a KBr beam splitter. Using the instrument OPUS software, the resolution was set to 2 cm^{-1} for all scans. The samples were evaluated by averaging 36 scans in transmittance mode. All semiconductor samples were prepared using 50 grams of KBr to 1 gram of GaN powder. For the TTP-PO_3 data collection 100 grams of KBr to 0.1 gram of TTP-PO_3 was utilized. The OPUS software was employed to perform a background subtraction and smooth line profiles.

All XPS evaluation was performed on an Axis Ultra XPS manufactured by Kratos. The X-ray source was a monochromated Al Kα with beam energy of 1486.7. eV. A charge neutralizer was used with 2.0 A filament current to account for charging of the samples. The pressure was maintained within the sample chamber to 3 x 10^{-8} Torr. The samples were mounted onto an aluminum sliding sample holder using adhesive coated copper tape. For each sample, a survey scan was collected using a sweep pass energy of 160 eV. High resolution regional scans were gathered using a pass energy of 20 eV for C1s, Ga 2p, N1s, O 1s, and P 2p spectra. The software used to deconvolute and calibrate the peaks was Casa XPS version 2.3.12.8. A Shirley approximation was used to remove the background before peak deconvolution. The data was calibrated by setting the adventitious carbon C 1s peak to 284.8

eV. A Lorentzian fit was used to constrain the full width half-maximum of the deconvoluted peaks to the primary peaks. A second calibration was performed to adjust for the high degree of charging evident in the N 1s region scan. The N-Ga peaks for each sample was calibrated to 397.3 eV.[58]

The fluorescence data was obtained with an excitation wavelength of 455 nm at maximum LED source intensity. The sample was sonicated before testing to ensure dispersion of particles within the solution. All data was plotted and analyzed with Origin 9.0.

2.4 Results and Discussion

2.4.1 In-Situ Functionalization of GaN Powder with Porphyrin

Porphyrin molecules show promise for sensitization due to their reported high conversion efficiencies.[59] Stable bonding between the semiconductor and dye molecules is critical for stability and optimal electronic properties in photonic devices, which has been explored by a number of research groups. Brennan et al. investigated various anchoring groups for attaching porphyrin molecules to semiconductor surfaces.[60] The use of porphyrin dyes to successfully sensitize TiO_2 was described by Odobel et al.[53] In this study, we performed an in-situ functionalization of GaN powder with a porphyrin derivative TTP-PO_3 using a recently reported in situ approach.[1] The covalent attachment of the porphyrin to the GaN was investigated to determine success and stability of the reaction.

The selection of porphyrin derivative for this study was based primarily on the side groups and the ability to bind to GaN in addition to containing a desirable structure to modulate the optical response. The attachment of phosphonate groups to gallium nitride through *in-situ* functionalization was recently quantitatively studied.[1] A water-soluble

porphyrin was needed in order to be compatible with phosphoric acid used during the *in situ* procedure. The TTP-PO_3 salt provides a water-soluble molecule containing phosphonate side groups available for attachment through a bidentate mode. In future studies of porphyrin dye attachment to GaN, the incorporation of a metal center within the molecule will be explored.

Prior to the functionalization method displayed in Figure 2.1 the GaN powder was washed with various solvents and treated with hydrochloric acid. The hydrochloric acid was used to remove the native thin oxide layer which forms on the GaN during storage under normal room temperature and humidity environmental conditions. During functionalization, H_3PO_4 serves as an etchant that encourages the formation of a controlled oxide layer in addition to removing nitrogen rich regions from the surface. By adding TTP-PO_3 while etching, phosphonic groups preferentially bind to metal rich areas on the surface as well as to protonated and hydroxyl terminated regions. This in turn provides a binding site for TTP-PO_3 as well as caps existing gallium oxide to hinder dissolution in water. The 7.125 μM solution of TTP-PO_3 used in this study falls within the concentrations ranges that other surface modification procedures have utilized (1 μM to 1 mM.)[61] Identification of bonding and subsequent changes in surface chemistry at the GaN interface is best performed with surface sensitive techniques such as XPS. XPS gathers information about the binding energies of species at the sample surface and provides qualitative as well as quantitative information of changes in chemical composition following chemical treatments. FT-IR assesses the presence of distinct functional groups. An additional advantage of using porphyrin as an adsorbate is in its distinct fluorescent spectra with peaks with strong intensity. This provides a method of

both testing successful functionalization as well as quantification of the stability of the dye attachment to the GaN interface.

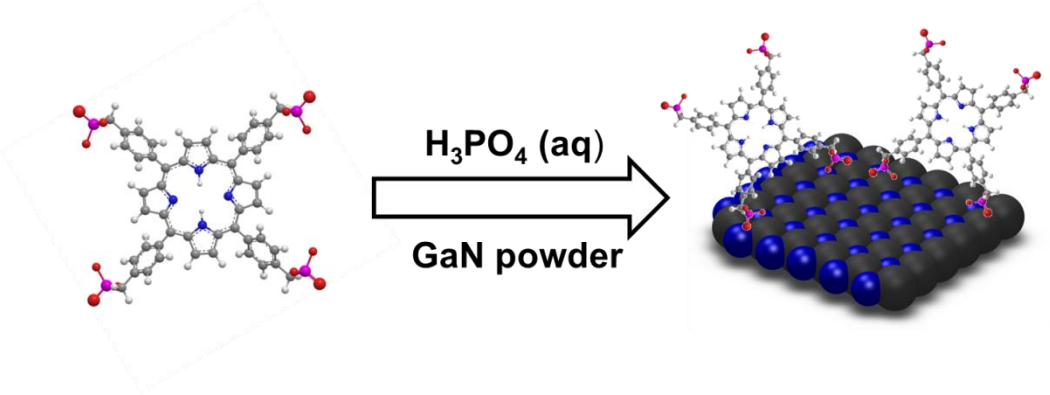

Figure 2.1. Schematic diagram of the in situ functionalization process showing bidentate binding of the porphyrin on the surface of the GaN powder.

2.4.2 Stability of Porphyrin in Phosphoric Acid

An important consideration in this study was the possible aggregation or degradation of TTP-PO_3 in solution, DI water, or with phosphoric acid. In a typical UV-Vis absorbance spectrum, a sharp Q band is used to provide evidence of the monomeric species of TTP-PO_3. If aggregation occurs, this peak will blue-shift as well as broaden in the UV-Vis spectrum. In Figure 2.2, no aggregation or degradation was observed in TTP-PO_3 dissolved in water or mixed with phosphoric acid etching solution. The solutions were left for 4 hours before they were tested to allow enough time for aggregates to form. These results provided evidence that TTP-PO_3 was compatible with the solution conditions necessary for the *in situ* method of functionalization.

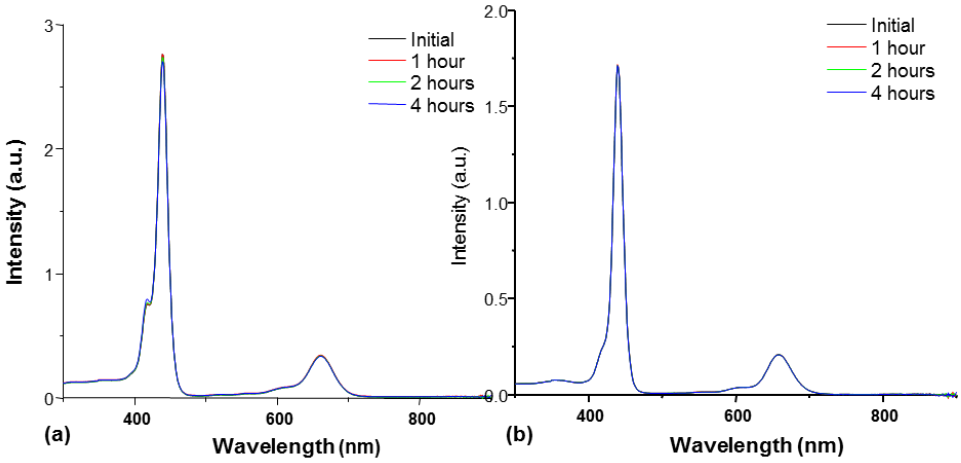

Figure 2.2. Room temperature UV-Vis spectra of (a) 7.125 μM TTP-PO_3 in DI water and (b) 50% 7.125 μM TTP-PO_3 in DI water and 50% phosphoric acid.

2.4.3 Morphological Characterization by SEM

SEM quantified the homogeneity of the GaN powder. Images, such as those seen in Figure 2.3, show that the aggregate size of the GaN powder varies widely and the overall surface holds little homogeneity. SEM was also used to probe for evidence of aggregation of organic contamination and TTP-PO_3. We observed that the powder was free of organic particulates from environmental contamination. The overall aggregate size was recorded to be dissimilar in various batches and ranged from less than 1 μm up to sizes greater than 5 μm. For this study, uniformity of the particulates making up the powder was not a concern as the binding at the GaN powder interface was the primary focus. The aggregates appeared amorphous with no consistent shared geometry shapes, which led to the conclusion that the aggregate composition was heterogeneous.

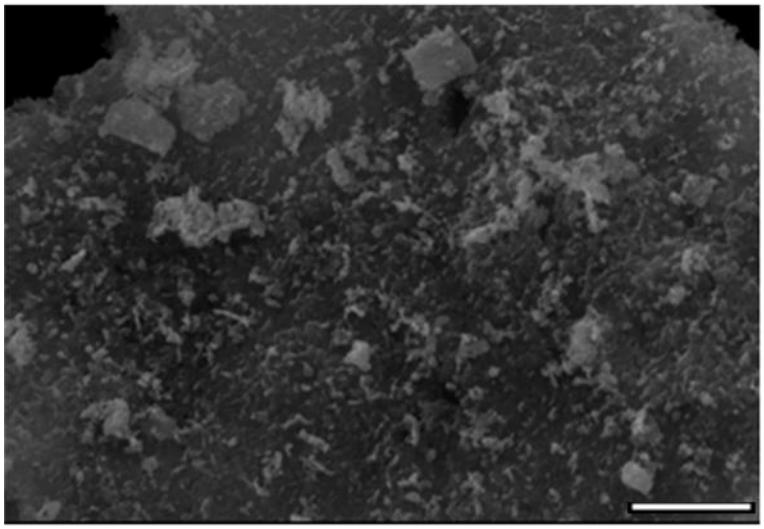

Figure 2.3. SEM image of GaN powder showing the size and heterogeneity of aggregrates within the powder. Scale bar is 5 μm.

2.5 Surface Characterization

2.5.1 X-Ray Photoelectron Spectroscopy

XPS was utilized to confirm successful attachment of TTP-PO_3 to the GaN powder. Multiple survey and high-resolution regional scans were collected following cleaning, etching, and functionalization. In the samples that underwent etching, the presence of a P 2p peak was expected due to residual phosphonic acid groups on the surface. The collection of C 1s spectra provides a calibration technique as well as probing mechanism into TTP-PO_3.[62] However, the adventitious carbon peak lies in close proximity with the expected peak for the porphyrin (285.0 eV). The Ga 2p region was collected to determine the presence of specific gallium species on the surface. These regional scans offer evidence of oxide species, Ga_2O_3 and other sub oxides, forming on the surface.[18]

A peak centered near 1120 eV was present in the survey scan for each of the samples. This peak was attributed to gallium content from both the powder and surface oxide seen within the Ga 2p spectra. Another peak near 530 eV, again recorded in the survey scans for all three types of samples, indicates the presence of oxide groups on the surface as seen from the O 1s region. In accordance with the identification of gallium, the peak centered near 400 eV confirmed presence of nitrogen, which is as expected and was observed within the high resolution N 1s spectra. A peak centered near 135 eV was present for the etched only GaN powder, as well as the etched and functionalized GaN powder, which was distinctly absent for the cleaned powder. This peak was attributed to P 2p as a result of etching and functionalization. For all three types of samples, carbon contamination was present and verified due to the emergence of a peak centered at 284.8 eV.

The high-resolution regional scan of Ga 2p was used to determine the nature of the gallium species on the surface of the samples. The Ga 2p spectra is preferred over the Ga 3d spectra for high resolution scans for its lower kinetic energy of radiation, therefore providing higher surface sensitivity.[63] Casa XPS was used to analyze and fit the data. For all three samples, a peak was present and centered near 1118 eV which was attributed to the Ga-N bonding expected on the surface.[64] Each sample contained a species centered near 1116 eV which was due to Ga-Ga bonding near the surface.[65] The species present for each sample near 1119.75 eV was attributed to Ga_2O_3.[64] The existence of sub oxide species such as Ga_2O, GaO, GaOOH and GaO_2 can be verified by peaks found at 1118.5 eV.

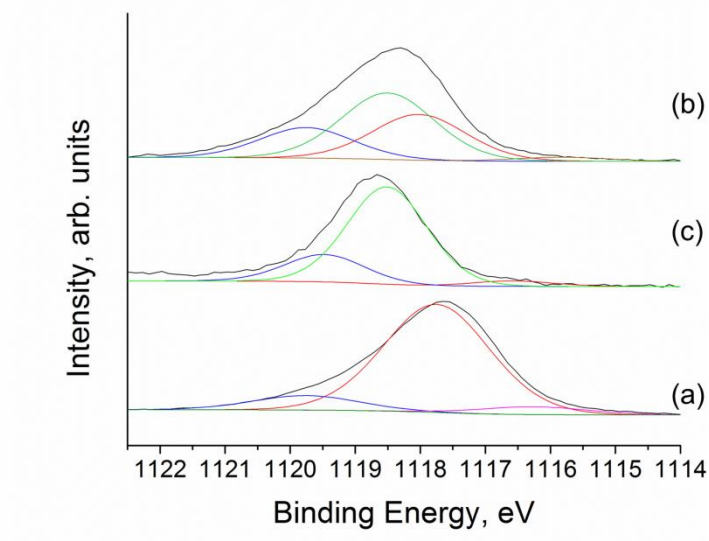

Figure 2.4. Ga 2p regional XPS spectra of (a) clean GaN powder, (b) clean, etched GaN powder, and (c) functionalized GaN powder.

The ratio of gallium species recorded in the spectra provided information about the nature of the gallium on the surface of the samples. In the clean GaN powder the presence of sub oxide species was not evident from the data. The percent area of Ga_2O_3 in the Ga 2p peak of the clean GaN powder was 11.43% and the percent area of Ga-N was 82.08%. In the etched only sample of GaN sub oxide species were a significant portion of the peak. The percent area of Ga_2O_3 was 20.12%, of sub oxides was 67.51% and of Ga-N was 8.69%. In the functionalized samples of GaN powder the percent area of Ga_2O_3 was 20.69%, of sub oxide species was 45.46% and of Ga-N was 31.11%. As expected, the etching process shows evidence of the production of oxide and sub oxide species in the GaN powder samples that were used.

The peak centered near 285 eV was attributed to C 1s and was used for calibration of the data in Casa XPS. The C 1s peak was analyzed and for each sample, and the existence of

two species contributing to this peak was evident. The species with the lowest binding energy was attributed to adventitious carbon and was calibrated to 284.8 eV.[66] The atmospheric contamination of samples with hydrocarbon molecules was evident due to the C 1s spectra. The presence of a species near 286 eV in the fitted peak can be contributed to the C-N bond present in the porphyrin.[63] Due to the powder nature of the samples, the ability to distinguish between peaks in this region was difficult.

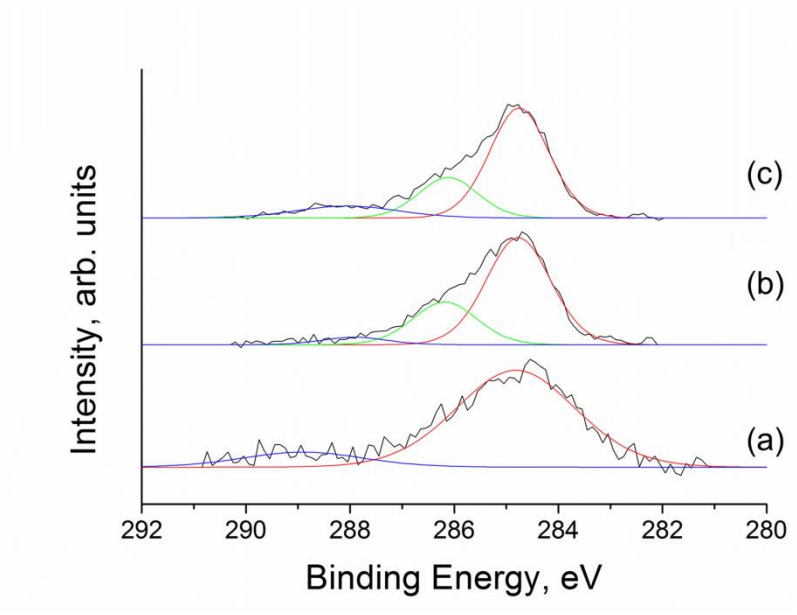

Figure 2.5. C 1s regional XPS spectra of (a) clean GaN powder, (b) clean, etched GaN powder, and (c) functionalized GaN powder.

Evidence of the phosphoric acid used for etching was gathered from the emergence of a P 2p peak centered near 135 eV. A high-resolution scan was performed to investigate whether this peak was only present in the samples that were etched. The functionalized sample would be expected to have a peak in this region both due to the phosphoric acid as well as the phosphonic groups that are present on the porphyrin molecule. As expected, the

clean GaN powder showed no peak in the P 2p high resolution scan and both the etched and functionalized powder samples exhibited peaks in this region.

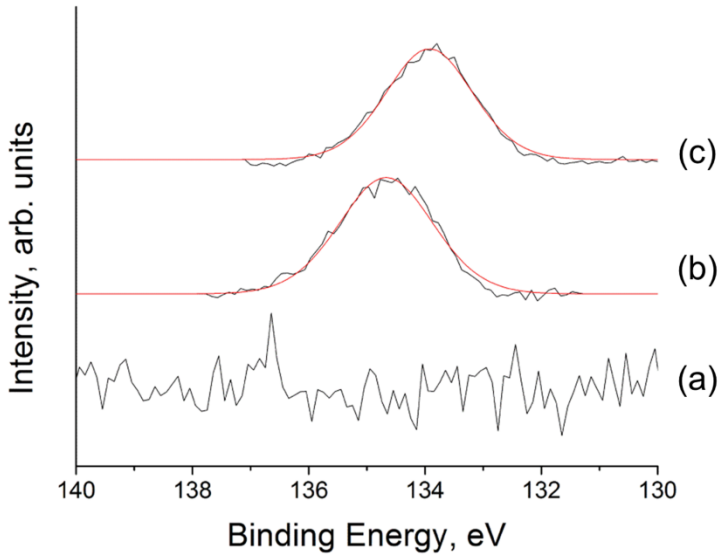

Figure 2.6. P 2p regional XPS spectra of (a) clean GaN powder, (b) clean, etch GaN powder, and (c) functionalized GaN powder.

The presence of a peak attributed to amine and amide groups can be deduced from analysis of N 1s spectra.[40] Macquet et al. investigated porphyrins without metal centers.[67] The expected value of the binding energies of the N 1s peaks was reported to be 400 and 398 eV. The calibration method used may account for differences in less than 1 eV. The N 1s peaks of thin film porphyrins were studied by Sarno et al.[68] The presence of a peak centered at around 400 eV for a porphyrin salt was reported by Silipigni et al.[62] All high-resolution data collected in the N 1s region of the functionalized samples showed evidence of charging. The etched and clean GaN powders both contained three species within the single N 1s peak, while the functionalized powder contained an additional peak at higher binding energy. The peak at this binding energy was attributed to a single species. For each sample, the N 1s peak

that is attributed to N-Ga bonding was used for calibration because it is present in all samples. This peak is present close to 397 eV and was calibrated to 397.3 eV to account for the charging.[58] The spectra of all three samples are shown in Figure 2.4. Due to the Al Kα source used with the XPS instrument, there was an overlap between the Auger peaks of the Ga and the N 1s peaks. The Ga Auger peaks (LMM 1 and LMM 2) were present at lower binding energy than the N-Ga peak for each sample, around 395.4 and 392.1 eV. The functionalized sample contained a species centered near 400.8 eV, which was not present in any of the other samples. The presence of the amine groups found on the TTP-PO_3 contributes to this peak and provides evidence that the GaN was successfully modified with the porphyrin derivative.

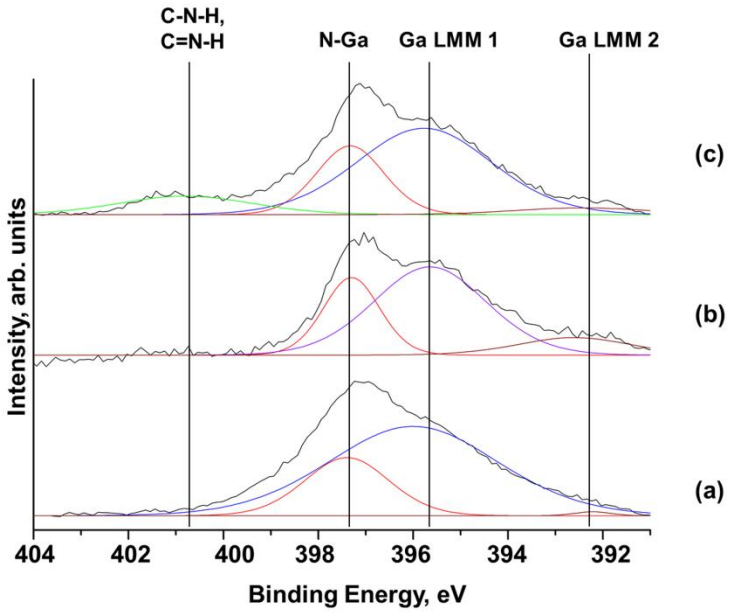

Figure 2.7. N 1s regional XPS spectra of (a) clean GaN powder, (b) clean etched GaN powder, and (c) functionalized GaN powder. Peak assignments are displayed with the peak near 400.8 eV present only in the functionalized powder.

2.5.2 Infrared Spectroscopy

FT-IR signatures of GaN powders have been studied by a number of research groups. For example, Baraton and Gonsalves investigated the infrared spectra of both aluminum and gallium nitride for nanostructured powders.[69] The synthesis of GaN nanowires was successfully accomplished by Wei and Shi, and evidence for this was gathered by FT-IR.[70] Shi and Xue obtained FT-IR spectra for the determination of suitable growth conditions for GaN nanowires.[71] This prior work has presented evidence of two strong peaks near 560 cm^{-1} and 610 cm^{-1}. The band at 560 cm^{-1} is attributed to the bond between gallium and nitrogen stretching in the material.[71]

Prior work on nanostructured GaN demonstrated high levels of uniformity and homogeneity. The samples in this study possess low homogeneity due the milling method utilized for their preparation. Xiao et al. examined GaN powders[72] and reported a broad peak located between 500 and 700 cm^{-1} and discussed its varied position following different treatment temperatures. A second, smaller peak was found near 1630 cm^{-1} that corresponded to GaN powder. A third, medium sized peak resided near 3410 or 3420 cm^{-1}, the location of which depended on experimental parameters. The complexities involved in determining specific peak assignments for GaN have been previously examined in the literature.[69] Additionally, a broad peak near 2100 cm^{-1} was assigned to Ga-H due to a nitrogen vacancy previously discussed by others.[73]

The two pellets with clean and functionalized powder were expected to show peaks consistent with the presence of GaN whereas the pellet with just the porphyrin powder was expected to show an absence of these peaks. Spectroscopic investigations into porphyrin

molecules by Ogoshi et al.[74] reported theoretically calculated FT-IR peaks and assigned them based on the stretching or bending modes of the molecules. Santiago et al. gathered FT-IR data between 1800 and 400 cm^{-1} for an iron porphyrin under various pH conditions.[75] The spectra contain various common species at expected wavenumbers including large peaks near 1650 cm^{-1} and 1000 cm^{-1}. The peak near 1000 cm^{-1} was attributed to the stretching mode the P-O bond. A peak present near 1650 cm^{-1} was attributed to the stretching modes of the bond between the ring structure carbons and nitrogen within the porphyrin.[74] Brennan et al. performed various spectroscopy techniques to compare functional groups for porphyrin attachment to TiO_2.[60] The FT-IR spectra that were obtained for the iron porphyrin under different pH environments showed the same peaks hear 1650 and 1000 cm^{-1}.

In all of our FT-IR characterization there was clearly evident peak broadening due to the non-homogeneity of the aggregates in the powder. A broad peak resided near 550 cm^{-1}. This peak is consistent with previously reported data that attributed its existence to the Ga-N bond stretching mode within the crystals.[71] A small, broad peak was evident near 2100 cm^{-1} as well, confirming GaN purity via stretching mode of hydrogen present in a nitrogen vacancy within the powder.[73] Figure 2.5 confirms the two characteristic peaks of GaN through the broad peak near 550 cm^{-1} and the small peak near 2100 cm^{-1} for cleaned GaN powder. The presence of porphyrin was seen with a peak residing near 1000 cm^{-1} present only on functionalized GaN powder. The peak at 1000 cm^{-1} is attributed to the P-O-H bonds.[60] Additionally, a peak present near 1450 cm^{-1}, attributed to the stretching of the C-N bond within the porphyrin ring, as well as a strong peak [74] near 1650 cm^{-1} for C=N stretching mode within the porphyrin ring were recorded.[75]

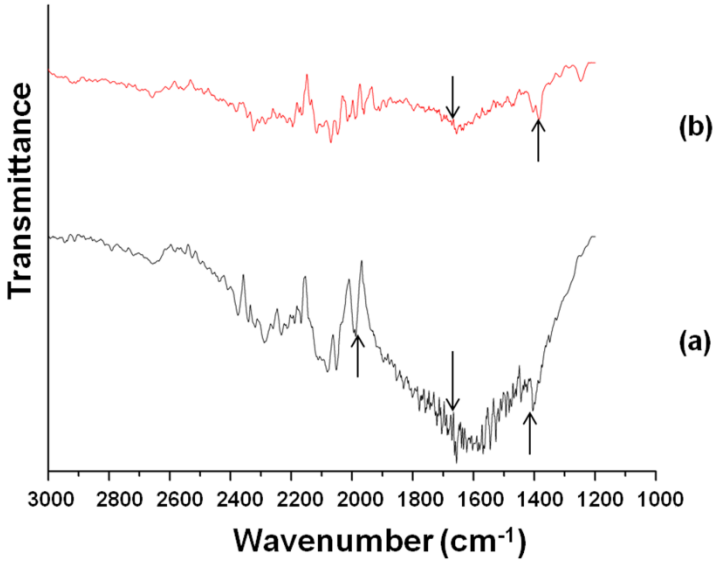

Figure 2.8. FTIR regional scan between 3000 and 1200 cm^{-1} of KBr mixed with (a) functionalized powder and (b) TTP-PO_3.

2.5.3 Stability Testing Using Fluorescence Spectroscopy

By utilizing a porphyrin adsorbate, the naturally strong fluorescent signal can be used to confirm successful functionalization both pre and post soaking following the *in situ* procedure. The fluorescence spectra of porphyrin molecules have been well studied in previous literature. Typically, porphyrin molecules possess distinct Soret bands near 430 nm as well as two Q-band peaks near 550 and 590 nm. [60] Emission peaks are expected near 620 and 670 nm as well. The spectral sweep used in this work started at 550 nm and moved to higher wavelengths, meaning the useful peaks which would be expected to be present and easily observed would be the emission peaks near 620 and 670 nm.

Typical fluorescence data gathered throughout our study is displayed in Figure 2.6. The 7.125 μM solution of TTP-PO_3 in DI water was used to provide a point of reference for

investigating the presence of the porphyrin in other solutions. In order to investigate and compare this to the fluorescence of the functionalized sample, it was mixed with DI water and sonicated in order to disperse the powder particles of the sample. The two spectra were compared and expected to possess the same signature peaks. The difference in concentration of the two solutions as well as the nature of the solution (loose modified GaN powder vs. dissolved porphyrin molecules) accounts for changes in intensity of the characteristic peaks. A small peak centered near 610 nm was seen in the shadow of an overwhelming peak at 690 nm for TTP-PO_3 in water. The spectrum of the sonicated solution of the modified GaN powder showed peaks in the expected positions supporting the notion of successful functionalization of the semiconductor surface.

A sample of the functionalized powder was left under ambient temperature and humidity in DI water for a period of 20 days to test for any possible porphyrin leaching in solution. The degree of stability was assessed by measuring the amount of any porphyrin dissolved in the water solution. We note that the powder exhibited the same characteristics shown in Figure 2.6 (b) even after the water soak. The soaking solution containing the functionalized powder was centrifuged in order to separate the particulates. Presence of leached TTP-PO_3 into solution would produce the characteristic porphyrin signature. The spectrum of the soaking solution shows no peaks at the expected wavelengths of 610 and 690 nm as seen in Figure 2.6 (c). The absence of these peaks supports the assessment that TTP-PO_3 did not desorb from the GaN surface and dissolve into the water solution. This, in turn, provides evidence that the binding between the porphyrin and GaN is stable for at least 20 days within an aqueous environment.

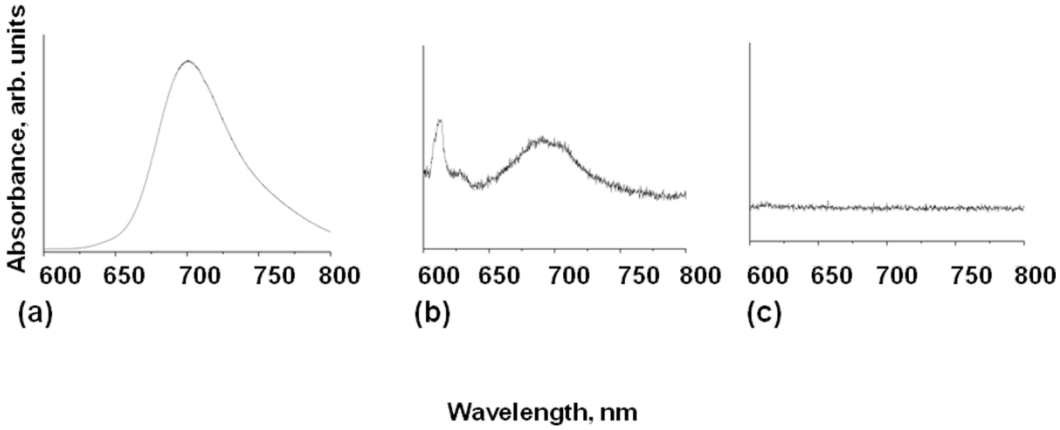

Figure 2.9. Fluorescence spectroscopy spectra of (a) 7.125 μM solution of TTP-PO_3 in DI water, (b) sonicated solution of functionalized powder in DI water, and (c) wash of functionalized powder in DI water after 20 days.

2.6 Conclusion

In conclusion, the attachment of a porphyrin derivative to GaN powder was performed using an *in-situ* functionalization procedure. XPS analysis confirmed the existence of amine groups on the modified GaN powder. The presence of C-N and C=N peaks in the FT-IR spectrum of the functionalized powder provided further evidence for the attachment of the porphyrin to the semiconductor surface. The stability of the bound porphyrin to the GaN interface was tested for a period of 20 days in water solution. No desorbed porphyrin was detected after the soaking period. We attribute this stability in solution to the covalent attachment of the porphyrin to the GaN powder surface. Future studies will focus on additional porphyrin derivatives containing metal centers due to their potential to enhance the optoelectronic properties of GaN.

3. *In-situ* and *Ex-situ* Functionalization of Nanostructured Gallium Oxyhydroxide with a Porphyrin Dye

Brady L. Pearce,[1] Nora G. Berg,[1] Matthew S. Rahn,[2] Albena Ivanisevic[1]*

[1]Department of Materials Science and Engineering, North Carolina State University, Raleigh, North Carolina, 27695, USA

[2]Department of Materials Science and Engineering, Pennsylvania State University, State College, Pennsylvania, 16801, USA

3.1 Abstract

The surface attachment of a porphyrin dye to nanocrystalline GaOOH was performed using two routes of solution based functionalization. The first method of functionalization utilized an *in-situ* incorporation of dissolved porphyrin salt in solution during the microwave synthesis step. Additionally, synthesized GaOOH nanorods were mixed in porphyrin solution after the microwave process to make an *ex-situ* GaOOH/TTP-PO_3. X-Ray Photoelectron Spectroscopy confirmed the presence of expected surface species and provided evidence of increased surface coverage of TTP-PO_3 on GaOOH in the *ex-situ* GaOOH/TTP-PO_3 as compared to the *in-situ* one. Size and morphology changes were investigated using SEM and, along with analysis of XRD, the *in-situ* samples showed larger crystallite sizes. This was confirmed with PL due to the higher bandgap energy evident in the *ex-situ* GaOOH/TTP-PO_3 compared to the *in-situ* sample. A stability study was performed using Fluorescence Spectroscopy which indicated no leaching of porphyrin from the *in-situ* GaOOH/TTP-PO_3. However, porphyrin leaching was evident from the *ex-situ* GaOOH/TTP-

PO_3 sample. The stability of the *in-situ* GaOOH/TTP-PO_3 makes it attractive for a number of interfacial applications.

3.2 Introduction

The use of wide bandgap semiconductor materials as optoelectronic platforms for attaching functional organic molecules shows great promise for various applications ranging from biomedical to green energy.[76] Gallium oxyhydroxide (GaOOH) is an inorganic material with a bandgap of 4.75 eV. GaOOH is of particular interest for semiconductor research due to its nature as a precursor for both gallium oxide[13] (Ga_2O_3) and gallium nitride (GaN).[14] Performing solution based functionalization of GaOOH with phosphonic side group containing molecules is inherently simple due to the surface oxide layers present in the material. The surface attachment of dye molecules to wide bandgap semiconductors can potentially find applications in solar cell research including dye-sensitized solar cells (DSSCs)[26] as well as imaging and biosensing. A substantial amount of research has focused on the use of several wide bandgap materials such as TiO_2[21] and ZnO.[77] There is a need for exploring alternative wide bandgap semiconductors with higher electron mobility than TiO_2[26] and better interfacial stability than ZnO.[78]

Nanostructured materials are especially attractive for surface functionalization due to the high surface area available for the immobilization of organic molecules.[21] The high surface area to volume ratio also is useful in enabling high photocatalytic activity of the nanostructured material.[79] Ga_2O_3 nanowires have been functionalized for sensing atmospheric hydrocarbons.[80] Nanoribbons of β-Ga_2O_3 with various adsorbed organics were studied to determine surface coverage and hydrogen bonding effects on surface binding.[81]

The functionalization of Ga_2O_3 nanowires with pyruvic acid was studied for capacitance-based gas sensing.[82]

The fabrication of GaOOH nanostructures has been investigated using various methods and precursor materials. Using gallium nitrate ($Ga(NO_3)_3$) and various additives, a microwave-assisted method has been used to form GaOOH nanorods,[83] along with a hydrolysis method in the presence of lanthanide ions[84] and a calcination reaction with sodium carbonate.[85] $Ga(NO_3)_3$ was also utilized with a sodium hydroxide (NaOH) titration and hydrothermal treatment to form GaOOH nanostructures,[86] with a sodium doceyl benzene sulfonate surfactant[87] and in the presence of no surfactant.[88] Hydrothermal treatment of $GaCl_3$ in the presence of urea was performed to make various nanostructured GaOOH crystals with diamond-like cross sections[89] and ultrasound radiation sonication on $GaCl_3$[90] in a benzene saturated solution[91] produced GaOOH nanostructures. The growth of α-GaOOH as well as iron oxyhydroxide in various concentrations using an alkaline precipitation reaction has been reported.[92] A high pressure phase, β-GaOOH, was synthesized using a high-pressure chamber.[93] The synthesis of GaOOH nanorods from ball-milled GaN powders was done to make GaOOH particles ranging in size from 10 to 80 nm.[94] Room temperature synthesis of GaOOH nanostructures was accomplished by Kisailus et al.[95] To the best of knowledge, no prior studies have attempted to modify the nanostructured inorganic material with organic adsorbates in solution.

In this study we report the synthesis and surface attachment of GaOOH nanorods with a porphyrin dye using two methods: an *in-situ* route and an *ex-situ* process where the nanostructures were submerged in porphyrin solution after synthesis. The use of subsequent

characterization techniques provided a comparison between the two functionalization methods. The microwave synthesis technique[96] was chosen due to the ease of preparation using solutions with just DI water and the reactants. X-Ray Diffraction (XRD) scans were evaluated to assess the crystallinity of the product after various processing techniques. The morphological properties of the nanostructures were investigated using Scanning Electron Microscopy (SEM). Photoluminescence (PL) Spectroscopy was used to investigate the effect of the presence of the dye on the luminescent properties of GaOOH. The properties of the interface between the dye and semiconductor were investigated with XPS and the stability of the functionalized nanostructured materials was tested using Fluorescence Spectroscopy.

3.3 Materials and Methods

3.3.1 Microwave Synthesis and Functionalization

The gallium nitrate hydrate powder and sodium hydroxide were obtained from Sigma Aldrich. Solutions of 0.1 M $Ga(NO_3)_3$ and 5 M NaOH were made with deionized (DI) water (18.2 MΩ*cm). The NaOH solution was added drop wise to the $Ga(NO_3)_3$ solution until a pH of 8 was reached. The resultant solution was placed in a CEM Discover LabMate microwave reaction vessel. The instrument was set to a maximum power of 200 W, the temperature was set to 120˚C and the reaction was programmed to run for 20 minutes. Prior to being left overnight to dry in an oven, the samples were washed with DI water and filtered. One sample was placed in the oven without performing the DI wash or filtration step.

The *in-situ* GaOOH/TTP-PO_3 samples were synthesized using the same procedure except the $Ga(NO_3)_3$ was added to a solution of 7.125 µM meso-tetra(4-phosphonomethylpheny) porphine tetrasodium (TTP-PO_3) salt (Frontier Scientific) in DI

water before the drop wise titration with NaOH. To produce the *ex-situ* GaOOH/TTP-PO_3, some of the filtered GaOOH product was added to a solution of 7.125 µM TTP-PO_3 in a centrifuge tube and left mixing on a rocking platform for 24 hours. The resulting product was washed with DI water and filtered and left to dry overnight in a dessicator.

3.3.2 Characterization

The SEM used was a FEI Verios 460L Field Emission SEM. The detector on the instrument was a concentric higher energy electron detector for each of the images taken. The clean GaOOH sample was imaged at a working distance of 6.1 mm with a stage bias of 1500 V. The current was set to 50 pA and the voltage was 2.00 kV. The *ex-situ* GaOOH/TTP-PO_3 was imaged at a working distance of 7.0 mm with a stage bias of 1200 V. The current was set to 0.20 nA with a voltage of 2.00 kV. The *ex-situ* GaOOH/TTP-PO_3 was imaged at a working distance of 6.8 mm with a stage bias of 1300 V. The current was set to 50 pA and the voltage was 2.00 kV.

XRD analysis was done using a Rigaku SmartLab X-Ray Diffractometer. A Cu Kα x-ray source was used with a voltage of 40 kV and a current of 44 mA. The powder diffraction was done with Bragg-Brentano optics. All scans were collected from 2 of 10 degrees to 80 degrees. A step size of 0.05 degrees was utilized for a scan time of 2 seconds and a resolution of 0.0002.

The PL data was obtained to determine the optical properties of each sample submersed in DI water in quartz cuvettes. A homemade optical bench top setup with a 193 nm Coherent Xantos XS Argon Fluoride Eximer laser was used to excite the samples. Various lenses were utilized and aligned to collimate and focus the beam onto the samples.

The samples contained in the quartz cuvettes were mounted on the optical table. A UV enhanced CCD connected to a fiber optic cable was used as a detector to collect data. Analysis and acquisition of the data was performed using LightField software, manufactured by Princeton Instruments. The data was normalized and analyzed using Orgin 9.0 to determine peak positions.

The XPS data was obtained with a Kratos Analytical Axis Ultra XPS. A monochromated Al Kα (energy of 1486.7 eV) X-ray source was employed in all characterization with a 2.0 A filament charge neutralizer in order to reduce the effects of charging. The sample chamber pressure was maintained at 3.0×10^{-8} Torr. All samples were mounted to an aluminum sliding sample holder with double sided copper tape. A survey scan was collected for each of the samples with a pass energy of 160 eV. High resolution regional scans of C 1s, O 1s, Na 1s, P 2p, Ga 2p, Ga 3d and N 1s were obtained with a pass energy of 20 eV. Casa XPS Version 2.3.12.8 was utilized to fit the peaks and determine atomic percentages of each sample from the survey scans. Background subtraction was done using a Shirely approximation and all peaks were calibrated by setting the adventitious carbon C 1s peak to 284.8 eV. The full width at half-maximum of the deconvoluted peaks was constrained to the primary peaks using a Lorentzian fit.

The fluorescence stability data was taken on a home-built system with a 455 nm excitation wavelength. The intensity of the LED was set to 100 %. All of the data obtained was plotted and analyzed with Origin 9.0.

3.4. Results and Discussion

3.4.1 Synthesis and Functionalization with Porphyrin Dye

The method of using microwave synthesis[96] to produce GaOOH nanorods was chosen over an autoclave technique[97] due to the ease of preparation with DI water as the only solvent. The porphyrin dye TTP-PO_3 was chosen for functionalization because of its water solubility as well as the assumption that the phosphonic groups provided a means of attachment to surface oxides for increased stability. The possible mechanism of GaOOH nanorod formation from Ga^{3+} ions in the presence of water has been explored. There exist many possible chemical routes for GaOOH nanorod synthesis, dependent on the precursor ion, as well as a mechanism which relies on metallic Ga.[90] The following reaction was described by Avivi et al.[90]

$$Ga^{3+} + 2\ H_2O \leftrightarrow GaOOH + 3\ H^+$$

The synthesized GaOOH material was white with a flake like consistency following the filtration and drying process. The SEM image of the clean GaOOH is displayed in Figure 3.1(a). The GaOOH is heterogeneous in nature with both nanorod like features as well as other nanocrystallite particles. The nanocrystallite and nanorod structures varied in size with the lengths of the nanorods being from around 40 nm to as large as 100 nm. The nanorods that were formed did not seem to have a preferred direction and were randomly ordered in the sample.

The surface modification of semiconductor surfaces with a sensitizing agent such as a porphyrin dye has many applications in biosensing and optoelectronic devices. Investigating the surface interaction between the two molecules provides insight into the environmental

stability and the effect of the functionalization on the properties of the semiconductor. The use of porphyrin as a sensitizing agent for semiconductors was explored by Brennan et al.[60] Porphyrin dye was used to produce a DSSC with TiO_2 with a conversion efficiency of 3%.[59] In previous work with solution based functionalization on GaN, an etchant was required to produce a controlled oxide layer for phosphonic group attachment.[1] A particular advantage of the sensitization of GaOOH is the native presence of this oxide layer so no additional and harmful etchant is required to attach a soluble dye to the semiconductor surface.

The inclusion of TTP-PO_3 with the GaOOH nanorods in this work was done through two different methods to compare and contrast the various property modifications that occurred. The first functionalization method that was followed was a simple soaking procedure after the microwave synthesis of the nanostructured GaOOH. This sample is referred to as *ex-situ* due to it being processed outside of the original reaction. The samples were filtered to remove any unreacted nitrate then left rocking overnight in a solution of DI water and porphyrin. The native oxide layer present on the GaOOH provided a means of attachment for the phosphonic groups on the porphyrin dye. The resulting solid solution was filtered and dried and after this was a vibrant green color (Figure 2).

SEM images of the *ex-situ* GaOOH/TTP-PO_3 samples were inspected to determine the effects of the functionalization on the structure. The image obtained is displayed in Figure 1(b). These samples had the same nanorod and nanocrystallite structures as well as similar length distributions as the original, clean GaOOH. The SEM image provides evidence that the *ex-situ* functionalization process has no effect on the size and shape of the

nanocrystallites, suggesting a simple adsorption of the TTP-PO_3 onto the GaOOH nanocrystalites.

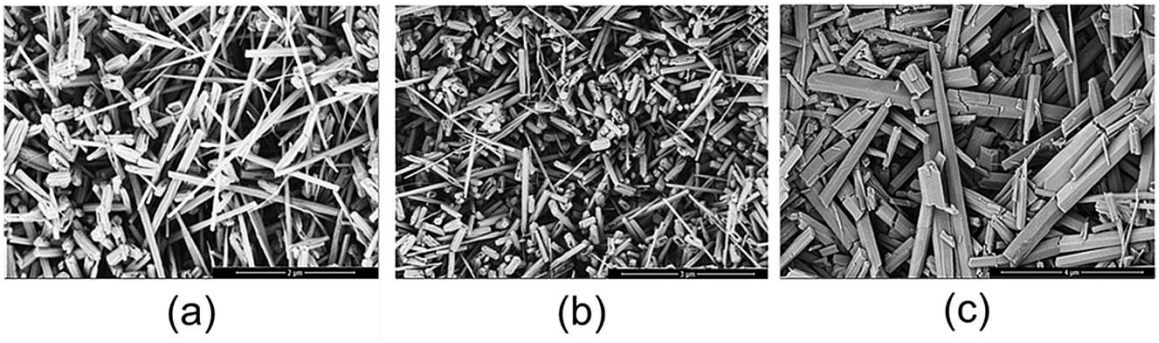

Figure 3.1. SEM images of (a) clean GaOOH nanorods, (b) *ex-situ* GaOOH/TTP-PO_3 and (c) *in-situ* GaOOH-TTP/PO_3.

In order to facilitate an even simpler, faster and more environmentally friendly approach, the second method was a one-step solution based *in-situ* functionalization and synthesis. Along with the precursor materials $Ga(NO_3)_3$ and NaOH, the TTP-PO_3 was added to the reaction mixture. The remaining solid product from the microwave process was washed with DI water, filtered and dried overnight. The solid was a pale yellow color and resembled the flake like structure of the clean GaOOH. The following is a modification of the original chemical equation to account for the presence of porphyrin.

$$Ga^{3+} + 2\ H_2O + \text{TTP-}PO_3 \leftrightarrow \text{GaOOH/TTP-}PO_3 + 3\ H^+$$

An SEM image was obtained to explore the effect the presence of TTP-PO_3 had on the size and structure of the nanocrystallites. The rods formed during the *in-situ* process were noticeably larger than the clean GaOOH, with lengths that ranged from 40 to 400 nm. The shapes and sizes were heterogeneous in nature with the general rod-like shape remaining

fairly consistent among the particles. As in the other two samples, no preferred orientation is evident in the rod structures.

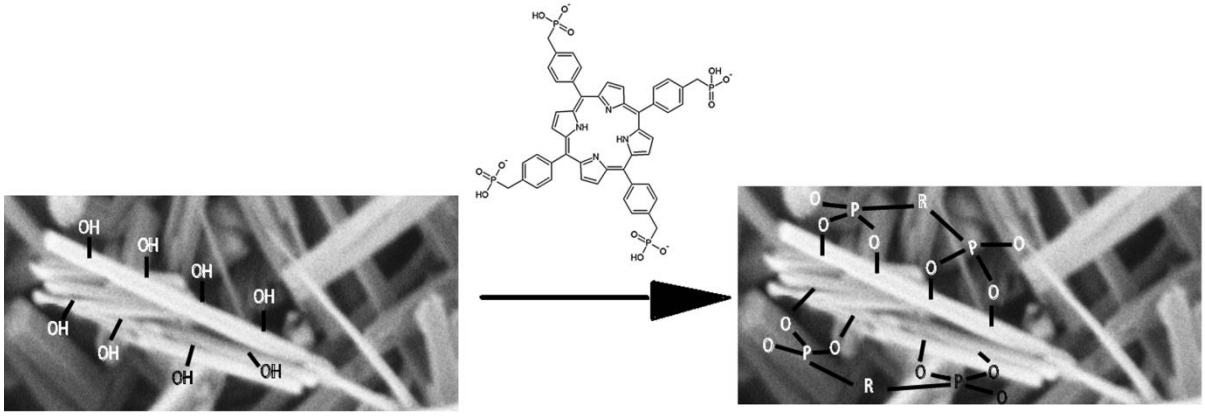

Figure 3.2. Scheme depicting the covalent interaction between TTP-PO_3 and the GaOOH nanorods pictured in the SEM image.

All three samples were used for XRD and XPS measurements and then submerged in DI water for various other measurements. The flake-like powders displayed varying degrees of color, which was especially evident in the DI water solution. Figure 3.2 shows all three of the samples with a safety laboratory glove as a background. The clean GaOOH was a bright white color with a lack of any other colors present in the sample. The *in-situ* GaOOH/TTP-PO_3 sample was a pale yellow color and the *ex-situ* GaOOH/TTP-PO_3 sample was a bright, vibrant green color which is visible in the image. The difference in coloration of the two functionalized samples suggests an increase in the amount of porphyrin on the surface of the *ex-situ* sample when compared to the *in-situ* sample.

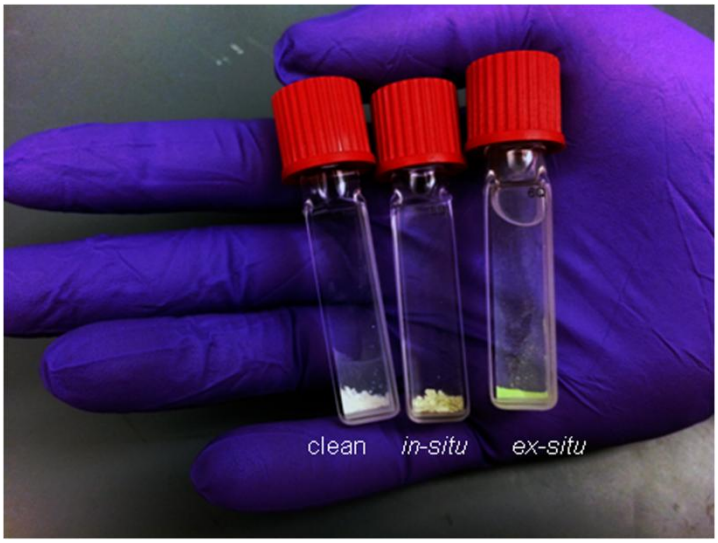

Figure 3.3. Optical photograph of the clean GaOOH, *in-situ* and *ex-situ* GaOOH/TTP-PO_3 submerged in DI water in quartz cuvettes.

3.4.2 Crystallographic Characterization with XRD

In order to investigate the crystalline qualities of the product formed and any effect either method of functionalization had on it, XRD spectra were obtained. The samples used were packed on a glass slide and analyzed using Bragg-Brentano powder diffraction. Differences in peak intensities for various crystallographic orientations were attributed to the heterogeneity of each sample. The original product was left unfiltered to probe for the presence of leftover nitrate. This sample was then filtered and an XRD spectrum was obtained to ensure that the process removed any unreacted precursor $Ga(NO_3)_3$ or NaOH. Beyond the discussion of the XRD data any mention of clean GaOOH refers to this filtered sample.

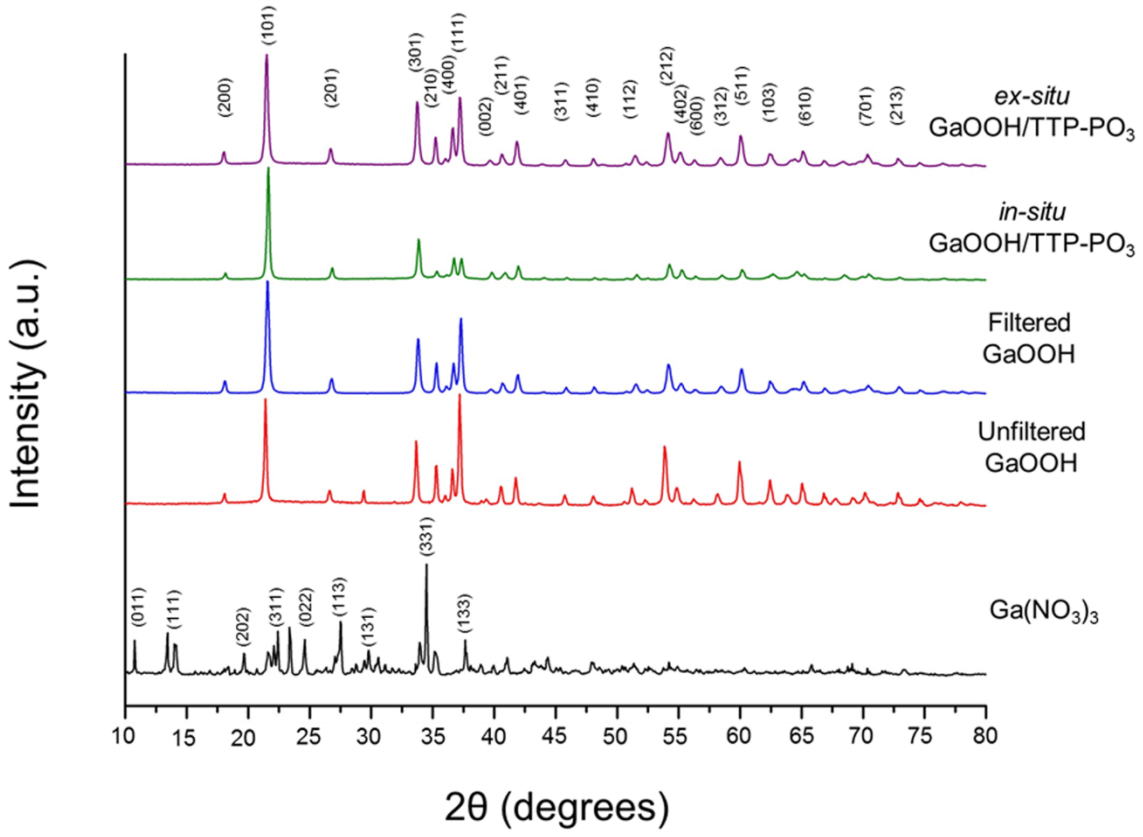

Figure 3.4. XRD spectra of the various GaOOH containing samples along with the $Ga(NO_3)_3$ precursor material. Assignments were made to peaks based on crystallographic orientation.

The Scherrer equation can be used to measure submicron grain sizes with XRD patterns. Materials with a high level of defects have a large number of other factors which lead to peak broadening; however it is reasonable to use the Scherrer equation to qualitatively compare average crystallite size of different materials. Although the discussion in this study will be limited to a qualitative comparison, it is important to note that line broadening is a function of both sample broadening and instrumental broadening. The crystallite sizes measured will still contain instrumental effects and are, again, only used as a method of

qualitatively comparing the two sizes. Based on previous results with this microwave method, the grain sizes expected will be in the submicron range. It is of interest, then, to investigate the broadening of the X-ray peaks found in the XRD patterns for each sample measured. The equation used in determining submicron crystallite size with XRD peak broadening is[98]

$$D = \frac{K\lambda}{B\cos\theta}$$

where λ is the wavelength of radiation (for Cu Kα, λ = 1.540562 Å), K is a constant (estimated to be 0.9), θ is the diffraction angle, D is diameter of the crystallites and B is the full width at half-maximum (FWHM) of the diffraction peak.

The XRD patterns of unfiltered and filtered GaOOH, *in-situ* and *ex-situ* GaOOH/TTP-PO_3 and the precursor material $Ga(NO_3)_3$ are shown in Figure 3.4. All spectra were normalized to the (101) peak except $Ga(NO_3)_3$ which was normalized to the (331) peak. Both the *ex-situ* and *in-situ* XRD patterns matched with a previously reported spectrum of GaOOH.[99] Peak assignments were made based on crystallographic orientation. The spectrum of the precursor material also matched with a previously reported spectrum of $Ga(NO_3)_3$.[100] Evidence of unreacted nitrate was present in the spectrum of the unfiltered GaOOH. After filtration, the spectrum was indicative of the removal of any unreacted nitrate with the apparent removal of the (131) peak of the nitrate.

The FWHM for the most distinct peaks in the three materials containing GaOOH nanocrystallites was selected to calculate crystallite size. The peak for the (hkl) of (101) is the most intense for each sample and the peak at (301) is the second or third most intense,

based on the sample. It would be of interest to use three peaks for the Scherrer equation to determine crystallite size; however the spectrum of the three samples does not contain a reasonable third peak to measure. The calculated crystallite size is meant to be qualitative in nature and used only as a means to compare sizes between samples, making the lack of a third peak inconsequential.

Table 3.1 displays the calculated FWHM and crystallite sizes for the clean, filtered GaOOH and the *in-situ* and *ex-situ* GaOOH/TTP-PO_3 samples. The qualitative crystallite size of clean GaOOH and *ex-situ* GaOOH/TTP-PO_3 were within 1 nm for each peak and the average values were within 0.1 nm of each other. The process of introducing the GaOOH sample to a porphyrin solution and rocking it overnight seems to have little to no effect on the size of the crystallites. This confirms the theory that the porphyrin is only surface bound on the *ex-situ* GaOOH/TTP-PO_3 samples with little bulk interaction to the nanostructured GaOOH. The qualitative crystallite size of the *in-situ* GaOOH/TTP-PO_3 was found to be the highest of the three samples, with the average size being over 4 nm larger than the other samples.

Table 3.1. FWHM of the peaks used and the qualitative crystallite sizes calculated from them.

	FWHM of (101) (radians)	**Qualitative Crystallite Size (nm)**	**FWHM of (301) (radians)**	**Qualitative Crystallite Size (nm)**	**Average Qualitative Crystal Size (nm)**
clean GaOOH	0.00512	27.6	0.00499	29.0	28.3
ex-situ GaOOH/TTP-PO_3	0.00499	28.3	0.00515	28.1	28.2
in-situ GaOOH/TTP-PO_3	0.00415	34.0	0.00460	31.5	32.8

3.4.3 Optical Properties

Photoluminescence (PL) Spectroscopy is especially useful when characterizing semiconductors functionalized for optoelectronic applications. The attachment of an optically active molecule, such as a porphyrin, to a semiconductor platform enhances the luminescent properties and allows for tunability of optoelectronic properties of the semiconductor. The use of PL in this experiment provides two specific pieces of information for the synthesized samples. One is the effect of the incorporation of the TTP-PO_3 on the surface or within the GaOOH nanostructures on the PL properties. Any peak shifting or changes in peak shape will provide evidence of the changes in PL properties that occur when the surface properties are altered due to molecular attachment. Second, any peak shifting to different energy levels can be compared to the XRD data which qualitatively provided a comparison of crystallite sizes of the various materials. A blue-shift is known to be indicative of smaller crystallite sizes in PL due to the increase in bandgap. The shift in PL for GaN nanowires compared to bulk samples has been previously reported.[101]

Figure 3.5 shows the PL spectra of the clean GaOOH, the *ex-situ* and *in-situ* GaOOH/TTP-PO_3 and a dilute TTP-PO_3 solution. All spectra were normalized to the peaks with highest intensity. Previous work with PL of GaOOH nanostructures indicated a peak at 367 nm.[102] The dilute TTP-PO_3 solution and the clean GaOOH were used as reference spectra to investigate the effects of the crystallite sizes and the incorporation of the dye on peak position. Peaks found at integral multiples of 193 nm are attributed to the laser, and in some cases this affected the shape of the characteristic peak of the material. Two intense

peaks near 650 and 705 nm in the TTP-PO_3 spectrum, a peak near 300 nm and a broad peak centered around 440 nm were observed. The intense peaks are consistent with the peak found using fluorescence spectroscopy, however the increased sensitivity of the PL detector allowed for the detection of two peaks as opposed to one large, broader peak. The spectrum of clean GaOOH contained a peak centered near 320 nm with a large shoulder consistent with the presence of defects in the material.[103] The close proximity of the GaOOH peak at 320 nm and the TTP-PO_3 peak at 300 nm is indicative of the ability to tailor optical properties of GaOOH with the porphyrin material.

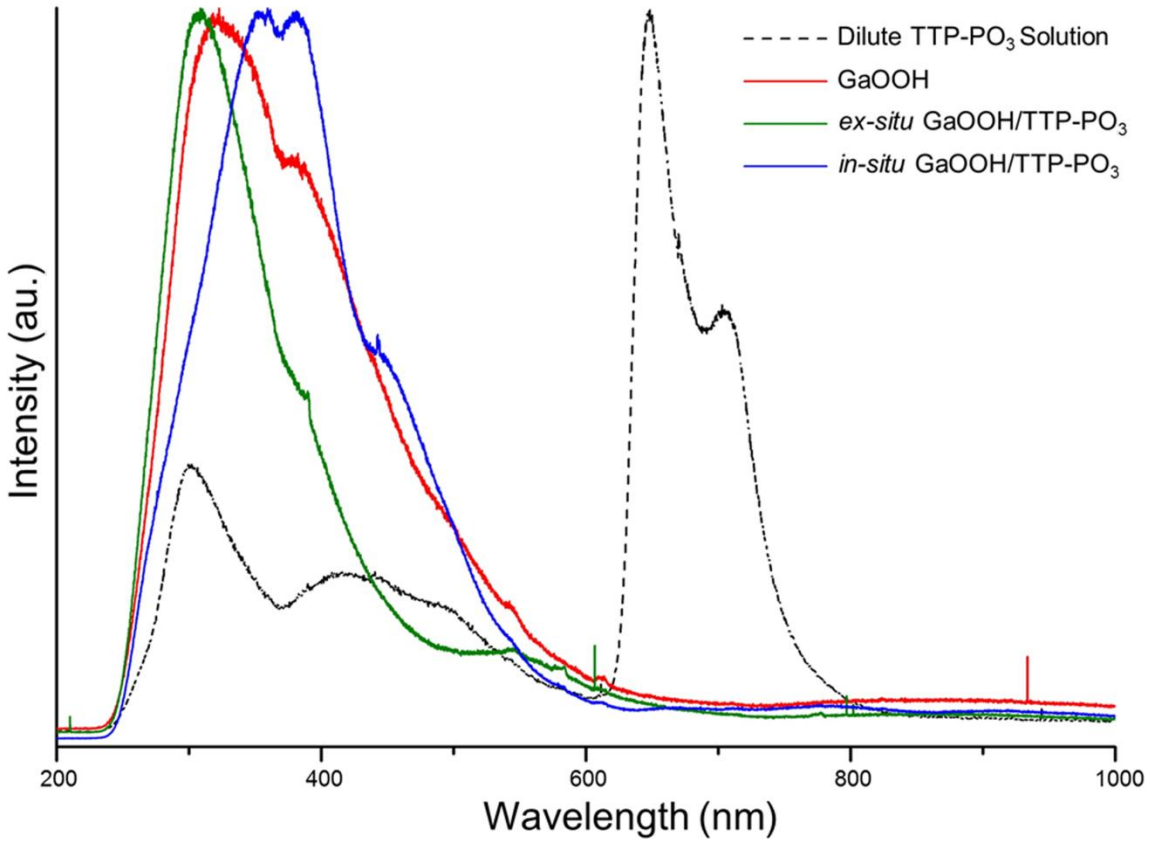

Figure 3.5. PL spectra of the dilute TTP-PO_3 solution, clean GaOOH, and the *ex situ* and *in situ* GaOOH/TTP-PO_3.

The spectra of the *in-situ* and *ex-situ* GaOOH/TTP-PO_3 materials provided information about the effect of porphyrin incorporation as well as crystallite size on the optoelectronic properties of GaOOH. SEM images and qualitative crystallite sizes calculated from the XRD data suggested that the *in-situ* GaOOH/TTP-PO_3 contained crystallites which were larger in size than the *ex-situ* GaOOH/TTP-PO_3. The *ex-situ* GaOOH/TTP-PO_3 contained a peak centered near 308 nm while the *in-situ* GaOOH/TTP-PO_3 had a peak centered near 366 nm. This significant blue-shift is consistent with the smaller crystallite size of the *ex-situ* GaOOH/TTP-PO_3 sample due to the higher band gap that is seen as crystallite size decreases in submicron materials. The shouldering in the *in-situ* GaOOH/TTP-PO_3 suggests the presence of a smaller peak near the 300 nm expected wavelength of TTP-PO_3.

The peak in the *ex-situ* GaOOH/TTP-PO_3 also blue-shifted from the clean GaOOH, although the reasoning for this is likely not crystallite size related since the SEM and XRD data suggested that both the samples had similar size distributions. The shift in the *ex-situ* GaOOH/TTP-PO_3 is instead likely due to the presence of the porphyrin and suggests the tunability of the optical properties with the use of this functional molecule. The effect of adsorbate attachment on the photoluminescence properties has been extensively reviewed and summarized in a review paper by Seker et al.[104] Hsu et al. demonstrated the shift of the position of the maximum peak from PL spectra of GaN nanowires due to silane attachment.[105] The emission peak lies in between the peaks seen near 320 nm for clean GaOOH and 300 nm for TTP-PO_3 in solution. When compared to the emission of the clean GaOOH, the *ex-situ* peaks contain significantly less shouldering as well. These observed

trends are likely due to the overlap of the bands of GaOOH and TTP-PO_3 giving it added intensity centered between the two characteristic peaks of these materials.

3.4.4 Surface Characterization by X-Ray Photoelectron Spectroscopy

The use of XPS provided a surface sensitive technique to explore the attachment of TTP-PO_3 to the GaOOH nanorods, the nature of oxide species on the surface of GaOOH and the effect of the different processing techniques. XPS of GaOOH nanoparticles[106] and nano-spindles[107] has provided information about the surface species present on this type of material. Survey scans were obtained to investigate the elements present on each of the sample surfaces and high resolution regional scans were used to determine the nature of different types of bonding on each sample. Quantitatively, the overall atomic percentages of each element were determined with the survey scans and the N 1s and O 1s regional scans were fitted to determine the percent contribution of each species. The high resolution C 1s spectra provided information about the nature of carbon species on the surfaces of the samples and all spectra were calibrated by setting adventitious carbon to 284.8 eV.[66]

The samples that were measured using XPS included the precursor $Ga(NO_3)_3$ material, the clean GaOOH, *ex-situ* and *in-situ* GaOOH/TTP-PO_3 and the TTP-PO_3 salt. In the survey scan of the $Ga(NO_3)_3$ a peak was present near 284 eV which is attributed to C 1s. Other peaks present were located near 398, 532 and 1118 eV attributed to N 1s, O 1s and Ga 2p, respectively. The clean GaOOH, *ex-situ* GaOOH/TTP-PO_3 and *in-situ* GaOOH/TTP-PO_3 survey scans contained similar peaks attributed to C 1s, N 1s, O 1s and Ga 2p. In the survey scan of the TTP-PO_3 salt peaks were present near 133, 284, 398, 532 and 1072 eV corresponding to P 2p, C 1s, N 1s, O 1s and Na 1s, respectively. Various other peaks were

present in the survey scans including Auger and other orbital level peaks; however the C 1s, N 1s, O 1s, Ga 2p, P 2p and Na 1s peaks were used to identify the percentage of atomic species for each of the samples.

Table 3.2 shows the atomic percentages of all elements present on the surface of each of the samples. The TTP-PO_3 salt contained a small amount of Na and P which were not present in any other samples. Theoretically, the stoichiometric ratio of the TTP-PO_3 salt is $C_{48}H_{38}N_4Na_4O_{12}P_4$. The absence of an appreciable P peak in the functionalized samples is attributed to the small atomic percentage of P in the TTP-PO_3 material, which is assumed to exist as a small surface layer or in small percentages incorporated in the GaOOH. The high atomic percentage of C in the *ex-situ* GaOOH/TTP-PO_3 is attributed to the porphyrin being present in high concentrations, solely on the surface, as opposed to the low atomic percentage of C in the *in-situ* GaOOH/TTP-PO_3 where the porphyrin had the opportunity to incorporate within the nanocrystallites formed during the microwave process. Further evidence of the surface coverage of the *ex-situ* sample is found in the increased ratio of oxygen to gallium in these samples. A significant amount of the nitrogen content is attributed to unreacted nitrogen from the precursor material and was not used for comparing surface content of porphyrin.

Table 3.2. Atomic percentages of C, O, N, Ga, Na and P of the precursor $Ga(NO_3)_3$, the TTP-PO_3 salt, clean GaOOH and *in-situ* and *ex-situ* GaOOH/TTP-PO_3.

	C	**O**	**N**	**Ga**	**Na**	**P**
$Ga(NO_3)_3$	53.4±4.0	32.9±2.4	11.5±1.3	2.25±0.44	-	-
TTP-PO_3 Salt	75.5±1.4	17.18±0.21	1.60±0.11	-	4.25±0.91	1.48±0.22
GaOOH	31.5±2.0	25.5±7.5	29.2±4.9	13.73±0.69	-	-
in-situ GaOOH/TTP-PO_3	13.1±1.7	32.45±0.92	34.82±0.46	19.55±0.46	-	-
ex-situ GaOOH/TTP-PO_3	66.5±1.5	19.04±0.13	9.20±0.81	5.31±0.72	-	-

The ratio of specific surface atomic species to one another provided another means of investigating the nature of the sample surfaces. Table 3.3 shows the ratios of O to Ga, C to Ga and N to Ga for the precursor $Ga(NO_3)_3$, the clean GaOOH and the *in-situ* and *ex-situ* GaOOH/TTP-PO_3. The $Ga(NO_3)_3$ precursor had the highest O to Ga ratio, which is expected since the material is a hydrate powder. The *ex-situ* GaOOH/TTP-PO_3 had the highest O to Ga ratio of the synthesized products which is evidence of an increase in the presence of TTP-PO_3 on the surface when compared to the *in-situ* GaOOH/TTP-PO_3. The C to Ga ratio was also the highest for the *ex-situ* GaOOH/TTP-PO_3 in all of the synthesized materials which is further evidence of increased TTP-PO_3 surface coverage on these samples. The N to Ga ratios remained relatively consistent throughout the synthesized samples.

Table 3.3. Atomic ratios of O to Ga, C to Ga and N to Ga for the precursor $Ga(NO_3)_3$, clean GaOOH and *in-situ* and *ex-situ* GaOOH/TTP-PO_3

	O/Ga	**C/Ga**	**N/Ga**
$Ga(NO_3)_3$	15.5±2.3	14.2±8.2	5.34±0.57
GaOOH	2.294±0.038	1.10±0.64	2.11±0.25
in-situ GaOOH/TTP-PO_3	1.661±0.083	0.677±0.095	1.782±0.033
ex-situ GaOOH/TTP-PO_3	3.71±0.45	13.0±1.9	1.77±0.19

The high-resolution regional scans provided information regarding the nature of the atomic species present on the surface of the samples. All spectra were normalized to the peaks with highest intensity. Figure 3.6 shows the N 1s, O 1s, C 1s and Ga 2p spectra of the various samples. By fitting the peaks to determine the spectral composition of the regions, conclusions can be made as to what species are present on each sample. The N 1s and O 1s spectra provided evidence of the presence of porphyrin on the surface of the functionalized species as well as the N 1s spectra showing the absence of the precursor nitrate material. The C 1s spectra contained the adventitious carbon peak at 284.8 eV which overlapped with any peak attributed to the TTP-PO_3 (285 eV).[62] The nature of gallium species for $Ga(NO_3)_3$, GaOOH and the *ex-situ* and *in-situ* GaOOH/TTP-PO_3 was determined using the Ga 2p spectra.

The N 1s spectra of the $Ga(NO_3)_3$ was fitted into three separate peaks at 407.3, 398.6, 395.4 eV which are attributed to nitrate species[66], unconsumed (unreacted) N[108] and Ga

LMM Auger peaks.[66] The clean GaOOH sample contained two peaks in the N 1s spectra residing at 397.3 and 394.3 eV which were due to unreacted N and Ga LMM Auger peak. Fitting of the N 1s XPS data is especially useful for investigating the presence of pyrrolic nitrogens contained in porphyrin molecules.[109] Peaks centered around 399 and 402 eV provided evidence of the presence of TTP-PO_3 in the *in-situ* and *ex-situ* GaOOH/TTP-PO_3. These peaks are attributed to the pyrolle N and the intense satellite peak, respectively.[110] These peaks are absent in the clean GaOOH sample which is indicative of no porphyrin being present on these samples. The spectra of these samples also contained the unreacted N and Ga LMM Auger peaks located at 397.0 and 394.1 eV. High concentration of nitrogen bonded to oxygen species can result in charging of the surface during the XPS experiment. One can observe evidence of this from the approximately 2 eV shift to higher binding energies of unreacted N and Ga LMM Auger peaks in $Ga(NO_3)_3$.

The O 1s spectra of the $Ga(NO_3)_3$ spectra contained one intense peak at 532.8 eV which contributed to over 90 % of the area in this region at 532.8 eV. This peak is attributed to the nitrate species while the smaller peak near 534 eV is attributed to the water within the sample. The O 1s spectra of the TTP-PO_3 salt contained a peak in the same area (around 532.9 eV) however this is attributed to the phosphonic groups on the porphyrin. The clean GaOOH sample contained two peaks residing at 531.2 and 532.5 eV which are attributed to the Ga-O and hydroxide (OH) species in the sample.[111] Three peaks were present in the *in-situ* and *ex-situ* GaOOH/TTP-PO_3 samples with the Ga-O and OH peaks residing at the lower binding energies of 530.5 and 531.7 eV, respectively. The shifting to lower binding energies

for these peaks is attributed to the presence of a third peak near 533.0 eV, which is consistent with the existence of the phosphonic groups from the TTP-PO_3.

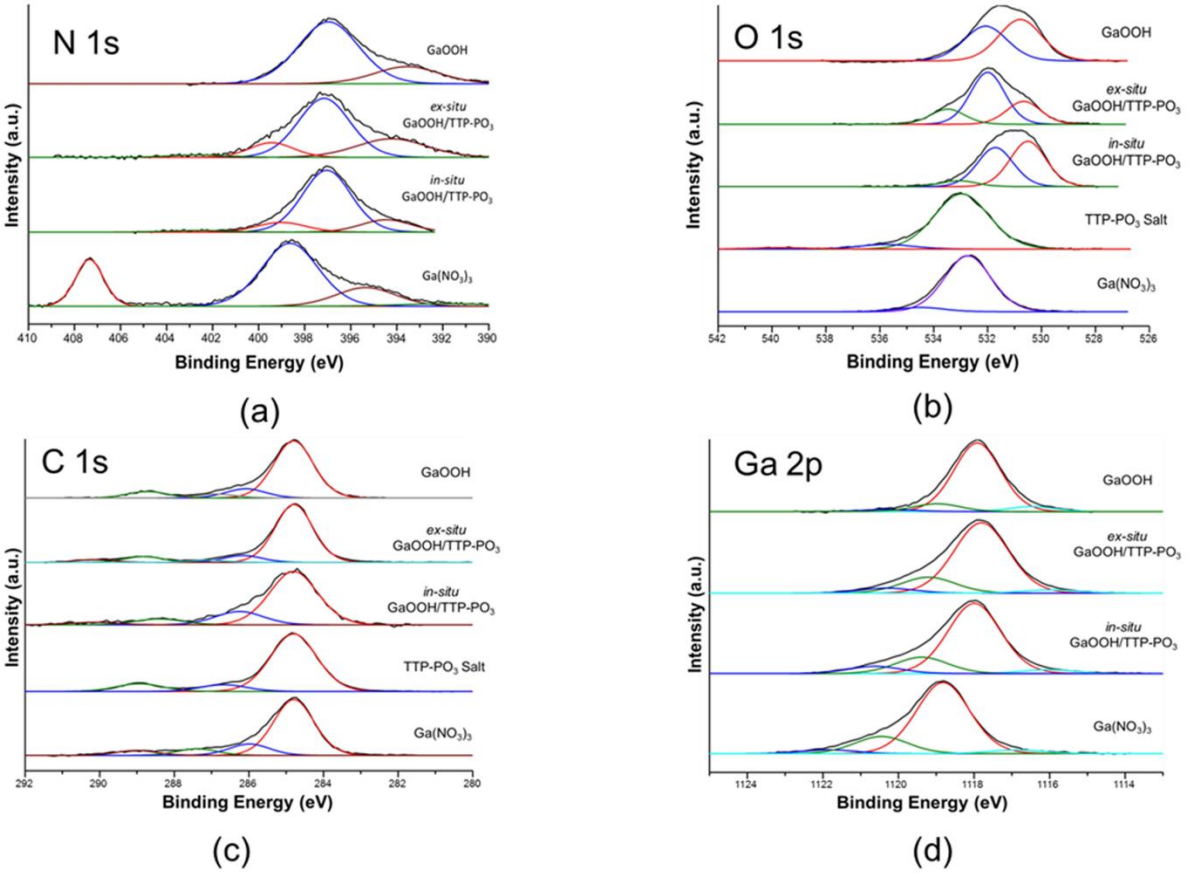

Figure 3.6. XPS spectra of the (a) N 1s of the precursor $Ga(NO_3)_3$, clean GaOOH, and the in situ and ex situ GaOOH/TTP-PO_3, (b) O 1s and (c) C 1s of the precursor $Ga(NO_3)_3$, TTP-PO_3 salt, clean GaOOH, and the in situ and ex situ GaOOH/TTP-PO_3 and (d) Ga 2p of the precursor $Ga(NO_3)_3$, clean GaOOH and the in situ and ex situ GaOOH/TTP-PO_3.

Quantitative XPS analysis was done to determine the percent contribution of each species within the N 1s spectra of the samples containing GaOOH. This was done to examine the surface coverage of the porphyrin on the functionalized samples and determine whether there was a significant difference between the two methods. Three runs were used and

averages were taken with the error signifying the standard error of the measurements. Displayed in Table 3.4 is the percentage each species contributed to the N 1s spectra. The clean GaOOH sample contained an average of 87.85±0.67 % unconsumed N and 12.15±0.67 % Ga LMM Auger peak. The *in-situ* GaOOH/TTP-PO_3 N 1s peak consisted of an average of 80.2±3.1 % unreacted N, 11.0±1.6 % Ga LMM Auger, 7.3±1.7 % pyrolle N and 1.48±0.22 % porphyrin satellite peak. The *ex-situ* GaOOH/TTP-PO_3 N 1s peak consisted of an average of 75.9±2.3 % unconsumed N, 11.7±1.4 % Ga LMM Auger, 8.3±1.1 % pyrolle N and 4.11±0.73 % porphyrin satellite peak. There is no significant difference between the *in-situ* and *ex-situ* pyrolle N percentages; however there is a significant difference in the porphyrin satellite peak. This could be attributed to the low atomic percentage of N in TTP-PO_3 providing a low signal for analysis. In both cases however, the averages show a higher surface percentage of species consistent with the presence of TTP-PO_3. When considered in conjunction with the increased C atomic percent of the surface of the *ex-situ* GaOOH/TTP-PO_3 this shows a possible increase in the surface coverage when using this method.

Table 3.4. The contribution of environment N, Ga LMM auger, pyrolle and satellite N peaks in percentages of N 1s spectra of clean GaOOH, *in-situ* and *ex-situ* GaOOH/TTP-PO_3.

	Environmental N	**Ga LMM**	**Pyrolle N**	**Satellite**
GaOOH	87.85±0.67	12.15±0.67	-	-
in-situ GaOOH/TTP-PO_3	80.2±3.1	11.0±1.6	7.3±1.7	1.48±0.22
ex-situ GaOOH/TTP-PO_3	75.9±2.3	11.7±1.4	8.3±1.1	4.11±0.73

The nature of the peaks in the O 1s spectra of the synthesized GaOOH containing samples was determined using the same method. Table 3.5 shows the percent each species contributed to the peaks in the O 1s spectra. The majority of the clean GaOOH was the metal oxide species with an average of 85.9±2.1 % and the hydroxide species being an average of 14.1±3.7 % of the N 1s spectra. The *in-situ* GaOOH/TTP-PO_3 contained an average of 47.7±1.9 % Ga-O species, 44.5±1.1 % OH species and 7.86±0.90 % P-O species. The *ex-situ* GaOOH/TTP-PO_3 sample contained an average of 27.9±2.9 % of Ga-O species, 54.93±0.95 OH species and 17.2±3.1 P-O species. The increase in the contribution of the phosphonic groups from the TTP-PO_3 in the *ex-situ* sample is support the notion that there is an increase in porphyrin surface coverage for these samples.

Table 3.5. The contribution of the Ga-O, OH and P-O peaks in percentages of the O 1s spectra for the clean GaOOH and the *in-situ* and *ex-situ* GaOOH/TTP-PO_3.

	Ga-O	**OH**	**P-O**
GaOOH	85.9±2.1	14.1±3.7	-
in-situ GaOOH/TTP-PO_3	47.7±1.9	44.5±1.1	7.86±0.90
ex-situ GaOOH/TTP-PO_3	27.9±2.9	54.93±0.95	17.2±3.1

3.4.5 Fourier Transformed-Infrared Spectroscopy

The Fourier Transformed-Infrared Spectroscopy (FT-IR) of the *in-situ* and *ex-situ* samples was investigated to explore the presence of functional organic groups from the pophyrin as well as vibrational frequencies associated with GaOOH. The use of FT-IR for the determination of TTP-PO_3 presence on GaN was previously used.[112] Figure 3.7 displays

the spectra of clean GaOOH by itself as well as the *in-situ* and *ex-situ* GaOOH/TTP-PO_3. The stretch found near approximately 1650 cm^{-1} can be attributed to the presence of C=N bond stretching in the pyrolle ring of TTP-PO_3. [75] The bands near 1030 and 950 cm^{-1} were found in each sample and can be attributed to typical bands found in GaOOH.[87] The weak bands present in the two functionalized samples between 1900 and 2200 cm^{-1} can be attributed to overtones of the aromatic rings present in the porphyrin.

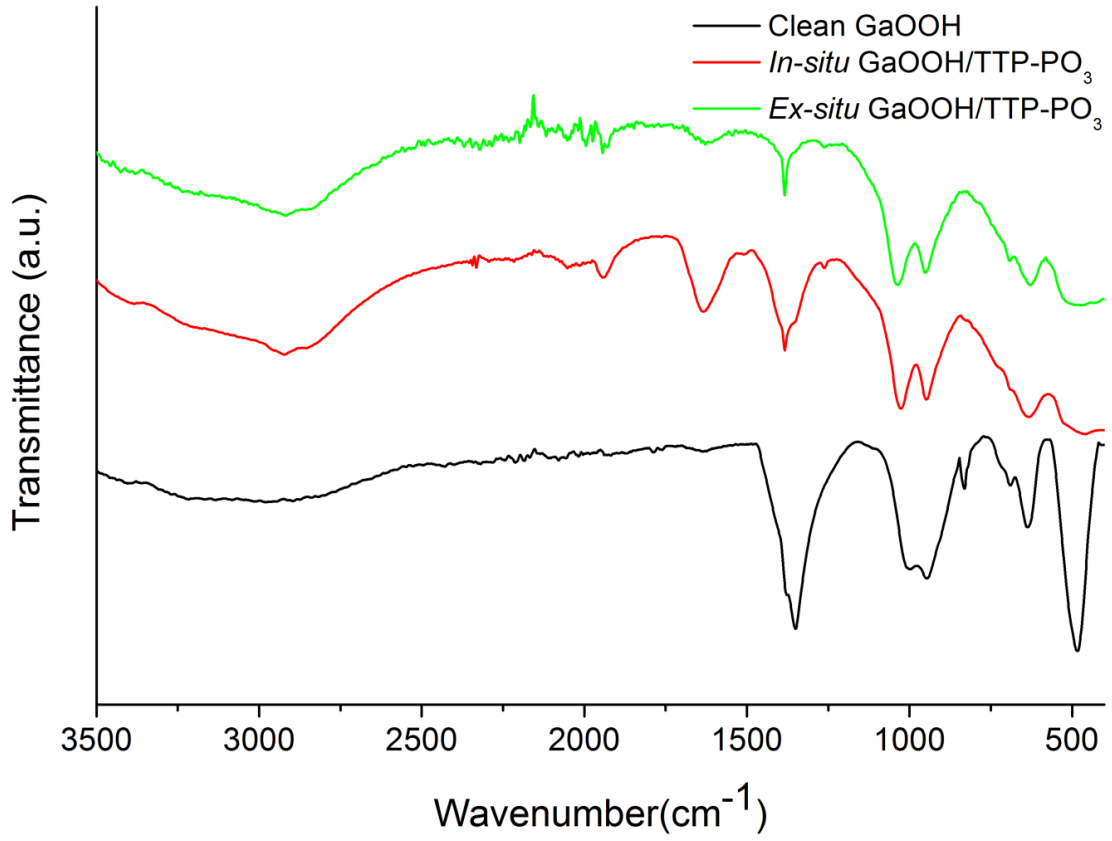

Figure 3.7. FT-IR spectra of the *in-situ* and *ex-situ* GaOOH/TTP-PO_3 as well as the clean GaOOH sample.

3.4.6 Stability Testing Using Fluorescence Spectroscopy

The stability of the porphyrin incorporation in the nanostructured materials is of particular interest for a number of applications that require substantial exposure to solution conditions such as solar cells and bioimaging probes. The *in-situ* and *ex-situ* samples were soaked in DI water to simulate unreacted conditions and measured with Fluorescence Spectroscopy to probe for leaching of porphyrin from the samples. A dilute sample of TTP-PO_3 in DI water was made to determine the position of the fluorescence peak of the porphyrin. The sedimented samples were shaken in solution and spectra were obtained. These spectra provided further evidence of functionalization based on the presence of peaks characteristic of the porphyrin dye present in the *in-situ* and *ex-situ* samples.

The *in-situ* and *ex-situ* samples were left in DI water for a period of 7 days after which the solution was filtered and tested for stability data. To ensure the removal of loose particles from these wash solutions, a filtration step was performed. A Nanosep centrifugal device with a molecular weight cut off of 3K and pore size of less than 5 nm was used. TTP-PO_3 that leached into the solution would be soluble in the DI water and remain the solution following the filtration step.

Figure 3.8 shows the fluorescence spectra of the dilute TTP-PO_3 solution, the filtered solution of the *in-situ* and *ex-situ* GaOOH/TTP-PO_3 and the sedimented *in-situ* and *ex-situ* GaOOH/TTP-PO_3 after shaking. The dilute solution contained a sharp peak near 695 nm which is consistent with the porphyrin. This same peak near 695 nm was present in the wash of the *ex-situ* sample while the wash of the *in-situ* sample showed the absence of any peak. This is consistent with the porphyrin leaching from the *ex-situ* GaOOH/TTP-PO_3 and

remaining contained in the *in-situ* GaOOH/TTP-PO_3. The sedimented *in-situ* GaOOH/TTP-PO_3 contained a peak near 675 nm after shaking and the sedimented *ex-situ* GaOOH/TTP-PO_3 contained a peak near 705 nm after shaking. The broad nature of the peaks and scattering due to the solid nature of the samples is likely the cause for the small shifts seen in the position of the fluorescence peaks.

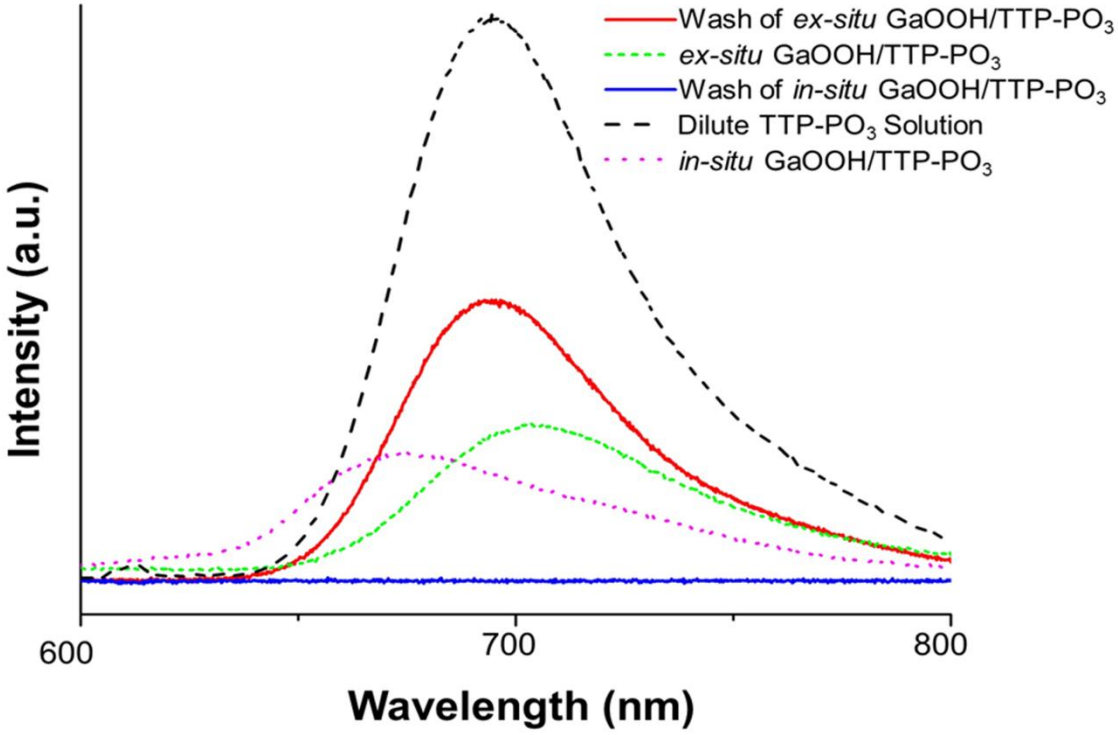

Figure 3.8. Fluorescence spectroscopy data of the dilute TTP-PO_3 solution along with the shaken *in-situ* and *ex-situ* GaOOH/TTP-PO_3 in DI water and the wash of the *in-situ* and *ex-situ* GaOOH/TTP-PO_3.

3.5 Conclusions

In conclusion, the synthesis and incorporation of porphyrin dye in GaOOH nanocrystallites was performed using two different methods. Subsequent characterization provided a comparison of the two methods. The *in-situ* GaOOH/TTP-PO_3 samples showed

evidence of larger crystallite size based on the PL, SEM and XRD data analysis. The *ex-situ* samples were smaller in crystallite size, however substantial leaching when submerged in DI water was evident from the Fluorescence Spectroscopy data. The XPS data showed evidence of increased surface coverage of the TTP-PO_3 on the *ex-situ* samples when compared to the *in-situ* samples. The larger size of the *in-situ* GaOOH/TTP-PO_3 crystallites suggests the possible incorporation of porphyrin inside of the hollow nanostructured semiconductor. Future work will be aimed to provide insight into this mechanism as well as into varying the size of the crystallites when the porphyrin is included in the synthetic procedure.

4. Synthesis and Optical Characterization of Mixed Nanostructured Aluminum-Gallium Oxyhydroxide

*Brady L. Pearce, Nora G. Berg and Albena Ivanisevic**

Department of Materials Science and Engineering, North Carolina State University, Raleigh, North Carolina, 27695, USA

4.1 Abstract

Nanostructured oxy-hydroxide materials with varied compositions of aluminum and gallium were synthesized in an environmentally friendly way with water as the only solvent. The tunability of optical properties of these materials through concentration ranges is particularly of interest for organic/inorganic hybrid materials in optoelectronic devices. Size comparisons of the materials were performed using DLS measurements. The measured size of the particles decreased with increasing Al. This supports the blue shift seen from the GaOOH emission wavelength to the $Al_{0.5}Ga_{0.5}OOH$ emission wavelength in the PL spectra. The XRD showed the formation of a possible amorphous layer in $Al_{0.5}Ga_{0.5}OOH$ and $Al_{0.2}Ga_{0.8}OOH$.

4.2 Introduction

Investigation into mixed aluminum and gallium containing oxides has seen increased attention due to their uses in catalysis and hydrogenation reactions. The mixed Al and Ga system with water has been researched, with the findings indicating that a boehmite structure of $Al_2O_3 \cdot H_2O$ exists up to the composition of approximately $70Al_2O_3 \cdot H_2O$, $30Ga_2O_3 \cdot H_2O$.[113] A one step precipitation reaction was followed to form mixed binary oxides of γ-Al_2O_3-α-Ga_2O_3 for catalysis applications.[114] The characteristics and properties of mixed $(Al_xGa_{1-x})_2O_3$

have been reported using precursor nitrate materials.[115] A solvothermal reaction has been used to produce spinel structured γ-Ga_2O_3 – Al_2O_3 mixed materials.[116]

The optical properties of these mixed oxide materials have, as of yet, not been extensively researched. Work in this field has focused mainly on the optical properties of mixed Al-Ga materials with various other metals. Examples of this are $Co(Al_{1-x}Ga_x)_2O_4$,[117] $Co_{3-x}M_xO_4$ (M=Al, Ga, In),[118] ZnX_2O_4 (X=Al, Ga, In)[119] and BaO-M_2O_3 (M=Ga, Al, In)-P_2O_3 glasses.[120] The wide band gap semiconductor GaOOH has recently been identified as a suitable material for the covalent attachment of phosphonic group containing organic dye molecules.[121] These composites are especially suitable for use in dye-sensitized solar cells (DSSCs).[25] It is hypothesized that by incorporating or substituting Al ions in GaOOH using varied concentrations, we can tune the optical properties, in particular the luminescent wavelength. This provides a unique advantage for DSSCs and other dye based optoelectronics. Band matching of the inorganic semiconducting material with the highest occupied and lowest occupied molecular orbitals (HOMO and LUMO) of the organic dyes could be done with added precision in conjunction with computational models. Another advantage to investigating AlOOH for this application is the increased stability seen in aluminum containing oxide materials when functionalized with organic molecules.[17]

In this study, aluminum nitrate nonahydrate and gallium nitrate hydrate precursors dissolved at various concentrations in DI water were titrated with sodium hydroxide and a previously reported hydrothermal microwave synthesis (GaOOH) was performed.[37] This titration and hydrothermal reaction has been done with AlOOH using an autoclave in previous work.[122] The advantages of using a microwave to replace this are numerous;

including the ability to perform a reaction which could take as long as a day within a 20 minute period. Corresponding ratios of mol:mol of Al:Ga were used to form the hypothesized compounds of AlOOH, $Al_{0.8}Ga_{0.2}OOH$, $Al_{0.5}Ga_{0.5}OOH$, $Al_{0.2}Ga_{0.8}OOH$ and GaOOH. The Al containing materials were more colloidal in nature as well as smaller in size than pure GaOOH, therefore these solutions were centrifuged to remove solvent instead of just being filtered. We found it easier to increase the yield using centrifugation rather than filtration. The effects of Al incorporation and concentration on the material diameter were investigated with Dynamic Light Scattering (DLS).

4.3 Results

The size characteristics of the nanocrystalline materials are important considerations for optical properties. The optical bandgap of materials is heavily influenced by size at nanometer scales. DLS provides a diameter measurement based on a spherical particle, the size measurements were still enough to provide size comparison data for increasing Al concentrations. In conjunction with photoluminescence spectroscopy (PL), these sizes can be used to explain any shifts in the emission wavelengths seen in the spectra which do not correspond to bandgap differences. The morphology of the GaOOH was investigated with SEM (Figure 4.1(a)). Microscopy measurements are a more reliable method of assessing the size of the synthesized materials. TEM was used to image the morphology of the hypothesized $Al_{0.5}Ga_{0.5}OOH$ material (Figure 4.1(b)). The materials are observed to conform to rod like morphologies, as expected from previous reports.[37, 122]

Table 4.1. Displayed are the DLS measurements of the average diameter of the mixed oxides.

Sample	Average Measured Diameter (nm)
AlOOH	86.3±3.6
$Al_{0.8}Ga_{0.2}OOH$	217±54
$Al_{0.5}Ga_{0.5}OOH$	357±23
$Al_{0.2}Ga_{0.8}OOH$	506±19
GaOOH	670±28

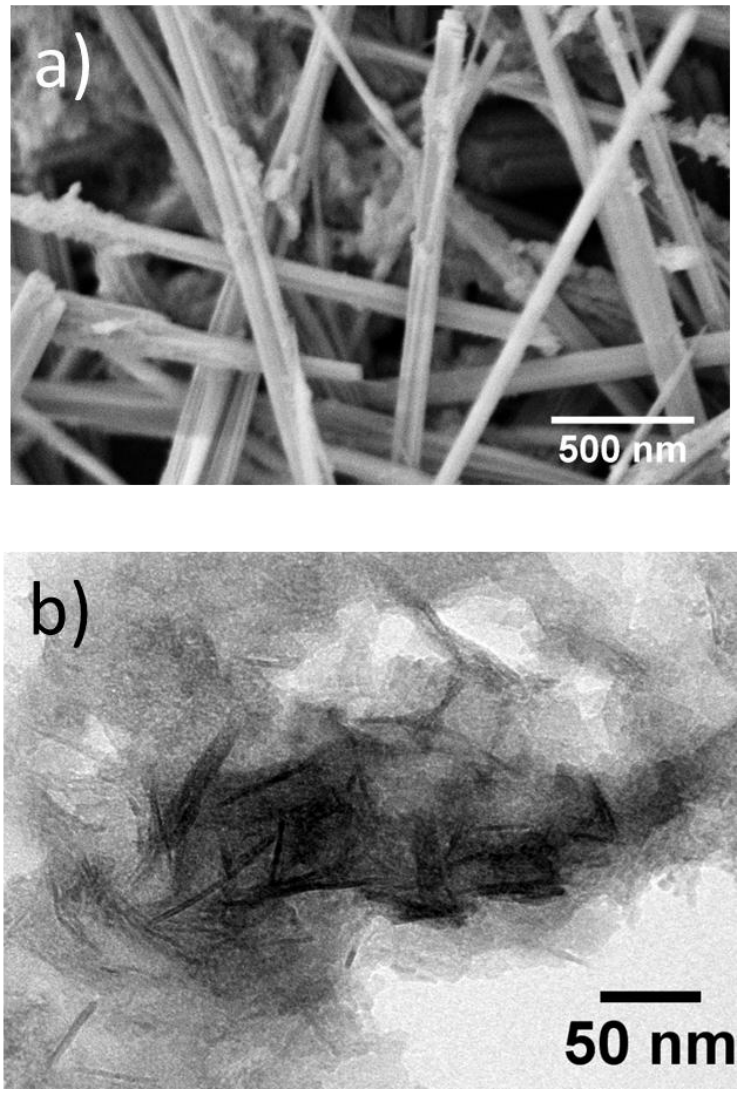

Figure 4.1. Displayed is the a) SEM image of GaOOH and b) TEM image of $Al_{0.5}Ga_{0.5}OOH$

The underlying goal of the synthesis of these mixed oxides was to provide a level of tunability to the optical properties of the materials for enhanced band matching with organic dye molecules. To explore the possibility of using these mixed oxides for this, PL data was obtained. This provided specific information about the luminescent emission of these materials and how this was affected by the composition. A homemade PL setup was used with an excitation wavelength of 193 nm. The laser used was a Coherent Xantos XS Argon Fluoride Eximer laser and different lenses were used to collimate and focus the beam on the sedimented samples in quartz cuvettes. Displayed in Figure 4.2 is the PL spectrum of each of the five materials going from top to bottom with increasing Al concentrations. Blue shifting is evident with increasing Al concentrations going from the high Ga concentrations to $Al_{0.5}Ga_{0.5}OOH$. The peaks present for each of the samples contained broad shoulders due to the expected high level of defects within the materials.

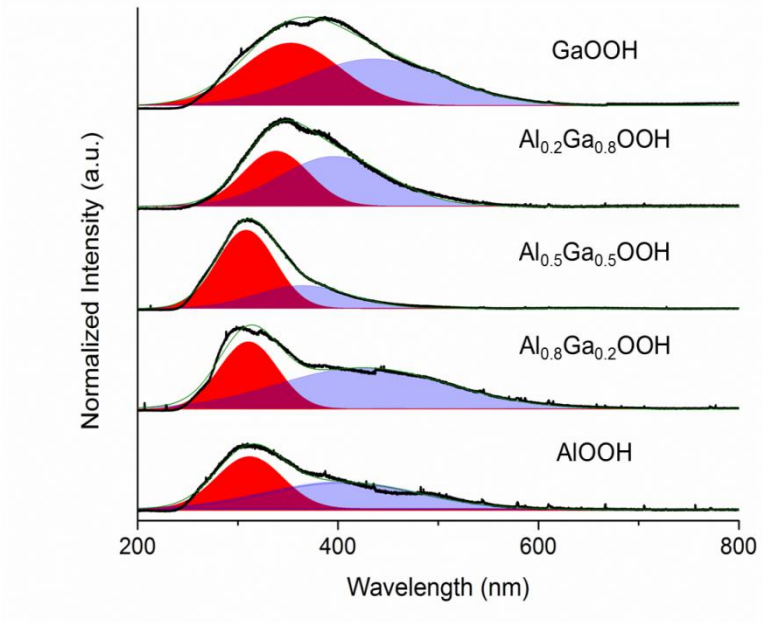

Figure 4.2. Depicted is the PL spectra of the various mixed oxides.

Peak fitting was done on individual spectra using Origin 8.0 to determine specific emission wavelengths. The main peaks of the hypothetical compounds AlOOH, $Al_{0.8}Ga_{0.2}OOH$, $Al_{0.5}Ga_{0.5}OOH$, $Al_{0.2}Ga_{0.8}OOH$, AlOOH were observed at 311.62, 306.39, 308.24, 337.94 and 352.85 nm, respectively. Blue shifting is seen from the high Ga concentration samples to the equal concentration samples and wavelength differences become negligible between peaks with added Al concentration. The band gap difference between AlOOH (4.51 eV)[15] and GaOOH (4.75 eV)[37] would suggest a red shift; however the effects of size at nanometer scales must be accounted for. In this study, it is evident that size effects overcome the material bandgap considerations.

The crystallinity of the various compounds was investigated with X-ray Diffraction (XRD), Figure 4.3. This data was obtained on a Rigaku SmartLab X-Ray Diffractometer. The spectra belonging to Al containing compounds indicated some leftover precursor material. The broad nature of the AlOOH peaks is indicative of nano-scale particles. At equal concentrations of Ga and Al, the nature of the peaks in the XRD spectrum suggests a possible amorphous region in these samples. This is observed in the TEM image of this sample, (Figure 4.1b) which shows nanostructured materials embedded in an amorphous matrix. This is also observed in the theoretical $Al_{0.2}Ga_{0.8}OOH$ sample. However, this sample contained well resolved peaks associated with GaOOH. The well resolved peaks from the GaOOH is consistent with the highly crystalline nanostructures seen in the SEM image (Figure 4.1a). It is possible the amorphous nature of these samples is due to the incomplete substitution of Ga into the boemite structure of AlOOH. Some microcrystal peaks are found in both the $Al_{0.2}Ga_{0.8}OOH$ and $Al_{0.5}Ga_{0.5}OOH$ spectra, with the broad, amorphous peaks. The peaks

found in the $Al_{0.2}Ga_{0.8}OOH$ can be attributed to GaOOH, whereas the peaks in the $Al_{0.5}Ga_{0.5}OOH$ are unique. It is expected that this material is likely mostly amorphous with a small amount of microcrystals within the matrix.

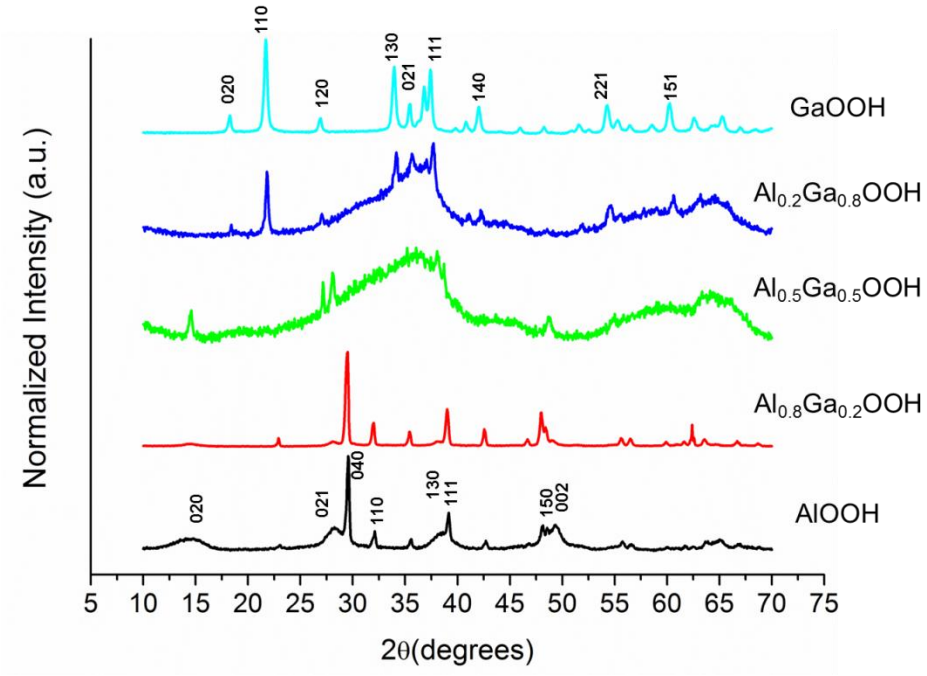

Figure 4.3. Shown are the XRD spectra of the various mixed oxides.

In order to obtain high resolution atomic ratios of Al:Ga for each of the compounds, Inductively Coupled Plasma-Mass Spectrometry (ICP-MS) was employed. The samples were prepared by dissolving less than 0.1 mg of each sample in a dilute nitric acid solution. A lab blank of just the nitric acid was used as a control. The average Al:Ga ratio of the three mixed compounds is displayed in Table 4.2. The AlOOH and GaOOH sample contained no Ga and Al, respectively, which was confirmed by XPS (Figure 4.4). The XPS data was obtained on a Kratos Analytical Axis Ultra XPS. Reaching exact values of molar ratios for Al and Ga in these samples is unlikely due to the inability to control the amount of unreacted precursors

following the solution based reaction. The Al:Ga ratio of $Al_{0.8}Ga_{0.2}OOH$, $Al_{0.5}Ga_{0.5}OOH$ and $Al_{0.2}Ga_{0.8}OOH$ were calculated to be 6.32±0.72, 1.687±0.050 and 0.48±0.026, respectively. These are believed to be reasonable representations of the theoretical values of 4, 1 and 0.25. It is noted that each sample contained higher levels of Al than the theoretical values, suggesting the possibility that the AlOOH reaction left less unreacted precursor than the GaOOH reaction.

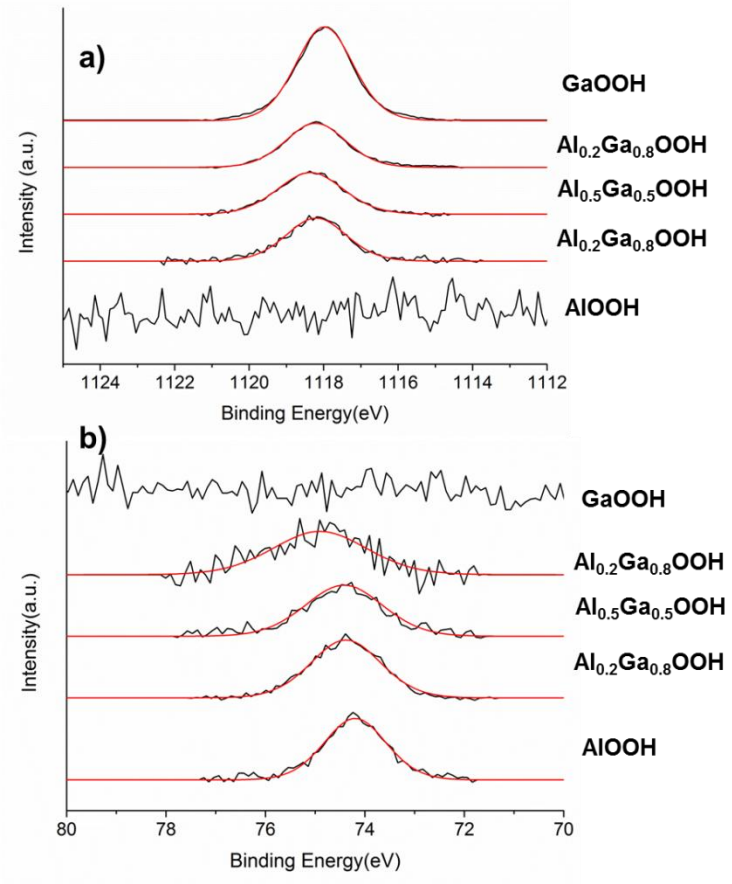

Figure 4.4. Displayed is the a) Ga 2p high resolution spectra and the b) Al 2p high resolution spectra of the mixed oxides.

Table 4.2. ICP-MS data of Al and Ga leaching of the mixed oxides.

Sample	Al Concentration (mol/L)	Ga Concentration (mol/L)	Al:Ga Ratio (mol:mol)
$Al_{0.8}Ga_{0.2}OOH$	$7.4\pm1.0 \times 10^{-5}$	$1.19\pm0.20 \times 10^{-5}$	6.36±0.72
$Al_{0.5}Ga_{0.5}OOH$	$8.5\pm3.1 \times 10^{-4}$	$5.0\pm1.8 \times 10^{-4}$	1.687±0.050
$Al_{0.2}Ga_{0.8}OOH$	$1.20\pm0.25 \times 10^{-4}$	$2.54\pm0.64 \times 10^{-4}$	0.484±0.026

4.4 Conclusions

The $Al_xGa_{1-x}OOH$ system was studied to determine its viability as an optically tunable inorganic for use in hybrid organic/inorganic optoelectronic devices. An example of this is DSSCs, where the efficiency of the device is directly impacted by the band matching between the HOMO of the organic dye and the conduction band of the inorganic material. Varied concentrations of precursor Al and $Ga(NO_3)_3$ were added and a microwave hydrothermal technique was used to synthesize nanostructured samples. Difference concentrations were used for this study in order to investigate the size differences measured with DLS based on the varied concentrations. In conjunction with these size differences and concentrations, PL data was taken which indicated a blue shift in the materials from the GaOOH to $Al_{0.5}Ga_{0.5}OOH$. The emission wavelengths beyond this concentration of Al did not show a significant change. The XRD spectra of each of the mixed oxides provided crystallographic information about the materials. Based on the collected data the method does not produce phase pure materials. These results indicate the possibility of tunability of the optical emission properties of this material system. This would prove to be valuable for a number of organic/inorganic hybrid materials for use in optoelectronics and bioelectronics. It would be of interest to investigate the properties of these materials as synthesized by conventional hydrothermal reaction to determine differences between the two synthetic

routes. The results of these syntheses suggest some reproducibility, however the concentration and crystallinity of the samples was uncontrolled.

5. Aqueous Stability of Nanostructured Aluminum and Gallium Oxyhydroxide Before and After Functionalization with Lysine

Brady L. Pearce[†], Nora G. Berg[†], Lin Jiang[‡], Albena Ivanisevic[†]

[†]Department of Materials Science and Engineering, North Carolina State University, Raleigh, North Carolina, 27695, USA

[‡]Materials Science and Engineering, University of New South Wales, Sydney, Australia

5.1 Abstract

Composites of nanostructured aluminum and gallium oxyhydroxide (AlOOH and GaOOH) and L-lysine were synthesized using an environmentally friendly approach. These composites were investigated to determine the effects of the functionalization on the aqueous stability and leaching of aluminum and gallium. The organic and inorganic components present in the samples were assessed with X-Ray photoelectron spectroscopy (XPS) and Fourier transformed-infrared spectroscopy (FT-IR). In the GaOOH-lysine composite, XPS provided evidence of both the presence of gallium and lysine. Crystallographic information was gathered using X-Ray diffraction (XRD). The FT-IR and XRD spectra of the composite materials were dominated by peaks related to lysine, due to the nature of these samples. Inductively coupled plasma-mass spectrometry (ICP-MS) data were collected of the functionalized and non-functionalized samples left in solution for periods of 1 day, 5 days and 7 days. This provided evidence of improved aqueous stability of the AlOOH-lysine composite with no effect seen in the GaOOH-lysine composite. The findings of this study will be used in determining the importance of lysine functionalization for future biomolecule-nanomaterial composites.

5.2 Introduction

The incorporation of the amino acid lysine to various functional materials to increase cell adhesion[30], biocompatibility[31] and aqueous stability[123] is of interest for a variety of applications including biosensors and targeted radiation therapy. The use of carboxylic acid containing molecules for bonding with materials such as AlOOH has been previously explored.[124] Lysine-alumoxane hybrid resins have been investigated to determine their effects on carbon fibers and epoxies.[125] For applications such as drug delivery, lysine can provide a means for specific drug transport across the blood-brain-barrier.[126] Lysine has proven to be an effective linker of various biomolecules to the surfaces of various gold samples for device capabilities such as biosensing.[127] The dendrimer structures of lysine have shown to provide an attachment mechanism for gold nanoparticles and DNA.[128] Graft polymers consisting of lysine and poly(ethylene glycol) (PEG) were investigated for adsorption on niobium oxide layers where altering the ratio of lysine to PEG directly affected the surface adhesion.[129]

The use of nanocrystalline materials for functionalization with organic moieties provides increased surface area for functional group attachment to the surface of the material. The materials of interest for this study, AlOOH and GaOOH, are typically researched for their effectiveness as precursors for conversion into Al_2O_3[130], AlN[131], Ga_2O_3[13] and GaN.[132] In addition to this, there are a number of reasons for considering these materials as the inorganic component of organic-inorganic composites. Particularly, the native hydroxide layer present on the materials provides an effective site for the attachment of organic molecules with functional side groups such as phosphonic and carboxylic groups. [112] The surface attachment

ensures long term stability of the interface between the two molecules. In this study, the functionalization of AlOOH and GaOOH nanostructured materials with L-lysine was performed. Toxicity occurs in biological systems at 700 mg/M^2 of gallium nitrate.[133] The importance of the surface functionalization of aluminum and gallium materials can be seen in Pourbaix diagrams.[134] The passivation of Al and Ga occurs in small pH window. Due to this, functionalization with molecules capable of improving the stability of these materials is of particular interestThe incorporation of the amino acid lysine to various functional materials to increase cell adhesion[30], biocompatibility[31] and aqueous stability[123] is of interest for a variety of applications including biosensors and targeted radiation therapy. The use of carboxylic acid containing molecules for bonding with materials such as AlOOH has been previously explored.[124] Lysine-alumoxane hybrid resins have been investigated to determine their effects on carbon fibers and epoxies.[125] For applications such as drug delivery, lysine can provide a means for specific drug transport across the blood-brain-barrier.[126] Lysine has proven to be an effective linker of various biomolecules to the surfaces of various gold samples for device capabilities such as biosensing.[127] The dendrimer structures of lysine have shown to provide an attachment mechanism for gold nanoparticles and DNA.[128] Graft polymers consisting of lysine and poly(ethylene glycol) (PEG) were investigated for adsorption on niobium oxide layers where altering the ratio of lysine to PEG directly affected the surface adhesion.[129]

The use of nanocrystalline materials for functionalization with organic moieties provides increased surface area for functional group attachment to the surface of the material. The materials of interest for this study, AlOOH and GaOOH, are typically researched for

their effectiveness as precursors for conversion into Al_2O_3[130], AlN[131], Ga_2O_3[13] and GaN.[132] In addition to this, there are a number of reasons for considering these materials as the inorganic component of organic-inorganic composites. Particularly, the native hydroxide layer present on the materials provides an effective site for the attachment of organic molecules with functional side groups such as phosphonic and carboxylic groups. [112] The surface attachment ensures long term stability of the interface between the two molecules. In this study, the functionalization of AlOOH and GaOOH nanostructured materials with L-lysine was performed. Toxicity occurs in biological systems at 700 mg/M^2 of gallium nitrate.[133] The importance of the surface functionalization of aluminum and gallium materials can be seen in Pourbaix diagrams.[134] The passivation of Al and Ga occurs in small pH window. Due to this, functionalization with molecules capable of improving the stability of these materials is of particular interest.

5.3 Materials and Methods

5.3.1 Synthesis of AlOOH and GaOOH Nanostructured Materials and Lysine Composites

Gallium nitrate hydrate, aluminum nitrate nonahydrate and sodium hydroxide, from Sigma Aldrich, were used as precursors for the formation of GaOOH and AlOOH nanorods using a previously reported hydrothermal microwave process.[37] This specific technique has not been reported for the synthesis of AlOOH nanorods. Due to the colloidal nature of the AlOOH solutions after microwaving, centrifugation was done in place of filtration. The oxide-lysine composites were made using a previously reported reflux reaction.[17] The L-lysine standard was obtained from Sigma Aldrich.

5.3.2 Characterization

X-ray Diffraction (XRD) spectra were obtained on a Rigaku SmartLab XRD. A Kratos Analytical Axis Ultra XPS provided surface sensitive information about the samples using a monchromated Al Kα source. A Bruker 1 95 9760 ALPHA FT-IR spectrometer equipped with a KBr beam splitter was used to gather FT-IR spectra in transmittance mode.

5.4 Results and Discussion

The nanomaterial synthesis and functionalization was done via a more environmentally green approach using water as a solvent and remaining at relatively low temperatures. A schematic representation of the various steps performed is shown in Figure 5.1. Included with this is SEM images of the GaOOH nanorods before and after functionalization. The nanorods are around 80 nm in width and 1 micron in length. To the best of our knowledge, this is the first reported use of GaOOH for this reaction in place of AlOOH.

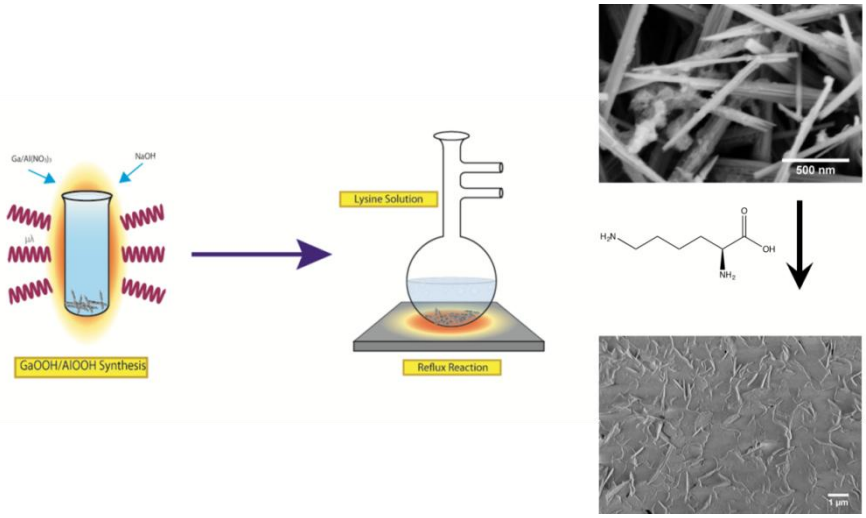

Figure 5.1. A graphical schematic depicting the processes followed for the synthesis of the composite materials. Included are SEM images of the GaOOH nanorods before and after lysine functionalization.

5.4.1 X-Ray Diffraction

The XRD spectra of the synthesized GaOOH and AlOOH nanorods and lysine composites showed the effectiveness of the reflux reaction (Figure 5.2). The GaOOH nanorods matched with the standard spectrum; however the AlOOH spectrum showed peaks consistent with possible leftover precursor material. The peaks attributed to AlOOH in this sample were significantly broad, which is attributed to the nano scale nature of the material. The significantly broader peaks in the AlOOH sample provide some evidence of smaller crystallite sizes in this sample when compared to the GaOOH. The composite materials both contained peaks that are consistent with the L-lysine standard which is also presented in the figure. The lack of any significant, observable crystallographic contributions from the GaOOH and AlOOH in the composites is attributed to the nature of the samples. It is hypothesized that the nanostructured oxides are surrounded by a crystalline lysine matrix whose XRD peaks are of significantly higher intensity.

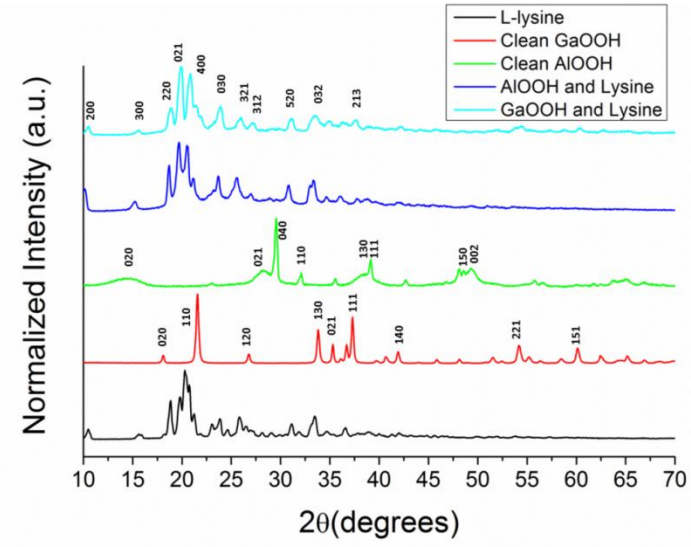

Figure 5.2. Displayed are the XRD spectra of the various samples including the L-lysine standard, the AlOOH and GaOOH composites and the clean nanostructured materials.

5.4.2 X-Ray Photoelectron Spectroscopy

Survey scans and high resolution regional XPS scans were taken for each of the samples. The N 1s, Ga 2p and Al 2p region scans provided evidence of the species present on the surface of each of the samples. In the Al 2p (Figure 5.3(a)) regional scan, the AlOOH sample has a peak near 74 eV which is not present in the AlOOH-lysine composite. It is believed that this is due to the AlOOH nanorods being buried in the lysine matrix along with the reduced response of Al in XPS when compared to Ga. The GaOOH and GaOOH-lysine composite both have a peak in the Ga 2p (Figure 5.3(b)) regional scan which is located near 1118 eV. Figure 5.3 (c) shows the N 1s regional scans of the various species indicating evidence of lysine presence in both the AlOOH and GaOOH containing lysine composites. This is based on the presence of two peaks near 399 and 400 eV on the composites as well as on the L-lysine standard.[135] No N 1s peak is present in the AlOOH sample and two peaks are present in the GaOOH at about 395 and 392 eV. These peaks are attributed to the Auger peaks Ga LMM 1 and 2.

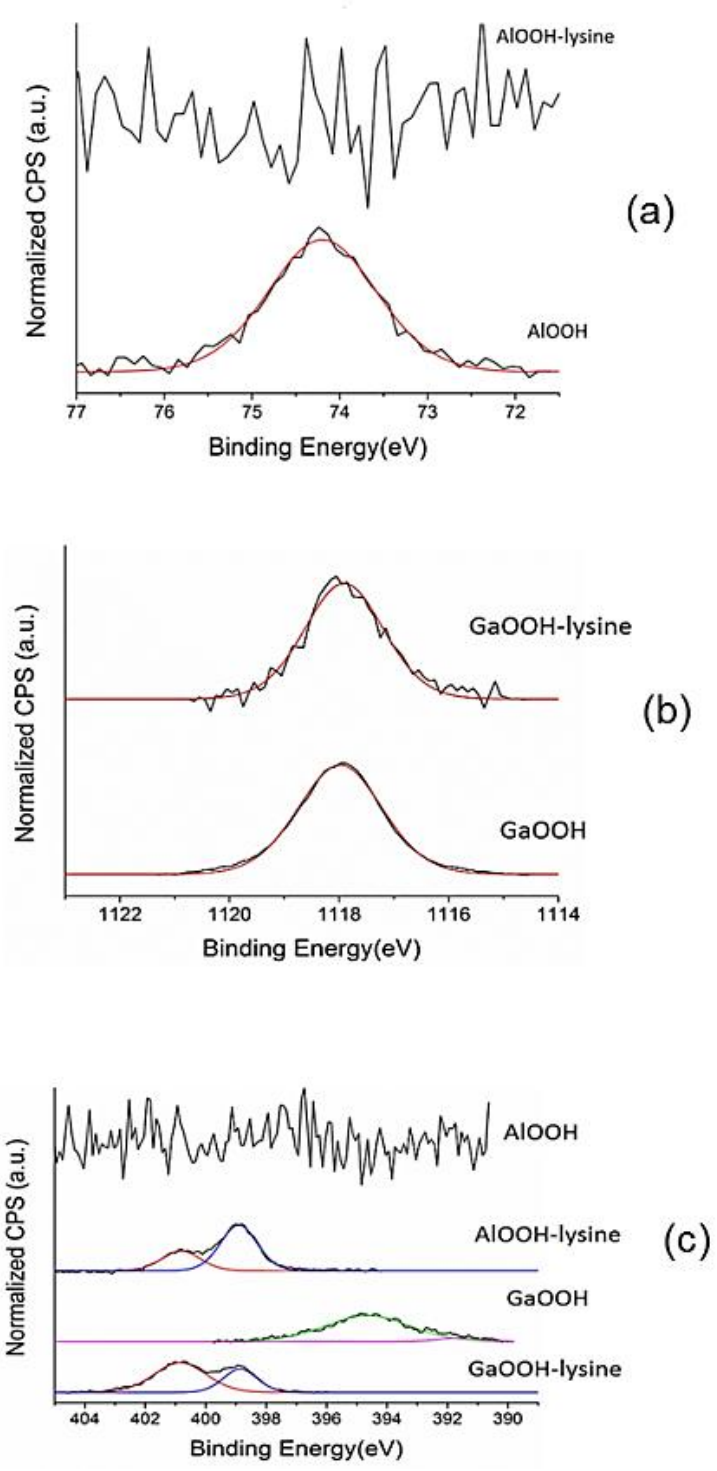

Figure 5.3. Depicted are the high resolution XPS spectra of various samples for (a) Al 2p, (b) Ga 2p and (c) N 1s.

5.4.3 Fourier-Transformed Infrared Spectroscopy

In order to evaluate the nature of the vibrational frequencies of the chemical species within the samples, FT-IR was used. The FT-IR spectra of both GaOOH[106] and AlOOH[136] nanostructured samples have previously been reported. Figure 5.4 displays the spectra of each of the four synthesized samples as well as of the lysine standard. The spectrum of the synthesized GaOOH nanorods contains expected peaks near 1030, 950, 690 and 630 cm^{-1}.[88] Peaks that are corresponding to the carboxylic acid group on lysine are found near 1600-1300 cm^{-1} in the spectrum of the standard. These peaks are also observed in the spectra of both of the lysine containing composites. In the AlOOH sample, peaks are seen near 1165, 1071, 737, 610 and 478 cm^{-1}, consistent with previously reported results.[136] The peaks from AlOOH or GaOOH are difficult to resolve in the composite materials due to their high level of overlap with the characteristic peaks of the organic material.

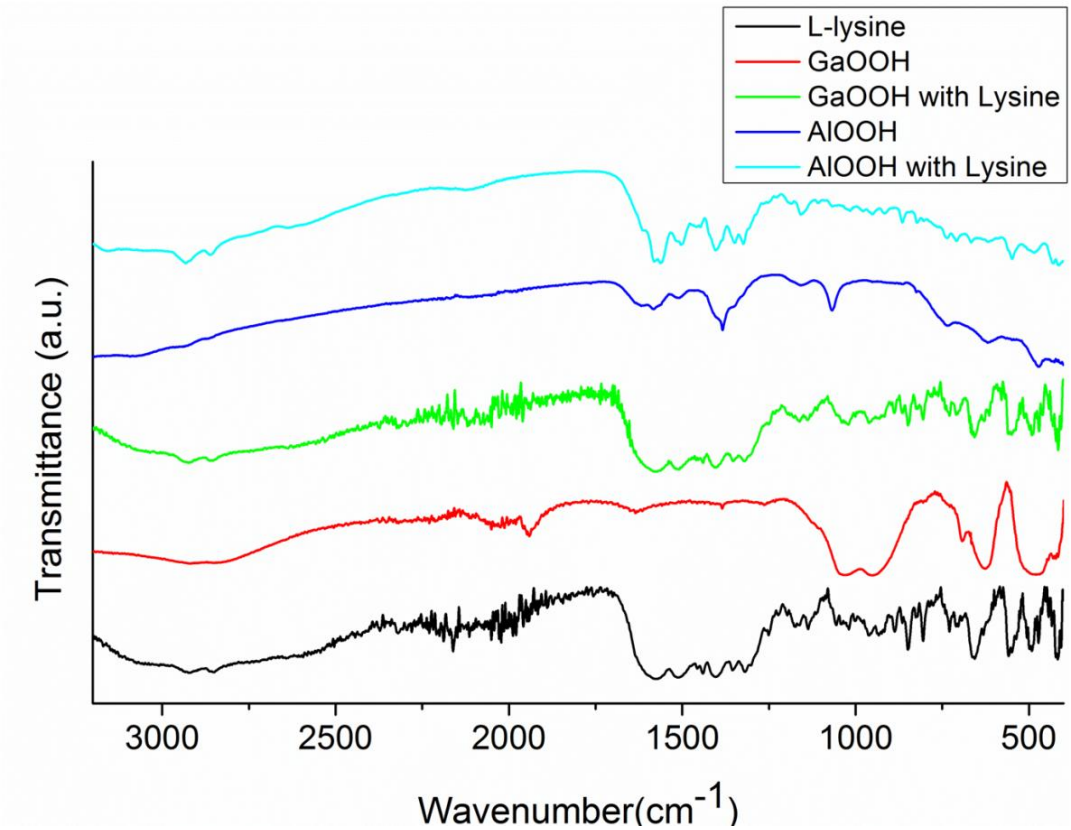

Figure 5.4. Shown are the FT-IR spectra of the various samples including the L-lysine standard, the AlOOH and GaOOH composites and the clean nanostructured materials.

5.4.4 Inductively Coupled Plasma-Mass Spectrometry Aqueous Stability

The leaching characteristics of the nanocrystalline materials and composites were investigated to determine the effect of the surface modification with lysine. Solutions of the various materials encompassed by DI water, soaked over periods of 1, 5 and 7 days, were measured with ICP-MS for Al and Ga leaching concentrations. The initial concentrations of GaOOH, GaOOH-lysine, AlOOH, Al-lysine were 8.7 mg, 9.1 mg, 9.4 mg and 8.6 mg in 10 mL, respectively. Table 5.1 shows the average and standard deviation. It is observed that the

presence of lysine does not reduce the presence of Ga leaching in the GaOOH samples and that these materials are relatively stable over time. In the AlOOH samples, however, the level of Al leached into solution is significantly less for the lysine functionalized composites. Statistical analysis was performed to determine if leaching levels over time were significantly different. These statistical tests are presented in the supplemental information. The values of leaching observed in the AlOOH were above reported toxicity values of between 50-200 ppb[137] and 9 ppm.[138] The values of observed leaching for the AlOOH-lysine composite were below this, indicating the advantage of functionalizing the aluminum containing nanostructures with lysine.

Table 5.1. Displayed is the ICP-MS data for Day 1, 5 and 7 of the various solutions of the submerged materials and the measured Ga or Al concentrations and percent of starting material leached.

Sample Type	Day 1		Day 5		Day 7	
	Ga Concentration (ppm)	Percent Leached (%)	Ga Concentration (ppm)	Percent Leached (%)	Ga Concentration (ppm)	Percent Leached (%)
GaOOH	1.487±0.036	0.2517±0.0060	1.187±0.036	0.2011±0.0054	1.092±0.024	0.1849±0.0040
GaOOH-Lysine	6.400±0.030	2.521±0.012	6.86±0.17	2.691±0.065	7.400±0.054	2.920±0.021
	Al Concentration (ppm)	Percent Leached (%)	Al Concentration (ppm)	Percent Leached (%)	Al Concentration (ppm)	Percent Leached (%)
AlOOH	24±20	5.6±4.7	31±16	7.7±3.9	25±22	6.0±5.2
AlOOH-Lysine	0.49±0.24	0.43±0.22	0.2093±0.0049	0.1860±0.0043	0.2110±0.0013	0.1885±0.0045

5.5 Conclusions

An environmentally friendly inorganic synthesis and functionalization process was followed to make GaOOH and AlOOH composites with lysine. Nanostructured forms of the

oxide materials were synthesized using a microwave hydrothermal process. The chemical and crystallographic nature of the composite was explored with XPS, FT-IR and XRD. The leaching characteristics of the composites were characterized using ICP-MS of DI water solution over a period of 7 days. The results indicated that the lysine incorporation on the AlOOH nanostructured materials improved the aqueous stability of the particles over a 7 day period. Understanding the effects of surface modification of nanostructured semiconductors provides pivotal information for future implementation of these composites into biomolecule based devices such as bacteriostatic glasses containing Ga.[139]

6. Optical Property Modulation from *In-situ* and *Ex-situ* Functionalization of Nanostructured Mixed Oxyhydroxides with a Porphyrin Dye

Brady L. Pearce[1], Albena Ivanisevic[1]

[1]Department of Materials Science and Engineering , North Carolina State University, Raleigh, North Carolina, 27695, USA

6.1 Abstract

A porphyrin dye was immobilized on the surface of nanocrystalline AlOOH and AlGaOOH. An *in-situ* procedure was used, in which the precursors were mixed with the soluble porphyrin dye prior to the microwave process. In a second methodology, the nanostructured materials were added to a porphyrin solution *ex-situ*, after the microwave process was complete. The presence of porphyrin onto the oxyhydroxide was confirmed with Fourier Transformed-Infrared Spectroscopy. The effect of porphyrin dye on the crystallographic nature of samples was examined with X-Ray Diffraction. The mixed AlGaOOH samples showed the formation of an amorphous layer and the AlOOH samples contained well resolved peaks attributed to the inorganic material of interest. Scanning Electron Microscopy images confirmed larger nanostructures in the AlOOH and AlGaOOH composites when the *in-situ* functionalization technique was employed as compared with the *ex-situ* one. Photoluminescence data indicated the presence of a peak attributed to the fluorescence of the porphyrin in the *en-situ* AlOOH sample, and a decrease in the full width at half maximum of the main excitonic peak of the semiconductors. This is attributed to the increased intensity from the added contribution of the organic dye near 300 nm. The results

demonstrate that a simple water based procedure can be used to modulate the optical signature of the mixed oxyhydroxides.

6.2 Introduction

Solution based functionalization research for wide bandgap semiconductors provides a scalable technique for developing hybrid inorganic/organic materials. Of particular importance in the functionalization of materials such as gallium nitride (GaN), is a preferentially grown surface hydroxyl layer.[2] The native presence of hydroxyl groups on the materials aluminum and gallium oxyhydroxide (AlOOH and GaOOH) present a unique advantage for one-step surface modification. Previous work has demonstrated the viability of using two different functionalization techniques for attaching a porphyrin molecule to the surface of GaOOH.[140] Poprhyrin molecules have shown great promise for photovoltaic applications, due to their elevated photon-to-electron conversion efficiency.[53]

Recent work has demonstrated the solution based synthesis of mixed Al and GaOOH, and indicated tunability of the optical properties based on the concentration of Al or Ga. Previous literature has indicated that the boehmite structure in the Al-Ga water system exists up to a 70% Al composition.[113] The optical tunability of these mixed composition, nanostructured oxyhydroxides provides these materials with unique viability in hybrid organic/inorganic composites. Solution based techniques have shown promise for developing Al and Ga mixed materials such as $(Al_xGa_{1-x})_2O_3$,[115] γ-Al_2O_3-α-Ga_2O_3[114] and γ-Ga_2O_3-Al_2O_3 spinel structures.[116]

In this work we explore the possibility of modulating the optical properties of mixed oxyhydroxides by modifying their surface with and organic dye molecule. The chemical nature of the compounds was investigated with Fourier Transformed-Infrared Spectroscopy (FT-IR). The effect of the presence of the organic dye on the crystallography of the

inorganic component was characterized with X-Ray Diffraction (XRD). The size characteristics of the nanostructured materials were explored using scanning electron microscopy (SEM). The optical properties of the composites were measured with photoluminescence (PL) spectroscopy.

6.3 Materials and Methods

6.3.1 Synthesis of Organic/Inorganic Composites

A previously reported synthesis procedure for making GaOOH nanorods was followed to produce the AlOOH and AlGaOOH nanostructure inorganics.[37] A 1:1 mol:mol ratio of $Al(NO_3)_3$ and $Ga(NO_3)_3$ precursor were titrated with 0.1 M NaOH to a pH of 8 for the AlGaOOH procedure. Due to the hypothesized size and nature of the nanostructured materials, centrifugation was used to separate the solid. Two different methodologies were employed to attach the porphyrin salt to the oxyhydroxide materials. An *in-situ* functionalization included adding the soluble porphyrin salt before the microwave process and an *ex-situ* functionalization was used after the microwave process. The product of the solution based synthesis was rocked in a solution of porphyrin salt for a period of 24 hours.

6.3.2 Characterization

The XRD spectra obtained in this study were produced with a Rigaku SmartLab XRD. The FT-IR spectra were gathered with a Bruker 1 95 9760 ALPHA FT-IR spectrometer in transmittance mode with a KBr beam splitter. PL data was obtained on a homemade optical bench top with a 193 nm Coherent Xanton XS Argon Fluoride Eximer laser. All SEM images were obtained with an FEI Verios 460L Field Emission SEM.

6.4 Results and Discussion

Previous work has indicated the importance of size considerations on the optical bandgap and emission characteristic of mixed AlGaOOH materials. This is particularly important for optoelectronic applications involving organic/inorganic hybrid materials. The synthesis of these composites was done with water as the only solvent and at low temperatures relative to typically used techniques.

6.4.1 X-Ray Diffraction

Crystallographic information of the *in-situ* and *ex-situ* AlOOH and AlGaOOH with porphyrin was gathered using XRD spectra. This was done in an effort to determine the effect of the presence of porphyrin during the microwave synthesis on the crystalline nature of the samples. The *in-situ* and *ex-situ* AlGaOOH had few well resolved peaks, with evidence of amorphous layers within the samples. The peaks found in the spectra of these samples lie at the same 2θ as peaks found in the AlOOH samples. The *ex-situ* and *in-situ* AlOOH XRD spectra contained well resolved peaks attributed to the presence of crystalline AlOOH.\

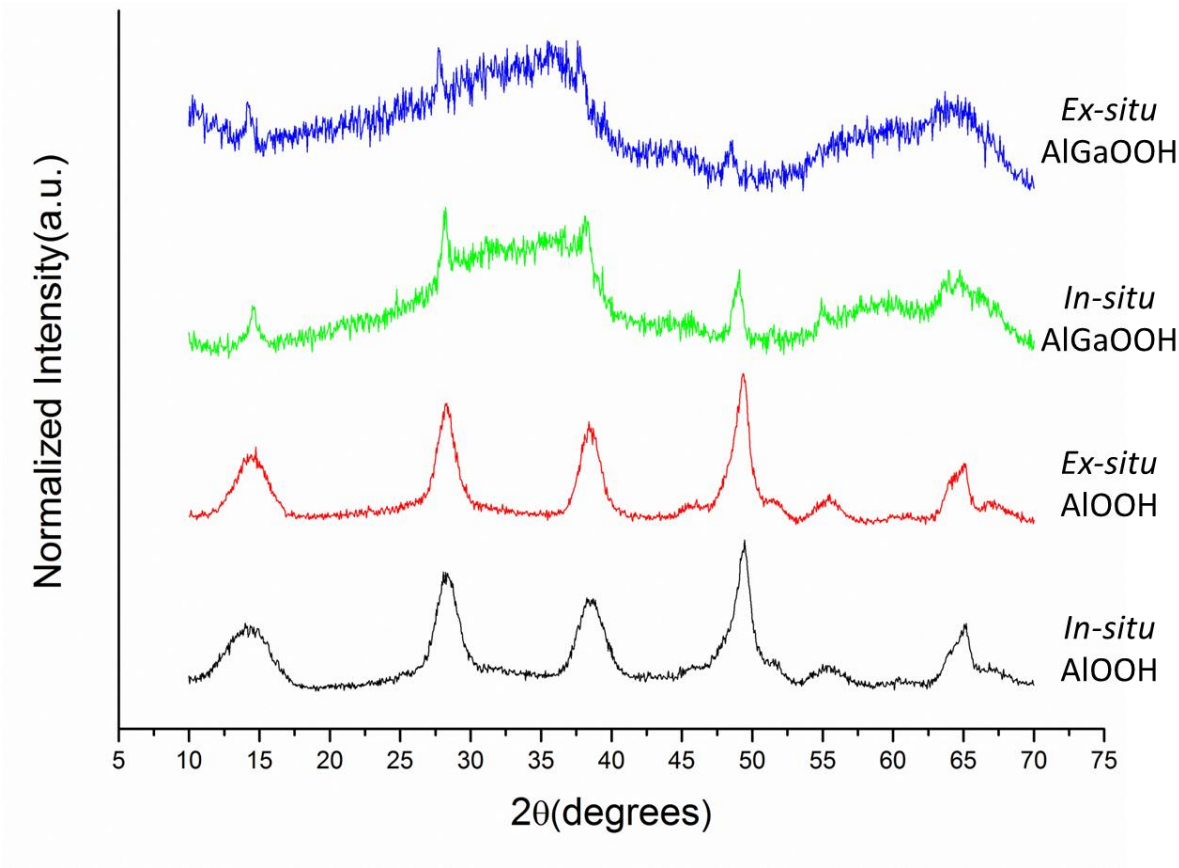

Figure 6.1. Displayed is the XRD spectra of the *in-situ* and *ex-situ* functionalized AlOOH and AlGaOOH.

6.4.2 Fourier-Transformed Infrared Spectroscopy

FT-IR spectra were obtained to determine the nature of chemical species within the hybrid organic/inorganic composites. In the *ex-situ* and *in-situ* AlOOH and AlGaOOH, a number of peaks were present which can be attributed to the presence of AlOOH. The band found near 1636 cm^{-1} can be attributed to water, while the bands found near 1080 cm^{-1} and 1160 cm^{-1} are attributed to different modes of the Al-O-H bonding in the AlOOH structure.[32] The band near 750 cm^{-1} can be attributed to the torsional vibrational mode of boehmite and the bands found near 630 cm^{-1} and 485 cm^{-1} are due to stretching bands of the Al-O bond.[32]

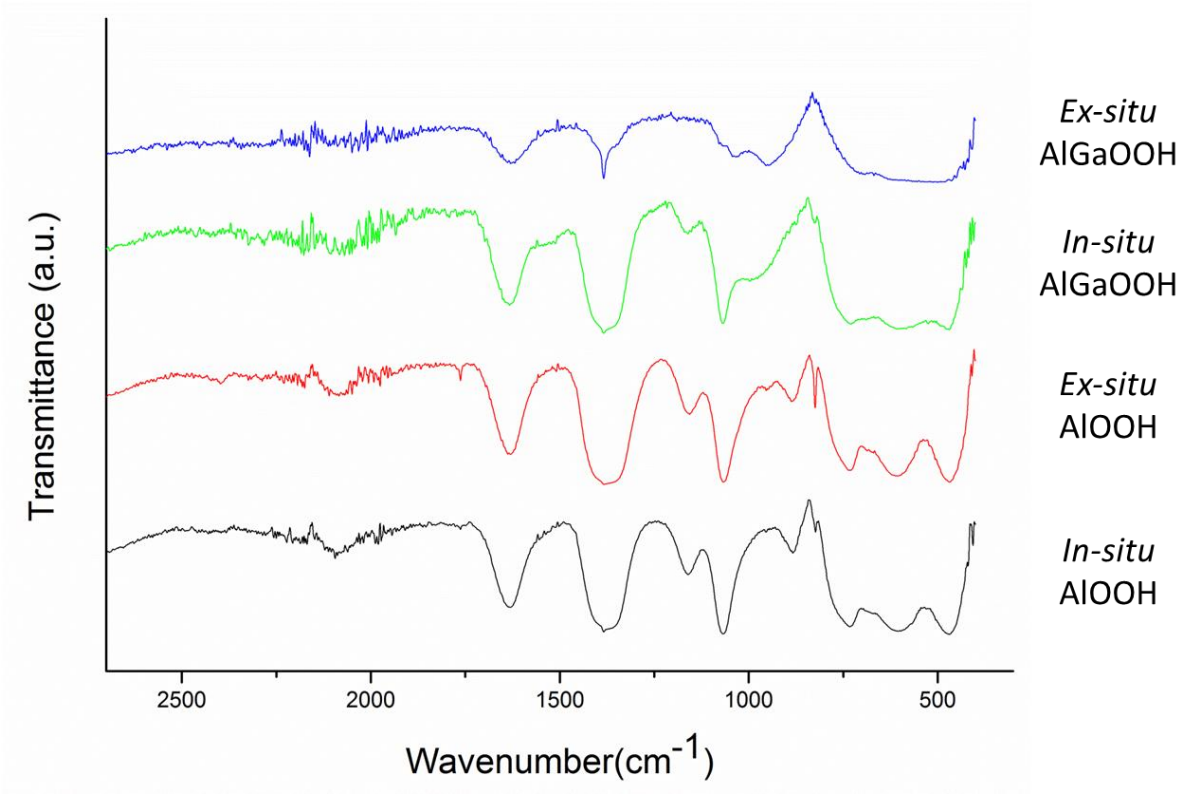

Figure 6.2. Depicted is the FT-IR spectra of the *in-situ* and *ex-situ* AlOOH and AlGaOOH.

6.4.3 Size Measurements from Scanning Electron Microscopy

Previous work with composites containing various concentrations of Al and Ga in AlGaOOH samples indicated a decrease in the size of the nanostructures of the materials with an increase in Al concentration. SEM images were gathered for each of the hybrid organic/inorganic composites in an effort to gather size measurements of the nanostructures. Each of these hybrid materials conformed to rodlike geometries with lengths much larger than the widths. The average length and width measurements for each are displayed in Table 6.1. It was observed that the presence of the porphyrin molecule during the microwave synthesis led to larger lengths and widths in these composites. In both the *in-situ* and *ex-situ*

materials, the AlOOH was measured to be smaller in both length and width than the AlGaOOH material.

Table 6.1. Displayed is the measurement of the FWHM of the main excitonic peaks of each composite.

	Average Length (nm)	Average Width (nm)
***In-situ* AlOOH**	386±28	54.7±5.0
***Ex-situ* AlOOH**	59.7±2.6	15.98±0.93
***In-situ* AlGaOOH**	907±64	107±15
***Ex-situ* AlGaOOH**	151±14	19.9±3.3

6.4.4 Optical Properties of Composites Using Photoluminescence

Recently, the mixed AlGaOOH system was identified as a suitable material for hybrid organic/inorganics, in particular for optoelectronics.[141] Research has indicated that nanostructured GaOOH has increased photocatalytic properties.[37] The incorporation of Al at mixed concentrations has been shown to provide tunability to the optical bandgap and emission wavelength of the material. It was found that the smaller size of nanostructures due to increasing Al concentration reduced the optical bandgap and decreased the emission wavelength found using PL spectra.

For applications such as dye-sensitized solar cells, the energy loss from the electron moving from the lowest unoccupied molecular orbital (LUMO) of the organic dye to the conduction band (CB) of the semiconductor can be compensated by tuning the CB to match the energy level of the LUMO. The PL spectra of the hybrid organic/inorganic materials are shown in Figure 3. The highest energy peaks for the *in-situ* AlOOH, *ex-situ* AlOOH, *in-situ*

AlGaOOH and *ex-situ* AlGaOOH were found at 302.1, 299.7, 302.1 and 297.1 nm, respectively. It is observed that for both samples, the *in-situ* sample contained a peak at higher wavelengths, or lower energy. This is attributed to the observed larger sized nanostructures found in the *in-situ* samples when compared with the *ex-situ* ones. In the PL spectra of *ex-situ* AlOOH, the low intensity of the main excitonic peak provided the observation of a peak near 650 nm, due to the fluorescence of the porphyrin dye. The spectra of this sample also contained a main peak with the lowest full width at half maximum (FWHM).

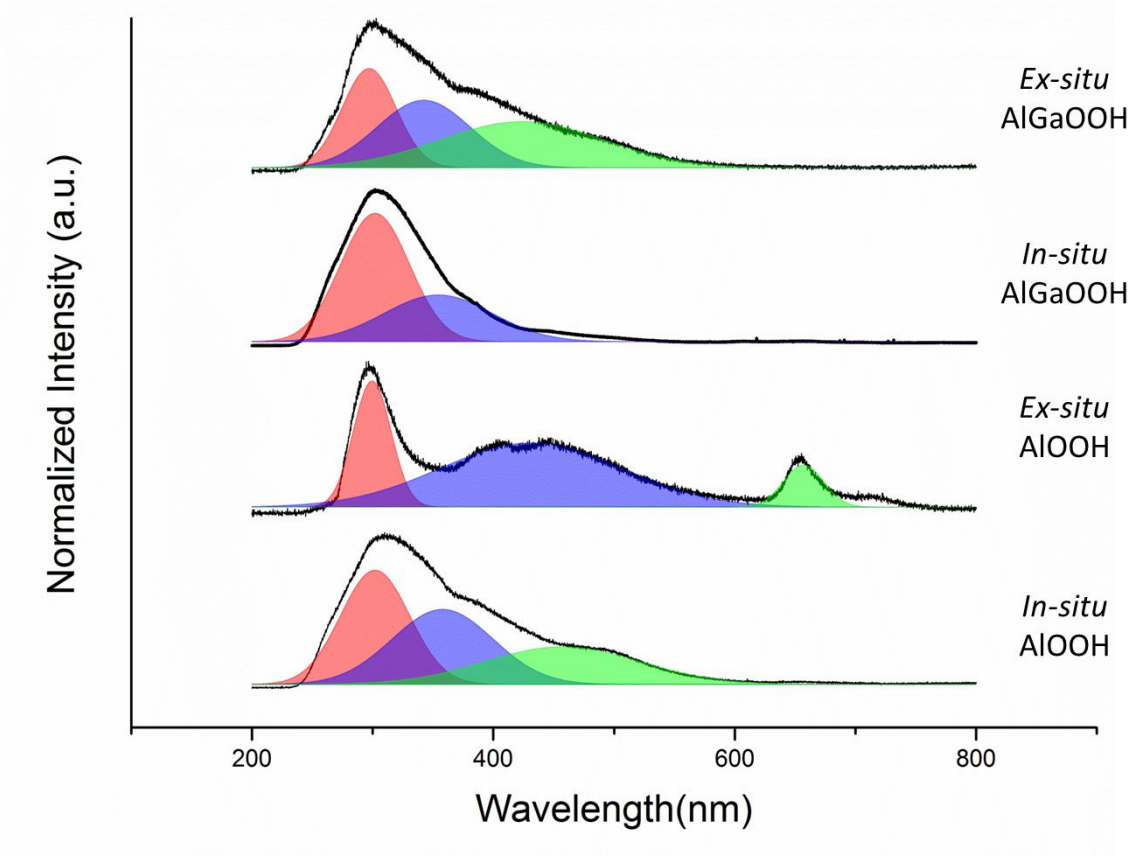

Figure 6.3. Shown is the PL spectra of the *in-situ* and *ex-situ* AlOOH and GaOOH.

The presence of an optically active organic dye molecule with an inorganic semiconductor is hypothesized to increase the bandwidth of emission during luminescence. This is demonstrated by the increased FWHM of the excitonic peaks found in each of the samples. The FWHM of the *in-situ* and *ex-situ* AlOOH were significantly smaller than the FWHM of AlOOH from previously published data of 76.7.[141] This was also the case with the *in-situ* and *ex-situ* AlGaOOH, with smaller FWHM of their excitonic peaks than that of AlGaOOH, 68.0.[141] This is likely due to an increase in the intensity of emitted photons from the presence of the porphyrin molecule. Porphyrins have been explored as sensitizers on oxide surfaces such as TiO_2.[142] The ease of functionalization with these dyes and their utility for different wide band gap materials is well documented in the literature.[2] Our materials' characterization data and spectroscopy data illustrates that this extremely simple method of chemical functionalization can be used to form stable dye-wide band gap surface complexes in water. Comparison between the PL data of in situ and ex-situ functionalization of AlOOH indicates that one can load considerably more dye onto to the oxide surface after synthesis. The observation supports the notion that phosphonate ligands have a higher affinity of AlOOH compared to previously studied GaOOH.[2]

Table 6.2. Displayed is the measurement of the FWHM of the main excitonic peaks of each composite.

	Excitonic Peak	FWHM
***In-situ* AlOOH**	302.1	67.3
***Ex-situ* AlOOH**	299.7	36.8
***In-situ* AlGaOOH**	302.1	67.1
***Ex-situ* AlGaOOH**	297.1	52.8
AlOOH[143]	311.62	76.7
AlGaOOH[143]	308.24	68.0

6.5 Conclusions

The surface attachment of organic dye molecules to nanostructured inorganic semiconductors has wide reaching applications in optoelectronics and bioelectronics. In oxyhydroxide materials such as GaOOH and AlOOH, the surface layer of hydroxyl groups can be used to provide attachment sites for organics with phosphonic group containing functional side groups. This study explored the *in-situ* and *ex-situ* functionalization of AlOOH and a mixed AlGaOOH with a porphyrin dye containing a phosphonic side group. The crystallographic nature of the samples was investigated with XRD, showing the formation of an amorphous region in the *in-situ* and *ex-situ* AlGaOOH, and well resolved peaks attributed to AlOOH in the *in-situ* and *ex-situ* AlOOH.

7. Conclusions and Future Outlook

The focus of this dissertation is the improvement of processing techniques and characterization of novel hybrid organic/nanostructured inorganic composites. Using a previously established functionalization technique,[1] a phosphonic group containing porphyrin dye molecule was attached to the surface of a nanostructured GaN powder. Fluorescence spectroscopy indicated stability of the organic/inorganic interface after a period of 20 days in water due to the lack of peaks attributed to desorbed porphyrin. The presence of organic and surface species attributed to the porphyrin and GaN were observed using FT-IR and XPS, respectively. The information gathered in this study provided evidence to promote the hypothesis that the surface attachment between dye and semiconductor was covalent in nature.

The surface attachment of phosphonic group containing organic molecules to GaN is known to rely on a surface hydroxyl group, preferentially grown on the GaN surface. In an effort to reduce processing steps even further, as well as investigate a novel material for these applications, GaOOH was studied. Two methodologies were performed to attach a phosphonic group containing porphyrin dye to microwave synthesized GaOOH. An *in-situ* method relied on introducing the soluble porphyrin into solution before the microwave process, while the *ex-situ* method introduced it after the process. Larger crystallites were observed in the *in-situ* composites when compared to the *ex-situ* ones. This was evidenced by PL, SEM and XRD data, and suggested interaction of the soluble porphyrin with the GaOOH precursors during the microwave synthesis. The *ex-situ* process showed increased surface coverage via the XPS data as well as the presence of desorbed porphyrin from fluorescence

spectroscopy data. The leaching of porphyrin from the interface provided possible evidence of pi-stacking of the organic molecule on the surface of the nanostructured GaOOH.

For optoelectronic applications of organic/inorganic composites, a key electron transfer process is the movement from the HOMO of the organic to the conduction band of the semiconductor. In applications such as DSSCs, the efficiency of the device depends heavily on the reduction of energy losses during this step. In an effort to improve this, mixed concentrations of Al and Ga precursors were used to synthesize the $Al_xGa_{1-x}OOH$ system. Size measurements, performed with DLS, indicated decreasing size with increasing Al concentration. These size differences were hypothesized to be the reason behind the blue shift seen from the GaOOH material to the $Al_{0.5}Ga_{0.5}OOH$. Amorphous regions seen in the XRD spectra indicated that the methodology used did not produce all phase pure materials.

Optoelectronic devices left in environmental conditions, as well as bioelectronics in varying pH environments, require solution stability to avoid the leaching of ions from the material. Lysine has shown promise for this application, and a previous technique demonstrated the cross-linking of this organic with the nanostructured form of AlOOH. This technique was followed using both AlOOH and GaOOH, and ICP-MS data showed that the leaching of Al and Ga ions into solution over a 7 day period indicated an improvement in the aqueous stability in the AlOOH-lysine composites. The lack of improved aqueous stability in the GaOOH-lysine composites is hypothesized to be due to the nature of the larger GaOOH particles. This likely hindered the cross-linking of lysine, and led to the GaOOH sitting in a sea of lysine.

The final study in this dissertation was to explore the attachment of the phosphonic group containing porphyrin dye on AlOOH and the mixed AlGaOOH material. The previous *in-situ* and *ex-situ* methodologies were followed. In the mixed AlGaOOH system, the XRD spectra showed the formation of an amorphous region, as expected from previous work. The FT-IR spectra of the composites indicated the presence of both porphyrin and AlOOH in all four materials of interest. Size measurements were performed with SEM images, indicating that the *in-situ* methodology produced larger nanostructured crystallites than the *ex-situ* method. The FWHM of the PL spectra in the composite materials indicated an increase in intensity near the excitonic peak wavelength. The spectra *ex-situ* AlOOH material contained a peak around 650 nm, which was due to the presence of the porphyrin.

There are a number of additional promising directions that can be explored in light of the results from this dissertation. One can build a prototype DSSC, with metal center containing porphyrins, to insight into their efficiency in devices. The incorporation of various other precursors, such as indium nitrate $In(NO_3)_3$, would provide additional insight into the effects of varying compositions on size and optical characteristics of various composites.

Additional future work can be centered on the continuation of exploring the understanding of the use of phosphonic acids derivatives for organic/inorganic devices.[2] In particular, modifying transparent conduction oxides with phosphonic group containing organics has shown promise in providing improvements in these devices and new functionalities. In OLEDs, phosphonic acid containing organics provide an increase in work function, which drives the improved efficiency of these devices.

8. References

1. Wilkins, S. J.; Greenough, M.; Arellano, C.; Paskova, T.; Ivanisevic, A., In Situ Chemical Functionalization of Gallium Nitride with Phosphonic Acid Derivatives during Etching. *Langmuir* **2014,** *30* (8), 2038-2046.

2. Pearce, B. L.; Wilkins, S. J.; Paskova, T.; Ivanisevic, A., A review of in situ surface functionalization of gallium nitride via beaker wet chemistry. *J. Mater. Res.* **2015,** *30* (19), 2859-2870.

3. Christiansen, S.; Albrecht, M.; Dorsch, W.; Strunk, H. P.; Pelzmann, A.; Mayer, M.; Kamp, M.; Ebeling, K. J.; ZanottiFregonara, C.; Salviati, G., Microstructure and growth morphology as related to electro-optical properties of heteroepitaxial wurtzite GaN on sapphire (0001) substrates. *Mater. Sci. Eng. B-Solid State Mater. Adv. Technol.* **1997,** *43* (1-3), 296-302.

4. Morkoc, H., *Handbook of Nitride Semiconductors and Devices, Material Properties, Physics and Growth*. John Wiley & Sons: Weinheim, 2009; Vol. 1, p 1311.

5. Guo, D. J.; Abdulagatov, A. I.; Rourke, D. M.; Bertness, K. A.; George, S. M.; Lee, Y. C.; Tan, W., GaN Nanowire Functionalized with Atomic Layer Deposition Techniques for Enhanced Immobilization of Biomolecules. *Langmuir* **2010,** *26* (23), 18382-18391.

6. Rohrbaugh, N.; Bryan, I.; Bryan, Z.; Arellano, C.; Collazo, R.; Ivanisevic, A., AlGaN/GaN field effect transistors functionalized with recognition peptides. *Appl. Phys. Lett.* **2014,** *105* (13).

7. Bermudez, V. M., Adsorption of 1-octanethiol on the GaN(0001) surface. *Langmuir* **2003,** *19* (17), 6813-6819.

8. Kim, H.; Colavita, P. E.; Metz, K. M.; Nichols, B. M.; Sun, B.; Uhlrich, J.; Wang, X. Y.; Kuech, T. F.; Hamers, R. J., Photochemical functionalization of gallium nitride thin films with molecular and biomolecular layers. *Langmuir* **2006,** *22* (19), 8121-8126.

9. Peczonczyk, S. L.; Mukherjee, J.; Carim, A. I.; Maldonado, S., Wet Chemical Functionalization of III-V Semiconductor Surfaces: Alkylation of Gallium Arsenide and Gallium Nitride by a Grignard Reaction Sequence. *Langmuir* **2012,** *28* (10), 4672-4682.

10. Ito, T.; Forman, S. M.; Cao, C.; Li, F.; Eddy, C. R.; Mastro, M. A.; Holm, R. T.; Henry, R. L.; Hohn, K. L.; Edgar, J. H., Self-assembled monolayers of alkylphosphonic acid on GaN substrates. *Langmuir* **2008,** *24* (13), 6630-6635.

11. Schwarz, S. U.; Cimalla, V.; Eichapfel, G.; Himmerlich, M.; Krischok, S.; Ambacher, O., Thermal Functionalization of GaN Surfaces with 1-Alkenes. *Langmuir* **2013,** *29* (21), 6296-6301.

12. Tas, A. C.; Majewski, P. J.; Aldinger, F., Synthesis of gallium oxide hydroxide crystals in aqueous solutions with or without urea and their calcination behavior. *J. Am. Ceram. Soc.* **2002,** *85* (6), 1421-1429.

13. Muruganandham, M.; Amutha, R.; Wahed, M.; Ahmmad, B.; Kuroda, Y.; Suri, R. P. S.; Wu, J. J.; Sillanpaa, M. E. T., Controlled Fabrication of alpha-GaOOH and alpha-Ga2O3 Self-Assembly and Its Superior Photocatalytic Activity. *J. Phys. Chem. C* **2012,** *116* (1), 44-53.

14. Huang, C. C.; Yeh, C. S., GaOOH, and beta- and gamma-Ga2O3 nanowires: preparation and photoluminescence. *New J. Chem.* **2010,** *34* (1), 103-107.

15. Alemi, A.; Hosseinpour, Z.; Dolatyari, M.; Bakhtiari, A., Boehmite (gamma-AlOOH) nanoparticles: Hydrothermal synthesis, characterization, pH-controlled morphologies, optical properties, and DFT calculations. *Phys. Status Solidi B-Basic Solid State Phys.* **2012,** *249* (6), 1264-1270.

16. Zhao, S. R.; Nguyen, H. P. T.; Kibria, M. G.; Mi, Z. T., III-Nitride nanowire optoelectronics. *Prog. Quantum Electron.* **2015,** *44*, 14-68.

17. Vogelson, C. T.; Koide, Y.; Alemany, L. B.; Barron, A. R., Inorganic-organic hybrid and composite resin materials using carboxylate-alumoxanes as functionalized cross-linking agents. *Chem. Mat.* **2000,** *12* (3), 795-804.

18. Wilkins, S. J.; Paskova, T.; Ivanisevic, A., Effect of etching with cysteamine assisted phosphoric acid on gallium nitride surface oxide formation. *J Appl Phys* **2013,** *114* (6).

19. Wilkins, S. J.; Paskova, T.; Ivanisevic, A., Modified surface chemistry, potential, and optical properties of polar gallium nitride via long chained phosphonic acids. *Appl. Surf. Sci.* **2015,** *327*, 498-503.

20. Oregan, B.; Gratzel, M., A LOW-COST, HIGH-EFFICIENCY SOLAR-CELL BASED ON DYE-SENSITIZED COLLOIDAL TIO2 FILMS. *Nature* **1991,** *353* (6346), 737-740.

21. Tetreault, N.; Gratzel, M., Novel nanostructures for next generation dye-sensitized solar cells. *Energy Environ. Sci.* **2012,** *5* (9), 8506-8516.

22. Ozgur, U.; Alivov, Y. I.; Liu, C.; Teke, A.; Reshchikov, M. A.; Dogan, S.; Avrutin, V.; Cho, S. J.; Morkoc, H., A comprehensive review of ZnO materials and devices. *J Appl Phys* **2005,** *98* (4).

23. Hendry, E.; Koeberg, M.; O'Regan, B.; Bonn, M., Local field effects on electron transport in nanostructured TiO2 revealed by terahertz spectroscopy. *Nano Lett.* **2006,** *6* (4), 755-759.

24. Klaumunzer, M.; Kahnt, A.; Burger, A.; Mackovic, M.; Munzel, C.; Srikantharajah, R.; Spiecker, E.; Hirsch, A.; Peukert, W.; Guldi, D. M., Surface Functionalization and Electronic Interactions of ZnO Nanorods with a Porphyrin Derivative. *ACS Appl. Mater. Interfaces* **2014,** *6* (9), 6724-6730.

25. Hagfeldt, A.; Boschloo, G.; Sun, L. C.; Kloo, L.; Pettersson, H., Dye-Sensitized Solar Cells. *Chem. Rev.* **2010,** *110* (11), 6595-6663.

26. Zhang, S. F.; Yang, X. D.; Numata, Y. H.; Han, L. Y., Highly efficient dye-sensitized solar cells: progress and future challenges. *Energy Environ. Sci.* **2013,** *6* (5), 1443-1464.

27. Gratzel, M., Dye-sensitized solar cells. *J. Photochem. Photobiol. C-Photochem. Rev.* **2003,** *4* (2), 145-153.

28. Stergiopoulos, T.; Kontos, A. G.; Jiang, N.; Milliken, D.; Desilvestro, H.; Likodimos, V.; Falaras, P., High boiling point solvent-based dye solar cells pass a harsh thermal ageing test. *Sol. Energy Mater. Sol. Cells* **2016,** *144*, 457-466.

29. Chen, C. R.; Li, Y. C.; Young, T. H., Gallium nitride induces neuronal differentiation markers in neural stem/precursor cells derived from rat cerebral cortex. *Acta Biomaterialia* **2009,** *5* (7), 2610-2617.

30. Kuddannaya, S.; Bao, J. N.; Zhang, Y. L., Enhanced in Vitro Biocompatibility of Chemically Modified Poly(dimethylsiloxane) Surfaces for Stable Adhesion and Long-term Investigation of Brain Cerebral Cortex Cells. *ACS Appl. Mater. Interfaces* **2015,** *7* (45), 25529-25538.

31. Pla-Roca, M.; Isa, L.; Kumar, K.; Reimhult, E., Selective (Bio)Functionalization of Solid-State Nanopores. *ACS Appl. Mater. Interfaces* **2015,** *7* (11), 6030-6035.

32. Hou, H. W.; Xie, Y.; Yang, Q.; Guo, Q. X.; Tan, C. R., Preparation and characterization of gamma-AlOOH nanotubes and nanorods. *Nanotechnology* **2005,** *16* (6), 741-745.

33. Tavakoli, A.; Sohrabi, M.; Kargari, A., A review of methods for synthesis of nanostructured metals with emphasis on iron compounds. *Chem. Pap.* **2007,** *61* (3), 151-170.

34. Hayashi, H.; Hakuta, Y., Hydrothermal Synthesis of Metal Oxide Nanoparticles in Supercritical Water. *Materials* **2010,** *3* (7), 3794-3817.

35. Zhu, Y. J.; Chen, F., Microwave-Assisted Preparation of Inorganic Nanostructures in Liquid Phase. *Chem. Rev.* **2014,** *114* (12), 6462-6555.

36. Bilecka, I.; Niederberger, M., Microwave chemistry for inorganic nanomaterials synthesis. *Nanoscale* **2010,** *2* (8), 1358-1374.

37. Sun, M.; Li, D. Z.; Zhang, W. J.; Fu, X. Z.; Shao, Y.; Li, W. J.; Xiao, G. C.; He, Y. H., Rapid microwave hydrothermal synthesis of GaOOH nanorods with photocatalytic activity toward aromatic compounds. *Nanotechnology* **2010,** *21* (35).

38. Woodruff, D. P., Delchar, T. A. , *Modern Techniques of Surface Science*. Second ed.; Cambridge University Press: Cambridge, United Kingdom, 1994.

39. Fairley, N., Casa XPS. Casa Software Ltd: 2009.

40. Foster, C. M.; Collazo, R.; Sitar, Z.; Ivanisevic, A., Cell Behavior on Gallium Nitride Surfaces: Peptide Affinity Attachment versus Covalent Functionalization. *Langmuir* **2013,** *29* (26), 8377-8384.

41. Nemykin, V. N.; Galloni, P.; Floris, B.; Barrett, C. D.; Hadt, R. G.; Subbotin, R. I.; Marrani, A. G.; Zanoni, R.; Loim, N. M., Metal-free and transition-metal tetraferrocenylporphyrins part 1: synthesis, characterization, electronic structure, and conformational flexibility of neutral compounds. *Dalton Trans.* **2008,** (32), 4233-4246.

42. Rohrbaugh, N.; Bryan, I.; Bryan, Z.; Arellano, C.; Collazo, R.; Ivanisevic, A., AlGaN/GaN field effect transistors functionalized with recognition peptides. *Appl. Phys. Lett.* **2014,** *105* (13), 5.

43. Bermudez, V. M., Adsorption and photodissociation of 4-haloanilines on GaN(0001). *Surf. Sci.* **2002,** *519* (3), 173-184.

44. Bermudez, V. M., Functionalizing the GaN(0001)-(1x1) surface I. The chemisorption of aniline. *Surf. Sci.* **2002,** *499* (2-3), 109-123.

45. Bermudez, V. M., Functionalizing the GaN(0001)-(1x1) surface II. Chemisorption of 3-pyrroline. *Surf. Sci.* **2002,** *499* (2-3), 124-134.

46. Bermudez, V. M.; Long, J. P., Chemisorption of H2O on GaN(0001). *Surf. Sci.* **2000,** *450* (1-2), 98-105.

47. Bermudez, V. M., Investigation of the initial chemisorption and reaction of fluorine (XeF2) with the GaN(0001)-(1x1) surface. *Appl. Surf. Sci.* **1997,** *119* (1-2), 147-159.

48. Wilkins, S. J.; Paskova, T.; Ivanisevic, A., Modified surface chemistry, potential, and optical properties of polar gallium nitride via long chained phosphonic acids. *Appl. Surf. Sci.* **2015,** *327* (0), 498-503.

49. Arisio, C.; Cassou, C. A.; Lieberman, M., Loss of Siloxane Monolayers from GaN Surfaces in Water. *Langmuir* **2013,** *29* (17), 5145-5149.

50. Foster, C. M.; Collazo, R.; Sitar, Z.; Ivanisevic, A., Aqueous Stability of Ga- and N-Polar Gallium Nitride. *Langmuir* **2013,** *29* (1), 216-220.

51. Jung, Y.; Ahn, J.; Baik, K. H.; Kim, D.; Pearton, S. J.; Ren, F.; Kim, J., Chemical Etch Characteristics of N-Face and Ga-Face GaN by Phosphoric Acid and Potassium Hydroxide Solutions. *J. Electrochem. Soc.* **2012,** *159* (2), H117-H120.

52. Lopez-Gejo, J.; Navarro-Tobar, A.; Arranz, A.; Palacio, C.; Munoz, E.; Orellana, G., Direct Grafting of Long-Lived Luminescent Indicator Dyes to GaN Light-Emitting Diodes for Chemical Microsensor Development. *Acs Applied Materials & Interfaces* **2011,** *3* (10), 3846-3854.

53. Odobel, F.; Blart, E.; Lagree, M.; Villieras, M.; Boujtita, H.; El Murr, N.; Caramori, S.; Bignozzi, C. A., Porphyrin dyes for TiO2 sensitization. *J. Mater. Chem.* **2003,** *13* (3), 502-510.

54. Sunkara, M. K.; Pendyala, C.; Cummins, D.; Meduri, P.; Jasinski, J.; Kumar, V.; Russell, H. B.; Clark, E. L.; Kim, J. H., Inorganic nanowires: a perspective about their role in energy conversion and storage applications. *J. Phys. D-Appl. Phys.* **2011,** *44* (17), 9.

55. Jewett, S. A.; Makowski, M. S.; Andrews, B.; Manfra, M. J.; Ivanisevic, A., Gallium nitride is biocompatible and non-toxic before and after functionalization with peptides. *Acta Biomaterialia* **2012,** *8* (2), 728-733.

56. Millet, P.; Calka, A.; Williams, J. S.; Vantenaar, G. J. H., FORMATION OF GALLIUM NITRIDE BY A NOVEL HOT MECHANICAL ALLOYING PROCESS. *Appl. Phys. Lett.* **1993,** *63* (18), 2505-2507.

57. Swamy, A. K. N.; Shafirovich, E.; Ramana, C. V., Synthesis of one-dimensional Ga2O3 nanostructures via high-energy ball milling and annealing of GaN. *Ceram. Int.* **2013,** *39* (6), 7223-7227.

58. Carin, R.; Deville, J. P.; Werckmann, J., An Xps Study of Gan Thin-Films on Gaas. *Surf Interface Anal* **1990,** *16* (1-12), 65-69.

59. Cherian, S.; Wamser, C. C., Adsorption and photoactivity of tetra(4-carboxyphenyl)porphyrin (TCPP) on nanoparticulate TiO2. *J. Phys. Chem. B* **2000,** *104* (15), 3624-3629.

60. Brennan, B. J.; Portoles, M. J. L.; Liddell, P. A.; Moore, T. A.; Moore, A. L.; Gust, D., Comparison of silatrane, phosphonic acid, and carboxylic acid functional groups for attachment of porphyrin sensitizers to TiO2 in photoelectrochemical cells. *Physical Chemistry Chemical Physics* **2013,** *15* (39), 16605-16614.

61. Vericat, C.; Vela, M. E.; Corthey, G.; Pensa, E.; Cortes, E.; Fonticelli, M. H.; Ibanez, F.; Benitez, G. E.; Carro, P.; Salvarezza, R. C., Self-assembled monolayers of thiolates on metals: a review article on sulfur-metal chemistry and surface structures. *RSC Adv.* **2014,** *4* (53), 27730-27754.

62. Silipigni, L.; De Luca, G.; Quattrone, Q.; Scolaro, L. M.; Salvato, G.; Grasso, V., An XPS analysis of the interaction of meso-tetrakis(N-methylpyridinium-4-yl)porphyrin with exfoliated manganese thiophosphate. *J. Phys.-Condes. Matter* **2006,** *18* (24), 5759-5772.

63. Makowski, M. S.; Zemlyanov, D. Y.; Lindsey, J. A.; Bernhard, J. C.; Hagen, E. M.; Chan, B. K.; Petersohn, A. A.; Medow, M. R.; Wendel, L. E.; Chen, D. F.; Canter, J. M.; Ivanisevic, A., Covalent attachment of a peptide to the surface of gallium nitride. *Surf. Sci.* **2011,** *605* (15-16), 1466-1475.

64. Watkins, N. J.; Wicks, G. W.; Gao, Y. L., Oxidation study of GaN using x-ray photoemission spectroscopy. *Appl. Phys. Lett.* **1999,** *75* (17), 2602-2604.

65. Evans, S., Energy Calibration Secondary Standards for X-Ray Photoelectron Spectrometers. *Surf Interface Anal* **1985,** *7* (6), 299-302.

66. Fairley, N. *Casa XPS*, 2.3.16 PR; Casa Software Ltd: 2009.

67. Macquet, J. P.; Millard, M. M.; Theophanides, T., X-RAY PHOTOELECTRON-SPECTROSCOPY OF PORPHYRINS. *Journal of the American Chemical Society* **1978,** *100* (15), 4741-4746.

68. Sarno, D. M.; Matienzo, L. J.; Jones, W. E., X-ray photoelectron spectroscopy as a probe of intermolecular interactions in porphyrin polymer thin films. *Inorg. Chem.* **2001,** *40* (24), 6308-6315.

69. Baraton, M. I.; Gonsalves, K. E., An IR spectroscopic investigation of nanostructured AlN and GaN powder surfaces. *J. Clust. Sci.* **1999,** *10* (1), 133-154.

70. Wei, X. F.; Shi, F., Synthesis and characterization of GaN nanowires by a catalyst assisted chemical vapor deposition. *Appl. Surf. Sci.* **2011,** *257* (23), 9931-9934.

71. Shi, F.; Xue, C. S., Influence of reaction time on growth of GaN nanowires fabricated by CVD method. *J. Mater. Sci.-Mater. Electron.* **2011,** *22* (12), 1835-1840.

72. Xiao, H. D.; Liu, R.; Ma, H. L.; Lin, Z. J.; Ma, J.; Zong, F. J.; Mei, L. M., Thermal stability of GaN powders investigated by XRD, XPS, PL, TEM, and FT-IR. *J. Alloy. Compd.* **2008,** *465* (1-2), 340-343.

73. Brandt, M. S.; Ager, J. W.; Gotz, W.; Johnson, N. M.; Harris, J. S.; Molnar, R. J.; Moustakas, T. D., LOCAL VIBRATIONAL-MODES IN MG-DOPED GALLIUM NITRIDE. *Phys. Rev. B* **1994,** *49* (20), 14758-14761.

74. Ogoshi, H.; Nakamoto, K.; Saito, Y., INFRARED-SPECTRA AND NORMAL COORDINATE ANALYSIS OF METALLOPORPHINS. *J. Chem. Phys.* **1972,** *57* (10), 4194-&.

75. Santiago, P. S.; Moreira, L. M.; Tabak, M., Phosphate group effects upon the equilibrium of iron(III) meso-tetrakis (4-N-methylpyridiniumyl) porphyrin in aqueous solution. *J. Inorg. Biochem.* **2006,** *100* (11), 1715-1721.

76. Stutzmann, M.; Garrido, J. A.; Eickhoff, M.; Brandt, M. S., Direct biofunctionalization of semiconductors: A survey. *Phys. Status Solidi A-Appl. Mat.* **2006,** *203* (14), 3424-3437.

77. Ozgur, U.; Alivov, Y. I.; Liu, C.; Teke, A.; Reshchikov, M. A.; Dogan, S.; Avrutin, V.; Cho, S. J.; Morkoc, H., A comprehensive review of ZnO materials and devices. *J Appl Phys* **2005,** *98* (4), 041301-103.

78. Palacios-Lidon, E.; Pickup, D. F.; Johnson, P. S.; Ruther, R. E.; Tena-Zaera, R.; Hamers, R. J.; Colchero, J.; Himpsel, F. J.; Ortega, J. E.; Rogero, C., Face-Selective Etching of ZnO during Attachment of Dyes. *J Phys Chem C* **2013,** *117* (36), 18414-18422.

79. Jung, H. S.; Hong, Y. J.; Li, Y.; Cho, J.; Kim, Y. J.; Yi, G. C., Photocatalysis using GaN nanowires. *ACS Nano* **2008,** *2* (4), 637-642.

80. Mazeina, L.; Bermudez, V. M.; Perkins, F. K.; Arnold, S. P.; Prokes, S. M., Interaction of functionalized Ga2O3 NW-based room temperature gas sensors with different hydrocarbons. *Sens. Actuator B-Chem.* **2010,** *151* (1), 114-120.

81. Bermudez, V. A., Functionalization of beta-Ga2O3 Nanoribbons: A Combined Computational and Infrared Spectroscopic Study. *Langmuir* **2008,** *24* (22), 12943-12952.

82. Mazeina, L.; Perkins, F. K.; Bermudez, V. M.; Arnold, S. P.; Prokes, S. M., Functionalized Ga2O3 Nanowires as Active Material in Room Temperature Capacitance-Based Gas Sensors. *Langmuir* **2010,** *26* (16), 13722-13726.

83. Ge, S. X.; Zhang, L. Z.; Jia, H. M.; Zheng, Z., Microwave-assisted synthesis of various gallium oxyhydroxide nanorods and their controllable conversion into different gallium oxide polymorphs. *J. Mater. Res.* **2009,** *24* (7), 2268-2275.

84. Naidu, B. S.; Pandey, M.; Nuwad, J.; Sudarsan, V.; Vatsa, R. K.; Kshirsagar, R. J.; Pillai, C. G. S., Lanthanide-Ion-Assisted Structural Collapse of Layered GaOOH Lattice. *Inorg. Chem.* **2011,** *50* (10), 4463-4472.

85. Li, L. D.; Wei, W.; Behrens, M., Synthesis and characterization of alpha-, beta-, and gamma-Ga(2)o(3) prepared from aqueous solutions by controlled precipitation. *Solid State Sci.* **2012,** *14* (7), 971-981.

86. Yang, J.; Zhao, Y. Y.; Frost, R. L., Infrared and infrared emission spectroscopy of gallium oxide alpha-GaO(OH) nanostructures. *Spectroc. Acta Pt. A-Molec. Biomolec. Spectr.* **2009,** *74* (2), 398-403.

87. Quan, Y.; Fang, D.; Zhang, X. Y.; Liu, S. Q.; Huang, K. L., Synthesis and characterization of gallium oxide nanowires via a hydrothermal method. *Mater. Chem. Phys.* **2010,** *121* (1-2), 142-146.

88. Zhao, Y. Y.; Frost, R. L.; Yang, J.; Martens, W. N., Size and morphology control of gallium oxide hydroxide GaO(OH), nano- to micro-sized particles by soft-chemistry route without surfactant. *J. Phys. Chem. C* **2008,** *112* (10), 3568-3579.

89. Chen, S. G.; Luo, S. M.; Zhou, Y.; Chen, Y.; Liu, Y. Q.; Long, C. G., A simple hydrothermal route to GaOOH intersecting-rods with regular diamond-like cross section. *Mater. Lett.* **2008,** *62* (30), 4566-4569.

90. Avivi, S.; Mastai, Y.; Hodes, G.; Gedanken, A., Sonochemical hydrolysis of Ga3+ ions: Synthesis of scroll-like cylindrical nanoparticles of gallium oxide hydroxide. *J Am Chem Soc* **1999,** *121* (17), 4196-4199.

91. Wu, S.; Zhang, J.; Shi, L. H.; Tang, S. X.; Li, Y. G.; Jiang, L. N.; Cui, Q. L., Template-free synthesis of alpha-GaOOH hyperbranched nanoarchitectures via crystal splitting and their optical properties. *RSC Adv.* **2014,** *4* (16), 8209-8215.

92. Krehula, S.; Krehula, L. K.; Music, S., Synthesis and microstructural properties of alpha-Fe1-xGaxOOH solid solutions. *J. Alloy. Compd.* **2013,** *581*, 335-343.

93. Nikolaev, N. A.; Lityagina, L. M.; Dyuzheva, T. I.; Kulikova, L. F.; Bendeliani, N. A., Synthesis and single crystal growth of the new high-pressure phase of GaOOH. *J. Alloy. Compd.* **2008,** *459* (1-2), 95-97.

94. Xiao, H. D.; Ma, H. L.; Xue, C. S.; Hu, W. R.; Ma, J.; Zong, F. J.; Zhang, X. J.; Ji, F., Synthesis and properties of GaO2H nanorods. *Mater. Lett.* **2004,** *58* (30), 3925-3928.

95. Kisailus, D.; Choi, J. H.; Weaver, J. C.; Yang, W. J.; Morse, D. E., Enzymatic synthesis and nanostructural control of gallium oxide at low temperature. *Adv Mater* **2005,** *17* (3), 314-318.

96. Sun, M.; Li, D. Z.; Zhang, W. J.; Fu, X. Z.; Shao, Y.; Li, W. J.; Xiao, G. C.; He, Y. H., Rapid microwave hydrothermal synthesis of GaOOH nanorods with photocatalytic activity toward aromatic compounds. *Nanotechnology* **2010,** *21* (35), 1-7.

97. Pei, L. Z.; Yang, L. J.; Dong, Y. P.; Wang, J. F.; Fan, C. G.; Wang, S. B.; Chen, J.; Yin, W. Y.; Zhang, Q. F., Large-scale synthesis of submicron gallium oxide hydrate rods and their optical and electrochemical properties. *Cryst. Res. Technol.* **2010,** *45* (10), 1087-1093.

98. Cullity, B. D., *Elements of X-Ray Diffraction*. Addison-Wesley Publishing Company Inc.: London, 1978.

99. Li, S. J.; Zheng, C.; Lobring, K. C., Refinement of the crystal structure of gallium oxide hydroxide, GaO(OH). *Z. Krist.-New Cryst. Struct.* **2003,** *218* (1), 11-12.

100. Hendsbee, A. D.; Pye, C. C.; Masuda, J. D., Hexaaquagallium(III) trinitrate trihydrate. *Acta Crystallogr. Sect. E.-Struct Rep. Online* **2009,** *65*, I65-U201.

101. Cui, Z.; Li, E. L.; Shi, W.; Ma, D. M., Optical and field emission properties of layer-structure GaN nanowires. *Mater. Res. Bull.* **2014,** *56*, 80-85.

102. Lee, I.; Kwak, J.; Haam, S.; Lee, S. Y., Dipeptide-assisted growth of uniform gallium oxohydroxide spindles. *J. Cryst. Growth* **2010,** *312* (14), 2107-2112.

103. Lyu, S. C.; Cha, O. H.; Suh, E. K.; Ruh, H.; Lee, H. J.; Lee, C. J., Catalytic synthesis and photoluminescence of gallium nitride nanowires. *Chem. Phys. Lett.* **2003,** *367* (1-2), 136-140.

104. Seker, F.; Meeker, K.; Kuech, T. F.; Ellis, A. B., Surface chemistry of prototypical bulk II-VI and III-V semiconductors and implications for chemical sensing. *Chem. Rev.* **2000,** *100* (7), 2505-2536.

105. Hsu, C. W.; Ganguly, A.; Chen, C. P.; Kuo, C. C.; Paskov, P. P.; Holtz, P. O.; Chen, L. C.; Chen, K. H., Optical properties of functionalized GaN nanowires. *J Appl Phys* **2011,** *109* (5).

106. Huang, C. C.; Yeh, C. S.; Ho, C. J., Laser ablation synthesis of spindle-like gallium oxide hydroxide nanoparticles with the presence of cationic cetyltrimethylammonium bromide. *J. Phys. Chem. B* **2004,** *108* (16), 4940-4945.

107. Dar, M. I.; Sampath, S.; Shivashankar, S. A., Exploiting oriented attachment in stabilizing La3+-doped gallium oxide nano-spindles. *RSC Adv.* **2014,** *4* (90), 49360-49366.

108. Xu, N.; Boo, B. H., Pulsed laser deposition of nanocrystalline ZnSe : N thin films. *Semicond. Sci. Technol.* **2003,** *18* (4), 300-302.

109. Sun, Z. J.; Li, J. S.; Zheng, H. F.; Liu, X.; Ye, S.; Du, P. W., Pyrolyzed cobalt porphyrin-modified carbon nanomaterial as an active catalyst for electrocatalytic water oxidation. *Int. J. Hydrog. Energy* **2015,** *40* (20), 6538-6545.

110. Nemykin, V. N.; Galloni, P.; Floris, B.; Barrett, C. D.; Hadt, R. G.; Subbotin, R. I.; Marrani, A. G.; Zanoni, R.; Loim, N. M., Metal-free and transition-metal tetraferrocenylporphyrins part 1: synthesis, characterization, electronic structure, and conformational flexibility of neutral compounds. *Dalton Trans.* **2008,** *32* (32), 4233-4246.

111. Wang, S. G.; Ma, Y.; Shi, Y. J.; Gong, W. X., Defluoridation performance and mechanism of nano-scale aluminum oxide hydroxide in aqueous solution. *J. Chem. Technol. Biotechnol.* **2009,** *84* (7), 1043-1050.

112. Pearce, B. L.; Wilkins, S. J.; Rahn, M. S.; Ivanisevic, A., In situ functionalization of gallium nitride powder with a porphyrin dye. *J. Mater. Res.* **2015,** *30* (19), 2910-2918.
113. Hill, V. G.; Roy, R.; Osborn, E. F., THE SYSTEM ALUMINA GALLIA WATER. *J. Am. Ceram. Soc.* **1952,** *35* (6), 135-142.

114. de Leon, J. N. D., Binary gamma-Al2O3-alpha-Ga2O3 as supports of NiW catalysts for hydrocarbon sulfur removal. *Appl. Catal. B-Environ.* **2016,** *181*, 524-533.

115. Escribano, V. S.; Amores, J. M. G.; Lopez, E. F.; Panizza, M.; Resini, C.; Busca, G., Solid state characterization of coprecipitated alumina-gallia mixed oxide powders. *J. Mater. Sci.* **2005,** *40* (8), 2013-2021.

116. Nakatani, T.; Watanabe, T.; Takahashi, M.; Miyahara, Y.; Deguchi, H.; Iwamoto, S.; Kanai, H.; Inoue, M., Characterization of gamma-Ga2O3-Al2O3 Prepared by Solvothermal Method and Its Performance for Methane-SCR of NO. *J. Phys. Chem. A* **2009,** *113* (25), 7021-7029.

117. Lee, K.; Ruddy, D. A.; Dukovic, G.; Neale, N. R., Synthesis, optical, and photocatalytic properties of cobalt mixed-metal spinel oxides Co(Al1-xGax)(2)O-4. *J. Mater. Chem. A* **2015,** *3* (15), 8115-8122.

118. Newhouse, P. F.; Parkinson, B. A., Combinatorial optimization of spinel Co3-xMxO4 M = (Al, Ga, In) alloyed thin films prepared by ink jet printing: photoelectrochemical, optical, and structural properties. *J. Mater. Chem. A* **2015,** *3* (11), 5901-5907.

119. Karazhanov, S. Z.; Ravindran, P., Ab Initio Study Of Double Oxides ZnX2O4 (X=Al, Ga, In) Having Spinel Structure. *J. Am. Ceram. Soc.* **2010,** *93* (10), 3335-3341.

120. Prasad, S.; Reddy, M. S.; Kumar, V. R.; Veeraiah, N., Specific features of photo and thermoluminescence of Tb3+ ions in BaO-M2O3 (M = Ga, Al, In)-P2O5 glasses. *J. Lumines.* **2007,** *127* (2), 637-644.

121. Pearce, B. L.; Berg, N. G.; Rahn, M. S.; Ivanisevic, A., In situ and ex situ functionalization of nanostructured gallium oxy-hydroxide with a porphyrin dye. *Scanning* **2016**, n/a-n/a.

122. Yang, Q., The reaction conditions influence on hydrothermal synthesis of boehmite nanorods. *Inorg. Mater.* **2010,** *46* (9), 953-958.

123. Shan, C. S.; Yang, H. F.; Han, D. X.; Zhang, Q. X.; Ivaska, A.; Niu, L., Water-Soluble Graphene Covalently Functionalized by Biocompatible Poly-L-lysine. *Langmuir* **2009,** *25* (20), 12030-12033.

124. Alexander, M. R.; Beamson, G.; Blomfield, C. J.; Leggett, G.; Duc, T. M., Interaction of carboxylic acids with the oxyhydroxide surface of aluminium: poly(acrylic acid), acetic acid and propionic acid on pseudoboehmite. *Journal of Electron Spectroscopy and Related Phenomena* **2001,** *121* (1-3), 19-32.

125. (a) Shahid, N.; Villate, R. G.; Barron, A. R., Chemically functionalized alumina nanoparticle effect on carbon fiber/epoxy composites. *Compos. Sci. Technol.* **2005,** *65* (14), 2250-2258; (b) Omrani, A.; Simon, L. C.; Rostami, A. A., The effects of alumina nanoparticle on the properties of an epoxy resin system. *Mater. Chem. Phys.* **2009,** *114* (1), 145-150.

126. Zhang, T.; Go, M. A.; Stricker, C.; Daria, V. R.; Tricoli, A., Low-cost photo-responsive nanocarriers by one-step functionalization of flame-made titania agglomerates with L-Lysine. *J. Mat. Chem. B* **2015,** *3* (8), 1677-1687.

127. Shakiba, A.; Jamison, A. C.; Lee, T. R., Poly(L-lysine) Interfaces via Dual Click Reactions on Surface-Bound Custom-Designed Dithiol Adsorbates. *Langmuir* **2015,** *31* (22), 6154-6163.

128. Hussain, N.; Singh, B.; Sakthivel, T.; Florence, A. T., Formulation and stability of surface-tethered DNA-gold-dendron nanoparticles. *Int. J. Pharm.* **2003,** *254* (1), 27-31.

129. Pasche, S.; De Paul, S. M.; Voros, J.; Spencer, N. D.; Textor, M., Poly(L-lysine)-graft-poly(ethylene glycol) assembled monolayers on niobium oxide surfaces: A quantitative study of the influence of polymer interfacial architecture on resistance to protein adsorption by ToF-SIMS and in situ OWLS. *Langmuir* **2003,** *19* (22), 9216-9225.

130. Duan, X. C.; Kim, T.; Li, D.; Ma, J. M.; Zheng, W. J., Understanding the Effect Models of Ionic Liquids in the Synthesis of NH4-Dw and gamma-AlOOH Nanostructures and Their Conversion into Porous gamma-Al2O3. *Chem.-Eur. J.* **2013,** *19* (19), 5924-5937.

131. 이재범; Tai, K. S., Synthesis of AlN powders from AlOOH. *Korean Journal of Materials Research* **2006,** *16* (12), 771-776.

132. Liu, G. C.; Duan, X. C.; Li, H. B.; Liang, D., Preparation and photoluminescence properties of Eu-doped Ga2O3 nanorods. *Mater. Chem. Phys.* **2008,** *110* (2-3), 206-211.

133. Kelsen, D. P.; Alcock, N.; Yeh, S.; Brown, J.; Young, C., PHARMACOKINETICS OF GALLIUM NITRATE IN MAN. *Cancer* **1980,** *46* (9), 2009-2013.

134. Takeno, N., Atlas of Eh-pH diagrams: Intercomparison of thermodynamic databases. Environments, R. C. f. D. G., Ed. National Institute of Advanced Industrial Science and Technology: Japan, 2005.

135. Niedzialkowski, P.; Ossowski, T.; Zieba, P.; Cirocka, A.; Rochowski, P.; Pogorzelski, S. J.; Ryl, J.; Sobaszek, M.; Bogdanowicz, R., Poly-L-lysine-modified boron-doped diamond electrodes for the amperometric detection of nucleic acid bases. *J. Electroanal. Chem.* **2015,** *756*, 84-93.

136. Music, S.; Dragcevic, D.; Popovic, S.; Vdovic, N., Microstructural properties of boehmite formed under hydrothermal conditions. *Mater. Sci. Eng. B-Solid State Mater. Adv. Technol.* **1998,** *52* (2-3), 145-153.

137. Willhite, C. C.; Ball, G. L.; McLellan, C. J., Total allowable concentrations of monomeric inorganic aluminum and hydrated aluminum silicates in drinking water. *Crit. Rev. Toxicol.* **2012,** *42* (5), 358-442.

138. Water, O., 2012 Edition of the Drinking Water Standards and Health Advisories.

139. Mourino, V.; Newby, P.; Pishbin, F.; Cattalini, J. P.; Lucangioli, S.; Boccaccini, A. R., Physicochemical, biological and drug-release properties of gallium crosslinked alginate/nanoparticulate bioactive glass composite films. *Soft Matter* **2011,** *7* (14), 6705-6712.

140. Berg, N. G.; Pearce, B. L.; Snyder, P. J.; Rohrbaugh, N.; Nolan, M. W.; Adhikari, P.; Khan, S. A.; Ivanisevic, A., Interfaces with Tunable Mechanical and Radiosensitizing Properties. *ACS Applied Materials & Interfaces* **2016**.

141. Pearce, B. L.; Berg, N. G.; Ivanisevic, A., Synthesis and Optical Characterization of Mixed Nanostructured Aluminum-Gallium Oxy-hydroxide. *Materials Research Letters* **2016**.

142. Martini, L. A.; Moore, G. F.; Milot, R. L.; Cai, L. Z.; Sheehan, S. W.; Schmuttenmaer, C. A.; Brudvig, G. W.; Crabtree, R. H., Modular Assembly of High-Potential Zinc Porphyrin Photosensitizers Attached to TiO2 with a Series of Anchoring Groups. *J. Phys. Chem. C* **2013,** *117* (28), 14526-14533.

143. Pearce, B. L.; Berg, N. G.; Ivanisevic, A., Synthesis and Optical Characterization of Mixed Nanostructured Aluminum Gallium Oxy-hydroxide. *Materials Research Letters* **2016**.